

AD-A076 514

DAYTON UNIV OH RESEARCH INST

F/6 21/2

COMBUSTION DIAGNOSTICS USING LASER SPONTANEOUS-RAMAN SCATTERING--ETC(U)

APR 79 P P YANEY

F33615-76-C-2078

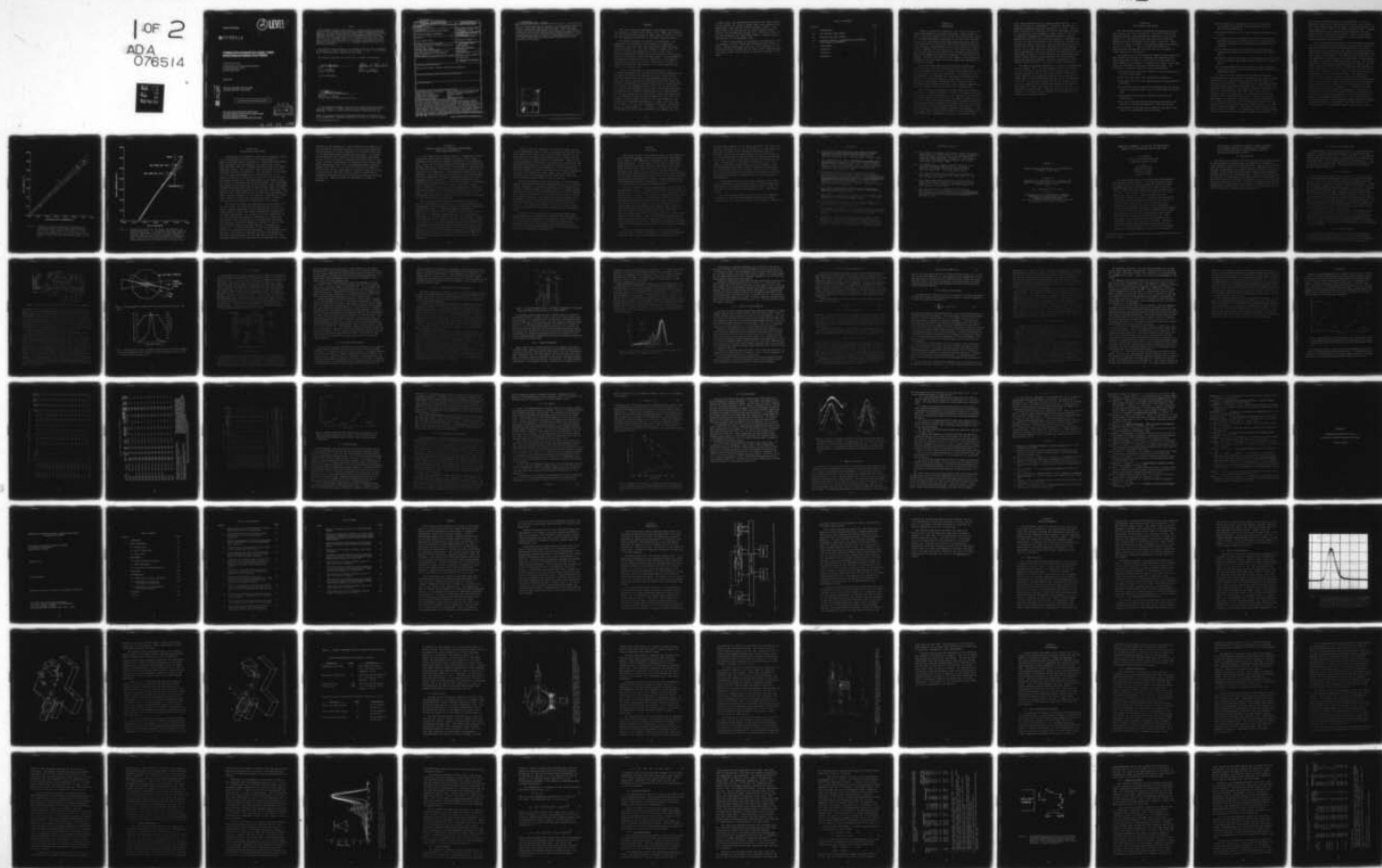
UNCLASSIFIED

UDR-TR-79-46

AFAPL-TR-79-2035

NL

1 OF 2
ADA
076514



AFAPL-TR-79-2035

② LEVEL II

AD A076514

COMBUSTION DIAGNOSTICS USING LASER SPONTANEOUS-RAMAN SCATTERING

PERRY PAPPAS YANEY

*UNIVERSITY OF DAYTON RESEARCH INSTITUTE
300 COLLEGE PARK AVENUE
DAYTON, OHIO 45469*

APRIL 1979

DDC FILE COPY

TECHNICAL REPORT AFAPL-TR-79-2035
Final Report July 1976 — October 1978

Approved for public release; distribution unlimited.

AIR FORCE AERO PROPULSION LABORATORY
AIR FORCE WRIGHT AERONAUTICAL LABORATORIES
AIR FORCE SYSTEMS COMMAND
WRIGHT-PATTERSON AIR FORCE BASE, OHIO 45433

DDC
RECEIVED
NOV 14 1979
B

79 13 11 120

NOTICE

When Government drawings, specifications, or other data are used for any purpose other than in connection with a definitely related Government procurement operation, the United States Government thereby incurs no responsibility nor any obligation whatsoever; and the fact that the government may have formulated, furnished, or in any way supplied the said drawings, specifications, or other data, is not to be regarded by implication or otherwise as in any manner licensing the holder or any other person or corporation, or conveying any rights or permission to manufacture, use, or sell any patented invention that may in any way be related thereto.

This report has been reviewed by the Information Office (OI) and is releasable to the National Technical Information Service (NTIS). At NTIS, it will be available to the general public, including foreign nations.

This technical report has been reviewed and is approved for publication.

W. M. Roquemore
NAME
W. M. ROQUEMORE
Project Engineer

Arthur V. Churchill
NAME
ARTHUR V. CHURCHILL
Chief, Fuels Branch

FOR THE COMMANDER

Blackwell C. Dunnam
NAME
BLACKWELL C. DUNNAM
Chief, Fuels and Lubrication Division

"If your address has changed, if you wish to be removed from our mailing list, or if the addressee is no longer employed by your organization please notify AFAPL/SFF, W-PAFB, OH 45433 to help us maintain a current mailing list".

Copies of this report should not be returned unless return is required by security considerations, contractual obligations, or notice on a specific document.

UNCLASSIFIED

SECURITY CLASSIFICATION THIS PAGE (When Data Entered)

REPORT DOCUMENTATION PAGE		READ INSTRUCTIONS BEFORE COMPLETING FORM
1. REPORT NUMBER AFAPL-TR-79-2035	2. GOVT ACCESSION NO.	3. RECIPIENT'S CATALOG NUMBER
4. TITLE (and Subtitle) COMBUSTION DIAGNOSTICS USING LASER SPONTANEOUS-RAMAN SCATTERING	5. TYPE OF REPORT & PERIOD COVERED Technical - Final report 1 July 1976-31 Oct. 1978	6. PERFORMING ORG. REPORT NUMBER UDR-TR-79-46
7. AUTHOR(s) Perry Pappas Yaney	8. CONTRACT OR GRANT NUMBER(s) F33615-76-C-2078	
9. PERFORMING ORGANIZATION NAME AND ADDRESS University of Dayton Research Institute 300 College Park Dayton, Ohio 45469	10. PROGRAM ELEMENT, PROJECT, TASK AREA & WORK UNIT NUMBERS Project 3048 Task 304805 Work Unit 30480576	
11. CONTROLLING OFFICE NAME AND ADDRESS Air Force Aero Propulsion Lab (SFF) Wright-Patterson Air Force Base, Ohio 45433	12. REPORT DATE April 1979	13. NUMBER OF PAGES 141
14. MONITORING AGENCY NAME & ADDRESS (if different from Controlling Office) 1613048 171304845	15. SECURITY CLASS. (of this report) Unclassified	15a. DECLASSIFICATION/DOWNGRADING SCHEDULE
16. DISTRIBUTION STATEMENT (of this Report) Approved for public release; distribution unlimited.		
17. DISTRIBUTION STATEMENT (of the abstract entered in Block 20, if different from Report)		
18. SUPPLEMENTARY NOTES		
19. KEY WORDS (Continue on reverse side if necessary and identify by block number) Spontaneous Raman Scattering Gated Detection with Pulsed Laser Raman Spectroscopy Multiple Regression Analysis Temperature Measurements Turbojet Engine Combustion Diagnostics J85-5 Remote Optical Probe Combustion Tunnel		
20. ABSTRACT (Continue on reverse side if necessary and identify by block number) An existing computer-controlled Raman Spectroscopy system, using a pulsed nitrogen laser and a double spectrometer, was up-graded and used to measure the temperatures in the combustion plume of an afterburning J85-5 turbojet engine. The computer-fitted temperatures had standard deviations between one and three percent. The agreement with simultaneous and sequential gas-sampling probe measurements and with sequential thermocouple measurements was within five percent. Upon completion of these studies, the system		

DD FORM 1 JAN 73 1473

EDITION OF 1 NOV 65 IS OBSOLETE

SECURITY CLASSIFICATION OF THIS PAGE (When Data Entered)

105400

JOB

UNCLASSIFIED

SECURITY CLASSIFICATION OF THIS PAGE (When Date Entered)

was extensively modified for use with a 10-inch diameter combustion tunnel. Forty-eight sets of Raman data were taken over a wide range of operating conditions of the tunnel. The temperatures ranged from 1000 to over 2000°K using methane fuel. The turbulent diffusion flame was characterized by an unsteady appearance and was orange-yellow in color. Poisson standard deviations for 21 of the measurements averaged four percent. Measurements and spectra of the laser-induced and non-laser-induced backgrounds were also obtained and analyzed.

ACCESSION for	
NTIS	Write Section <input checked="" type="checkbox"/>
DDC	Buff Section <input type="checkbox"/>
UNANNOUNCED	<input type="checkbox"/>
JUSTIFICATION	
BY	
DISTRIBUTION/AVAILABILITY CODES	
Dist. AVAIL. and/or SPECIAL	
A	

SECURITY CLASSIFICATION OF THIS PAGE (When Date Entered)

FOREWORD

This final report was prepared by the Research Institute of the University of Dayton (UD), Dayton, Ohio 45469 under Contract No. F33615-76-C-2078, Project No. 3048, Task 05, Work Unit 76 with Dr. W.M. Roquemore (AFAPL/SFF) as Government Project Monitor.

The report describes the results of experimental, computational, and theoretical investigations of combustion diagnostics using the laser Raman scattering (LARS) technique during the period of 1 July 1976 through 31 October 1978. Dr. Perry P. Yaney of the Department of Physics (PHY) was the Principal Investigator during the entire course of this research and he is the author of this technical report. The management of the program was carried out by Dr. Lloyd Huff of the Research Institute (RI) during the first 15 months with Dr. Eugene H. Gerber (RI) completing the program. The author submitted this report on 12 February 1979.

I wish to acknowledge the many contributions of the following colleagues: Mr. Ira Fiscus (RI) and his associates who designed and directed the construction of the scissors-jack-supported optics table for the modified LARS system, Mr. Dave Royer (RI) and his associates, particularly Mr. Mike Aulds, who designed, constructed, and repaired many circuits associated with the computer and computer-interface units, Mr. Al Gillio (RI), who unraveled the assembler program used in the LARS minicomputer and modified it to perform satisfactorily to our requirements, and Mr. Herb Mildrum of the Department of Electrical Engineering, who coordinated the many activities during the first half of the program. Special thanks is given to Dr. Louis Boehman of the Department of Mechanical Engineering, Dr. Duane Leet (RI), and Mr. Hal Swift (RI) for their invaluable assistance, particularly during the early months of this program. I especially wish to acknowledge the efforts and dedication of my students, Mr. Phil

R. Hemmer (PHY), who assembled and developed the Raman computer fitting routine, Mr. Terry H. Hemmer (PHY), who assisted in the experimental tests and the computer analyses, and Mr. Peter Magill (PHY), who performed an invaluable yeoman's effort in bringing the minicomputer software into a functional state. To my close colleague, Dr. Roger Becker (PHY), I express sincere appreciation for his dependable help.

I wish to acknowledge the cooperation and dedication of Dr. Mel Roquemore and the C-stand and combustion-tunnel staffs of AFAPL. Special thanks goes also to Dr. Paul Schreiber of the High Power Branch of AFAPL for the use of their capillary burner and various other items loaned to us during the course of this work.

TABLE OF CONTENTS

SECTION		PAGE
I	INTRODUCTION	1
II	THE ORIGINAL LARS SYSTEM	3
III	THE MODIFIED LARS SYSTEM	8
IV	COMPUTER STUDIES OF TEMPERATURE MEASUREMENTS USING RAMAN SPECTROSCOPY	10
V	CONCLUSIONS	12
	REFERENCES	14
	APPENDIX A	16
	APPENDIX B	47

SECTION I

INTRODUCTION

Dramatic changes have occurred in the last ten years in the supply and demand of the world's petroleum. These changes as well as those anticipated in the future have a significant impact on the combustion-engine technology for at least three reasons. First of all, fuel derived from high-grade petroleum resources will become more and more scarce while fuels which are obtained from low-grade, non-petroleum resources will become more common place. Secondly, the increasing cost of petroleum derived fuel and the high cost of fuel refined from low-grade resources will make a high combustion efficiency paramount in the design of new engines. Thirdly, our concern for the impact of the combustion products on the environment will place additional constraints on combustion designs.

One of the main obstacles to maintaining low pollution levels and high combustion efficiencies while burning non-traditional fuels is the lack of precise knowledge about the combustion process in practical combustors. The effects of this circumstance are to increase the time needed to design new combustors or to re-design old ones. Thus, there is a need to improve the combustion technology base that will be used in designing future combustion systems. This scenario impacts probably every aspect of military and civilian transportation.

One of the main impediments to understanding the combustion processes in a practical combustor has been the inability to make precise and reliable measurements in all combustion environments. These measurements are essential to the combustor modelling activities which strive to provide improved design prediction methods. Although hard probe techniques are available such as those using thermo-couples and gas sampling techniques, these devices are not very satisfactory in many complex combustion environments. These hard probes often perturb and interact with the environment in an irreversible way. Furthermore, in order to obtain the final

result many corrections must be applied which may not be well-known for unfamiliar environments. Therefore, the need for improved combustion diagnostic capabilities is clear. The Air Force recognized this need when in 1974 it contracted to modify an existing Laser Raman Scattering (LARS) system ⁽¹⁾ for use in combustion diagnostics.⁽²⁾ Although the results of that program were positive, they were not conclusive. Therefore, in 1976 the Air Force contracted with the University of Dayton to continue the work in this area. The two main tasks of this new program were to make definitive measurements with an improved version of the LARS system for comparison with standard hard probe measurements, and to perform extensive modifications of the LARS system to permit it to be used with the experimental combustion tunnel facility being planned by the Air Force Aero Propulsion Laboratory (AFAPL). The work accomplished in performing these two tasks is the subject of this final report.

Two reports have been generated as a result of the work done on this program. ^(3,4) The first report presents the results of the measurements made on the J85-5 turbojet engine using an upgraded version of the original LARS system.⁽³⁾ The second report describes the modified LARS system and the results obtained with it from measurements made with it on the combustion tunnel.⁽⁴⁾ In addition, an Operations and Maintenance Manual has been prepared which describes all aspects of the modified LARS system.⁽⁵⁾ Thus, this report is a review of the work presented in these reports. Complete detail on the work accomplished in the course of this program can be obtained by consulting the individual reports.

SECTION II

THE ORIGINAL LARS SYSTEM

The AVCO-Everett Research Laboratory developed the original LARS system on Air Force Contract No. F33615-71-C-1875 for the purpose of making field measurements of emission in jet engine exhausts.⁽¹⁾ Modifications were then made on the system by Computer Genetics Corporation on Air Force Contract No. F33615-74-C-2023 in order to improve the combustion diagnostic capabilities of the system.⁽²⁾ Many of these modifications were concerned with the computer code that was used to provide for remote operation of the system.

The objective of the University of Dayton program concerning the original LARS System was to upgrade and characterize the system adequately to permit it to be used for measurements in real combustion environments. Virtually every aspect of the LARS system was modified in some way to achieve this goal. The following is a partial listing of these modifications:

- The laser beam optics were changed to give a significantly smaller sample volume.
- The receiving optics were realigned and peaked up.
- The shape and size of the sample volume was experimentally measured.
- The tracking and precision of the spectrometer was greatly improved, especially when used in a high vibration environment.
- Reproducible and reliable alignment procedures were established.
- The laser emission spectrum was measured and means were provided to include the spectrum in the calculations.
- Procedures for determining the spectral instrument function of the system were set up and used.

- The procedures for adjusting the electronic detection instruments and adjusting the photo-multiplier tube voltage were established.
- Linear performance of the signal detection system was confirmed.
- Modifications of the computer code and the spectrometer electronic control unit were carried out in order that any available wavelength step size could be requested by the operator.
- Closed-loop control of the spectrometer wavelength was accomplished by adding an optical encoder to the spectrometer.
- Extensive changes were made in the computer code to facilitate the data handling and remote control activities of the computer.
- A computer-independent, chart-recorder readout capability was provided which greatly facilitated system alignment and performance checks.

In addition to the changes in the hardware and software identified above, completely new data handling and analysis procedures were set up and used which permitted precise Raman temperatures to be obtained. A description of the upgraded original LARS system and the analysis procedures used to obtain Raman temperatures was presented in the report presented by Roquemore and Yaney.⁽³⁾ The portion of that report due to Yaney which is concerned with the performance of the upgraded system and the analysis of the Raman data along with the results of the Raman measurements is presented in Appendix A. The work described in this report was concerned with the measurements made on the combustion plume of an afterburning J85-5 turbojet engine. In addition to these measurements, a measurement effort was made at the ramjet facility of AFAPL. This measurement effort which preceded the J85 work was brief and plagued by numerous difficulties. For

this reason no detailed record is presented here. The temperatures obtained were essentially low by about 200 to 400 °K due to the mismatch between the sample volume being probed by the LARS system and the size of the ramjet combustion zone. Although these measurements were quantitatively unacceptable the net result of that experience was positive. Namely, that measurements in that extremely high acoustic-noise environment can be accomplished with a Raman system.

One of the primary objectives of the J85 studies was to show that not only could viable temperature measurements be made in a practical combustor but that these measurements also would be consistent with those obtained from standard hard probe measurements. Both thermocouple and gas-sampling probe measurements were made during the J85 studies. The measured region was chosen to be compatible with the physical characteristics of these probes. Two types of measurement programs were carried out. One involved simultaneous Raman and gas-sampling probe measurements, and the other involved sequential Raman, gas-sampling, and thermocouple probe measurements. The success of these measurement efforts is summarized in Figures 1 and 2. Figure 1 shows the simultaneous measurements for fourteen separate runs. The agreement is excellent and the data falls well within the 4.5% deviation lines. The two points which do show some deviation were entirely due to an insufficient number of measurements of the background signal level during the Raman scan and are discussed in some detail in Section 5.2.2 in Appendix A. In Figure 2, the four different measurement efforts are summarized. Clearly, the agreement is well within uncertainties and fully vindicates the decision to use Raman spectroscopy as a non-intrusive optical probe for temperature measurements. We note that during this measurement program, one thermocouple element broke and a second was bent following a run sequence. The latter event is the suspected cause of the downward trend of the curve in Figure 2.

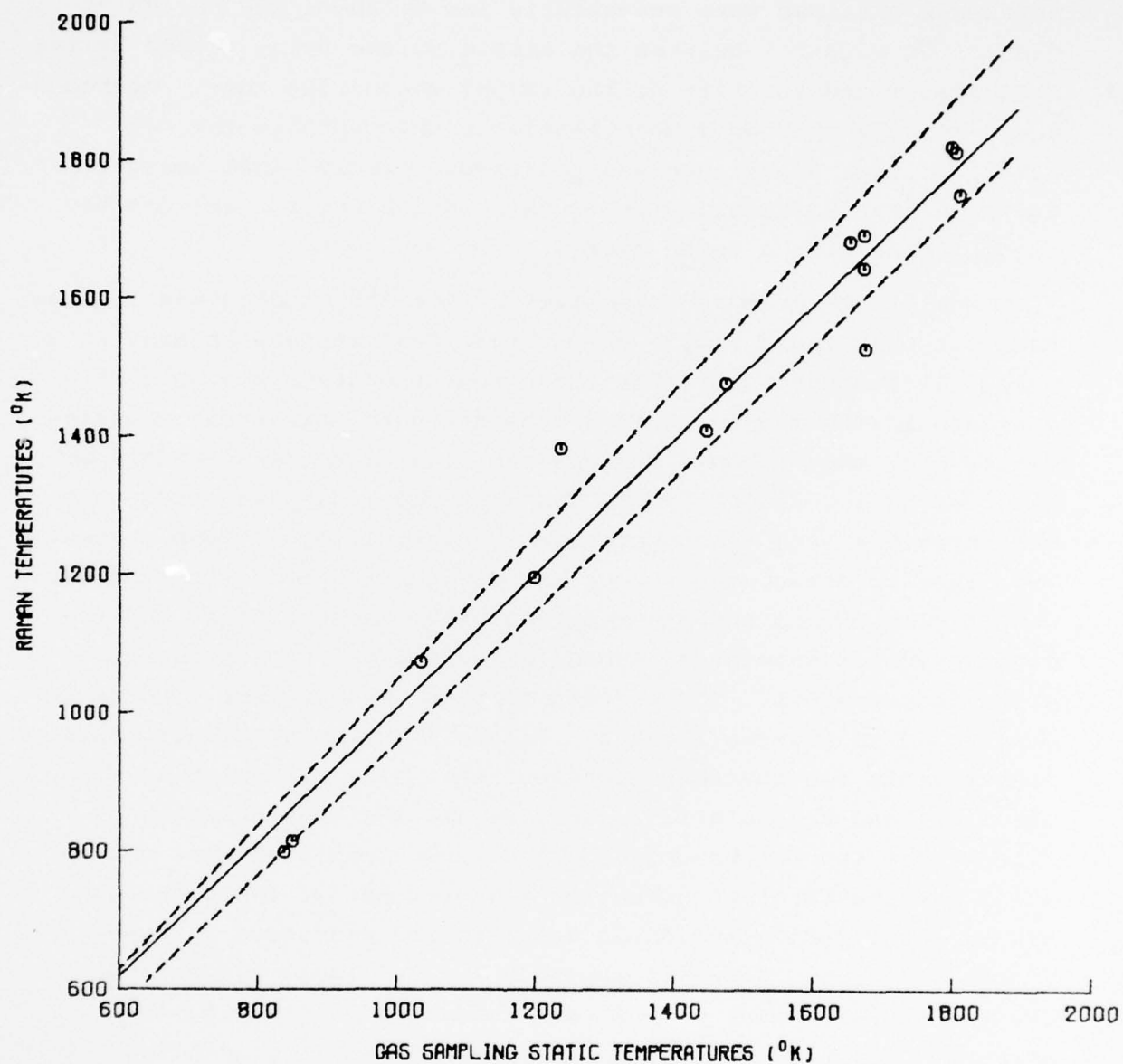


Figure 1. Comparison of Static Temperatures Obtained from Simultaneous Raman and Gas Sampling Measurements Carried Out During the July 1977 tests. The solid line is the linear curve fit to the points. The dashed lines identify the 4.5 percent deviation from the unity slope line and encompass 86 percent of the data.

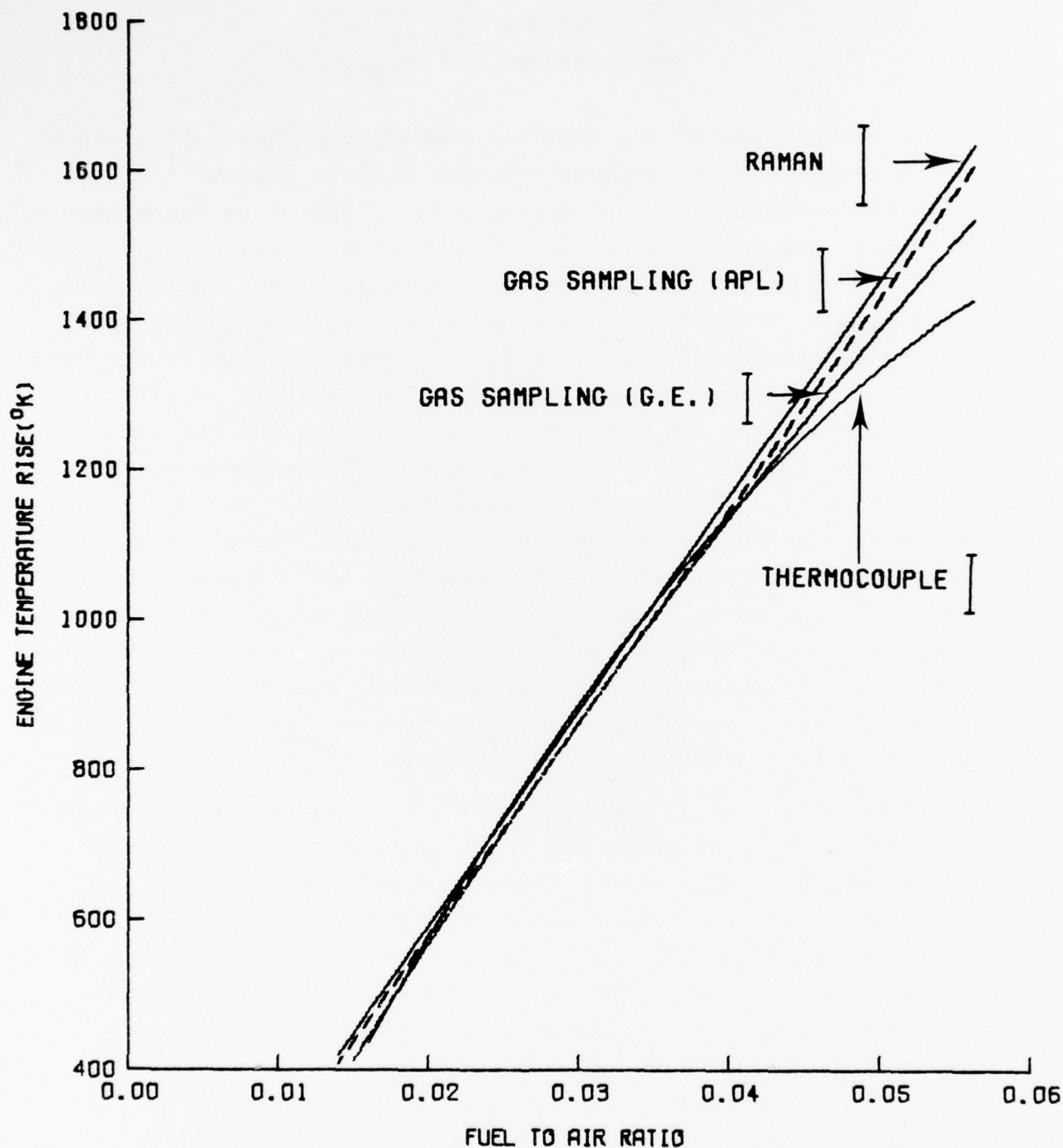


Figure 2. Regression Analyses of the Raman, Gas Sampling, and Thermocouple Data. All valid data were used, viz., 26 points of Raman data, 117 points of gas sampling data reported here (APL), 25 points of General Electric (GE) gas sampling data, and 55 points of thermocouple data. The error bar given with each curve is the standard deviation of the data from the fitted curve.

SECTION III

THE MODIFIED LARS SYSTEM

A description of the modified LARS system including a report on its performance is presented in the Interim Report⁽⁴⁾ which is included herein as Appendix B. Temperature measurements were performed using the system on a pre-mixed flame from a capillary burner and on a turbulent diffusion flame in the AFAPL combustion tunnel. The results of these measurements are also given and discussed in Appendix B. The performance of the system in all of these measurements was fully satisfactory in all aspects, including the optical, the electronic, and the mechanical facets, as well as in the performance of the computer software, and fully validated the design philosophy. This philosophy was subject to the constraints of the program. These constraints included the requirement that the modified LARS system use essentially all the major components of the original LARS system. The objective was to optimize the use, as well as the performance, of these existing components in the "modified" configuration. There was no option to evaluate the all-important choice of laser or other similar considerations in the design of the system.

The combustion tunnel was operated over a wide range of air and fuel flows. The flame was characterized by a highly turbulent, unsteady appearance, often orange-yellow in color, and which produced a high laser-induced fluorescence background in the Raman measurements. Out of about 70 sets of Raman data, 48 sets were analyzed and presented in Appendix B. Temperature measurements were accomplished by two measurement techniques. One technique, called the computer-fit method,⁽⁶⁾ was the same method used in analyzing the J85 data and is described in Appendix A. The second technique, called the N-wavelength method, was developed and used extensively in the combustion tunnel runs. This method is described in detail in Appendix B. Briefly, this method uses the fact that the ratio of the first hot band intensity to the intensity of the main peak is a linear

function of the temperature. These intensities are measured on the Q-branch of the Stokes spectrum of the nitrogen Raman band and they depend on an exact knowledge of the spectral pass band of the spectrometer-laser combination being used. Even though the measurements were plagued by high-fluorescence background levels, even to the point of obscuring the Raman signal in some cases, successful measurements of temperature were accomplished. These measurements were of the time-averaged variety requiring anywhere from about 3 to as much as 15 minutes to accomplish. The precision of these measurements generally became poor as the background level increased; however, nearly one-half of the measurements analyzed gave an average Poisson standard deviation of about 4%. Additional specific information is given in Appendix B.

SECTION IV

COMPUTER STUDIES OF TEMPERATURE MEASUREMENTS USING RAMAN SPECTROSCOPY

In the course of this work a number of problems were encountered which were solved by computer analysis. Two of these problems are of particular interest and deserve to be described here. The first of these problems centered around the difficulty brought about by the vibration of the spectrometer induced by the J85 turbojet engine. This problem is discussed in some detail in Section 5.2.4 in Appendix A. The problem was resolved into two questions. The first question concerned the relationship between the fitted temperature and the two parameters which were used to determine the slit function.⁽⁷⁾ The second question was concerned with the choices made for the slit parameters in analyzing the J85 Raman data.^(8, 9) The resolution to these two questions is presented in Section 3.3.3.3 of Appendix A. Basically the fitted temperature is a sensitive function of the slit parameters, and the vibration of the spectrometer during the J85 measurements would have introduced an error of about 20 °K upward if corrections had not been applied.

The second study was performed by Hemmer and Yaney⁽¹⁰⁾ and was concerned with the effect of time averaged temperature measurements on an environment in which a significant temperature distribution exists. A simulated composite spectrum was generated by a Gaussian (i.e., symmetric) distribution of temperatures. The apparent temperature due to a time-averaged measurement on the distribution was obtained by fitting a theoretical spectrum to the composite spectrum. In the range of 1000 to 3000 °K, the errors in the apparent temperature obtained from the simulated time-averaged measurements were less than 1% relative to the true mean temperatures of the assumed distributions. This was calculated for a standard deviation in the temperature distributions of 200 °K. With a mean temperature of 2000 °K, a 400 °K standard deviation introduced an error of less than 2% (downward).

Two facts must be considered in evaluating these results. In the temperature range of these calculations and for the chosen slit function, the ratio of the first hot-band intensity to the main peak of the nitrogen Raman spectrum used in these calculations is nearly a linear function of temperature. Thus, as long as the temperature distribution lies within the linear range, the temperature obtained from the composite spectrum is very close to the mean temperature of the distribution. These temperatures would be expected to deviate noticeably when the mean temperature is close to or outside the linear range. This would be particularly true for temperatures below about 1000° K where the first hot-band intensity drops to very low levels.

The second feature of these calculations is that they were carried out assuming essentially constant density (i.e., constant volume) conditions. To be more applicable to the combustors of interest, constant pressure conditions need to be studied wherein the density varies inversely with temperature. This will change the intensity weighting of the individual spectra which make up the composite spectrum. The result will be to introduce a non-linearity in the calculation which will probably increase the difference between the mean temperature and the fitted temperature of the composite spectrum. Clearly, the size of this increase will depend on the shape and width of the distribution chosen.

Although a final assessment of time-averaged temperature measurements using the Raman Stokes spectrum must await additional studies, in particular of temperatures below 1,000° K and of constant pressure conditions, the results reported here strongly suggest that viable temperature measurements can be obtained in combustion environments that can be characterized by well-defined temperature distributions.

SECTION V

CONCLUSIONS

The primary result of the work performed in this program is that reasonably accurate quantitative temperature measurements can be made in real combustion environments using spontaneous Raman scattering. In the course of this work, not only were methods developed to obtain precise temperatures from measurements made on Stokes Raman band of N_2 , but also these temperatures were shown to be in agreement with the temperatures obtained using standard probes. The essential thrust of this work is that such measurements are possible per se in situations where time-averaged measurements are viable. It was suggested that a time-averaged measurement is meaningful in the case where there is a well-defined distribution of temperatures.

The main limitation to these measurements was the nature of the background signal. Fluorescence background levels can be reduced by the use of a pulsed laser with gated direction (11,12) as was used in our work. Furthermore, considerable control over this background also can be exercised by the choice of laser wavelength which was not possible in this work. An example of the importance of this choice is seen in the fact that the fluorescence emission bands of six different liquid fuels all have their peaks at 3250 Å with the emission lower about two orders of magnitude above 4500 Å in all cases. (13) The choice of laser in our work was constrained to the nitrogen laser having a 3371-Å output. Thus, the fluorescence background was probably excited with high efficiency in our studies due to the short wavelength of the laser. There was no evidence that laser-induced soot incandescence contributed to the observed background signal.

However, high background levels, as such, were not the limiting factor in these measurements. If, when the background level was high, either the fractional concentration of the

nitrogen probe molecule in the sample volume was very low or the temporal fluctuations (e.g., due to turbulence) in the background were high, or both, then a meaningful measurement was not possible. Basically, the concentration must be high enough and the fluctuations small enough to permit an unambiguous detection of the first hot band in the Raman spectrum of the nitrogen molecule. In principle, if this band is detectable, then a temperature measurement is possible using this technique. In the two circumstances mentioned in which a temperature measurement was not possible using this technique, there is also a genuine need for clarification of what constitute meaningful temperature measurements regardless of whether they are time-averaged or instantaneous.

A significant feature of this work compared to many other optical techniques is the demonstration of accurate temperature measurements on a combustion zone probed optically on only one side and from a relatively remote position (viz., about three meters).

More detailed conclusions are given in the two appendices. In addition, a list of recommendations concerning the LARS measurements on the combustion tunnel are presented in Appendix B.

REFERENCES

1. D.A. Leonard, Field Tests of a Laser Raman Measurement System for Aircraft Engine Exhaust Emissions, Final Technical Report No. AFAPL-TR-74-100 (AVCO Everett Research Laboratory, Inc., Everett, Mass., October, 1974).
2. D.A. Leonard and B. Caputo, Development of a Raman System as a Combustion Diagnostic Tool, Final Technical Report AFAPL-TR-75-99 (Computer Genetics Corp., Wakefield, Mass., October, 1975); Interim Report, Task 19, Wright-Patterson Senior Investigator Program (Purdue University, West Lafayette, Ind., March 19, 1976).
3. W.M. Roquemore and P.P. Yaney, "Comparison of Thermo-couple, Gas-Sampling, and Raman Measured Temperatures in an Afterburning Turbojet Engine Plume," in the Proceedings of the 10th Materials Research Symposium on Characterization of High Temperature Vapors and Gases, J. W. Hastie, editor (National Bureau of Standards, September 18-22, 1978, Gaithersburg, Maryland, 1979, in press). Excerpts of this paper are given in Appendix A.
4. P.P. Yaney, Combustion Diagnostics Using a Pulsed-Laser Raman Spectroscopy System, Interim Report. This report is presented herein as Appendix B.
5. P.P. Yaney, R.J. Becker, P.R. Hemmer, and T.H. Hemmer, LARS Operations and Maintenance Manual, Volumes I, II, and III. (University of Dayton, 1979, unpublished).
6. P.R. Hemmer, P.P. Yaney, and W.M. Roquemore, "Computer Fits of Calculated Raman spectra of N_2 to observed spectra," Bull. Am. Phys. Soc. 22, 1039 (1977).
7. T.H. Hemmer, P.P. Yaney, and P.R. Hemmer, "Effect of Variations in Instrument Function on the Temperature Calculated from the Raman Spectrum of N_2 ," Bull. Am. Phys. Soc. 23, 162 (1978).
8. J. Ay, W.M. Roquemore, P.P. Yaney, and P.R. Hemmer, "Raman Measurements in the J85-5 Afterburning Turbojet Engine Plume," The Winter Annual Meeting of the American Society of Mechanical Engineers, Atlanta, Georgia, November 27-December 2, 1977, postdeadline paper, Session 4A. Presented by P.P. Yaney.

REFERENCES (cont'd)

9. P.P. Yaney, P.R. Hemmer, T.H. Hemmer, and W.M. Roquemore, "Determination of Temperatures in the Combustion Zone of a J85-5 Jet Engine Using the Laser-excited Vibrational-rotational Raman Spectrum of Nitrogen," in Thirty-Third Annual Molecular Spectroscopy Symposium (Ohio State University, June 12-16, 1976).
10. T.H. Hemmer and P.P. Yaney, "Computer Study of Time-Averaged Temperature Measurements on Combustion Temperatures Obtained from Raman Spectra of N₂," Bull. Am. Phys. Soc. (to be published, 1979).
11. P.P. Yaney, "Reduction of Fluorescence Background in Raman Spectra by the Pulsed Raman Techniques," J. Opt. Soc. Am. 62, 1297 (1972).
12. P.P. Yaney, "The Pulsed Laser and Gated Detection in Raman Spectroscopy--A Survey of the Spectra of Common Substances Including Studies of Absorbed Benzene," J. Raman Spectry. 5, 219 (1976).
13. W.M. Roquemore and F.N. Hodgson, "Fluorescence of Hydrocarbons in Jet Engine Exhaust," in the Proceedings of the International Conference on Environmental Sensing and Assessment (Institute of Electrical and Electronics Engineers, 1976).

APPENDIX A

RAMAN MEASURED TEMPERATURES IN AN AFTERBURNING
TURBOJET ENGINE PLUME

Excerpts of

"Comparison of Thermocouple, Gas Sampling, and
Raman Measured Temperatures in an Afterburning
Turbojet Engine Plume"

by

W.M. Roquemore and P.P. Yaney

in the

Proceedings of the 10th Materials Research
Symposium on Characterization of High
Temperature Vapors and Gases,

J.W. Hastie, editor (National Bureau of Standards,
Gaithersburg, Md., 1979, in press).

COMPARISON OF THERMOCOUPLE, GAS SAMPLING, AND RAMAN MEASURED
TEMPERATURES IN AN AFTERBURNING TURBOJET ENGINE PLUME

W. M. Roquemore
Air Force Aero Propulsion Laboratory
Wright-Patterson AFB, OH 45433

and
Perry Pappas Yaney¹
Department of Physics
University of Dayton
Dayton, OH 45469

This paper describes the results of plume temperature measurements made with three different probes: a Pt 13% RhPt thermocouple probe, a gas sampling probe, and a spontaneous-Raman-scattering optical probe. Measurements were made on the centerline of the chemically reactive plume of an afterburning J855 turbojet engine, about one meter from the nozzle exit. The engine was operated at 12 different fuel-air ratios ranging from 0.0094 to 0.0517. Thermocouple measurements were corrected for radiation and recovery. A combination gas-sampling-and-pressure probe was used to measure carbon dioxide, carbon monoxide and total hydrocarbon concentrations, and total gas stream pressures. Temperatures were calculated from the concentration measurements. Raman scattering measurements were made in a near-backscattering geometry using a pulsed nitrogen gas laser (3371 Å), a computer-controlled SPEX double spectrometer, and an 8850 RCA photomultiplier tube with EGG/ORTEC time-gated current-integration detection apparatus. Raman temperatures were determined by fitting calculated spectra to the experimental spectra of the nitrogen gas in the plume. Simultaneous Raman and gas sampling measurements made at nearly the same axial location in the plume were compared. An observed correlation between engine fuel-air ratio and temperature, was also used to compare the

¹Work reported here was performed through the auspices of the Research Institute of the University of Dayton.

three techniques. The temperatures measured by the Raman, gas-sampling, and thermocouple techniques were in agreement within the experimental error of about 5 percent except at maximum engine power where the thermocouple deviated by about 10 percent.

3.3 Raman scattering

Light scattering is the analysis of the intensity, polarization, and spectral content of the light collected from a well-defined region of a medium which is illuminated by an intense, monochromatic light source of known characteristics. Raman scattering is concerned specifically with that portion of the scattered light which is spectrally shifted (i.e., in wavelength) from the wavelength of the incident light due to the molecular oscillations of the medium. The use of Raman scattering as an optical diagnostic probe for temperature measurement spans three areas of overlapping endeavor. These are (1) the theoretical analysis of the basis for the measurement, (2) the design and operation of the experimental apparatus, and (3) the analysis of the data. The approaches taken in this work in these three areas are the subjects of this section. In Section 3.3.1, the apparatus used to make the measurements and the features important to its operation are described. A brief outline of spontaneous Raman scattering theory is given in Section 3.3.2 with the application of this theory to the calculation of temperature covered in Section 3.3.3.

3.3.1 Description of the Raman system

The Raman system used in this work was a modified version of the system described by Leonard [8]. It consisted of two separated subsystems. One subsystem was the optical transceiver unit which was located in the test cell with the engine. The other subsystem consisted of the signal-handling electronics, a Data General Nova 1220 minicomputer, and various power supplies. Two of the important features of these subsystems are: (1) the size and shape of the scattering volume referred to as the scattering "geometry," and (2) the electronic signal detection scheme. These features as well as the subsystems are described in the following sections.

3.3.1.1 The transceiver

The transceiver and its position relative to the engine is illustrated in figure 3. The transceiver components were mounted on a custom-made, aluminum pallet with dimensions of 2.9 m by 1.4 m. The laser was an AVCO model C5000 pulsed, nitrogen-gas laser with emission at 3371 Å. It was operated at 250 pps with about 100 mW average power. Its beam pattern consisted of a complex array of parallel "lines" of light in the far field having an overall measured half-angle divergence of approximately 1.2 mr by 10.4 mr. The beam at the laser (near field) consisted primarily of two very narrow, bright lines of light separated by 3.2 mm and 50 mm in length. The beam was directed and focused by means of a lens, a 135-cm-focal length, 45-cm-diameter spherical concave mirror, and five large, flat, beamfolding mirrors. The mirrors were adjusted to focus the two lines of light into a single line. Since the pulse length was about 10 ns, the pulse energy was 400 μ J, and with a peak power of about 40 kW, the peak intensity at focus was about 0.6 MW/cm². The laser beam was monitored by a ITT type F4000 high-current, biplanar, vacuum photodiode with S5 cathode response. The signal from this photodiode was used to monitor the laser power and to provide trigger signals for the electronics.

The receiver portion of the transceiver used a model 117 40-cm-diameter Cassegrain telescope supplied by Group 128, Inc. as the collecting optic. This telescope had a primary focal ratio of f/3 with an overall ratio of f/11. It was set up to give near unity magnification with the laser-illuminated volume at about three meters from the telescope. The light from the telescope was focused on the entrance slit of a SPEX model 1402 double spectrometer. The detector was an RCA 8850 photomultiplier tube (PMT) connected for fast-pulse detection.

3.3.1.2 Scattering geometry

The transceiver was positioned so that the axis of the collecting telescope was approximately horizontal and intersected the axis of the engine. The laser beam was directed from below the telescope up through the engine axis so that the long dimension of the beam was coincident with the vertical plane containing the telescope axis. This

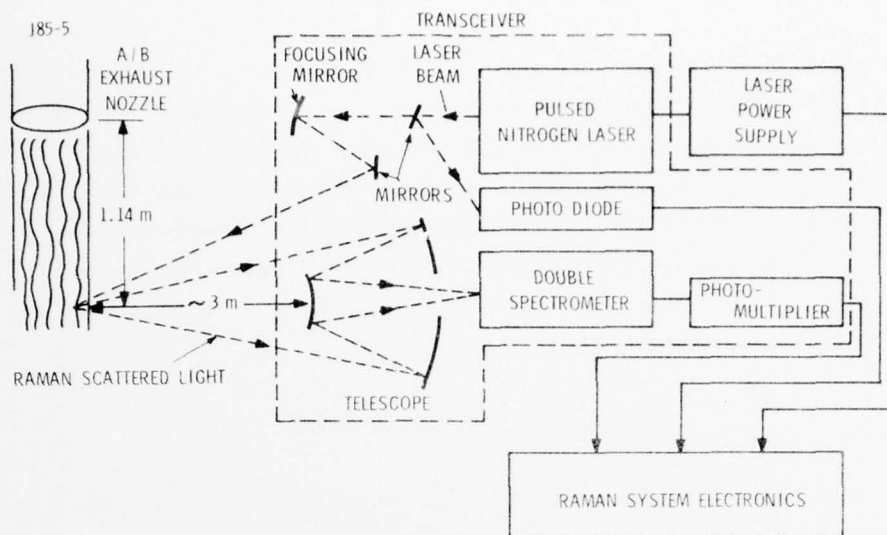


Figure 3. Raman transceiver subsystem with a schematic of the optical arrangement.

arrangement not only placed the long dimension of the laser beam parallel to the spectrometer slit, but it also allowed the transceiver to be placed at a safe distance from the combustion plume; however, it created a rather large, odd-shaped scattering volume from which the Raman signal was gathered. Because of the large divergence of the long dimension of the laser beam, the focused beam was originally almost 50 mm long. By replacing the final, 30-cm-long, beam-directing, flat mirror with a segmented mirror consisting of three 10-cm-long, flat mirrors each adjusted to project its beam segment onto a common line; the focused beam was reduced to a length of about 23 mm. The scattering volume as viewed from the engine nozzle is illustrated in figure 4. The "thickness" of this volume was determined by the width of the laser beam which was about 0.3 mm at the engine axis.

The scattering geometry was nearly "backscattering" with an angle between the beam direction the direction of the collected light along the telescope axis of 155° . A disadvantage of this near-backscattering geometry was that signals from across the whole diameter of the combustion plume could be detected as indicated in figure 4. The effective "depth-of-focus" of this geometry was determined by translating an ordinary microscope slide along the axis of the telescope and measuring the fluorescence signal from the slide due to the laser beam. These measurements are plotted in figure 5 along with the total temperature profile reported by General Electric for this same type engine [3] at the 1.14 m position from the nozzle of the afterburner. These graphs indicate that about 90 percent of the observed Raman signals came from within the constant temperature portion of the plume. This fact was the deciding factor in the choice of this axial station for the measurements. The remaining 10 percent of the observed signal which may have included the cooler portions of the plume could have biased our temperature measurements low by as much as 1 percent. However, since it was not possible to account for this error in any detailed manner, it had to be neglected.

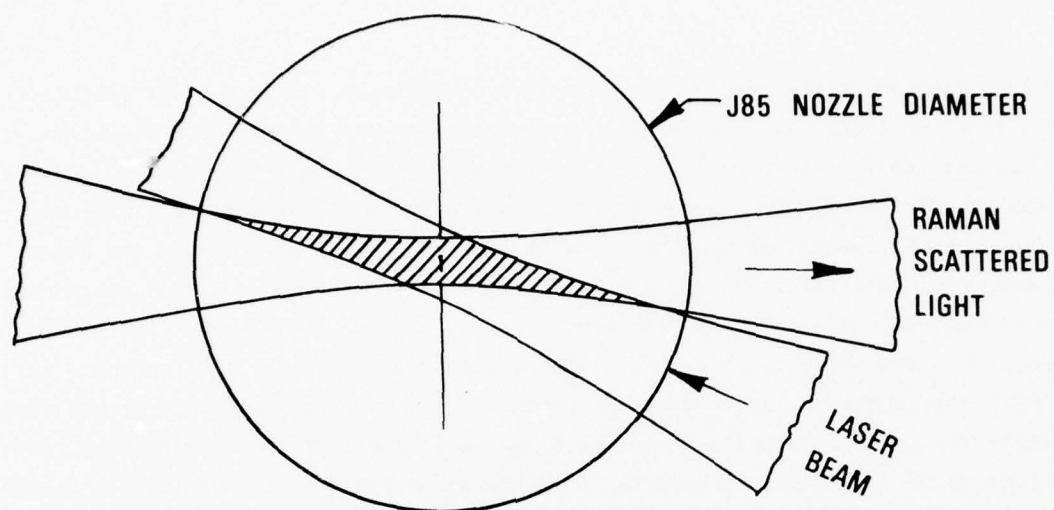


Figure 4. Scattering geometry as viewed along the axis and from the exit nozzle of the engine.

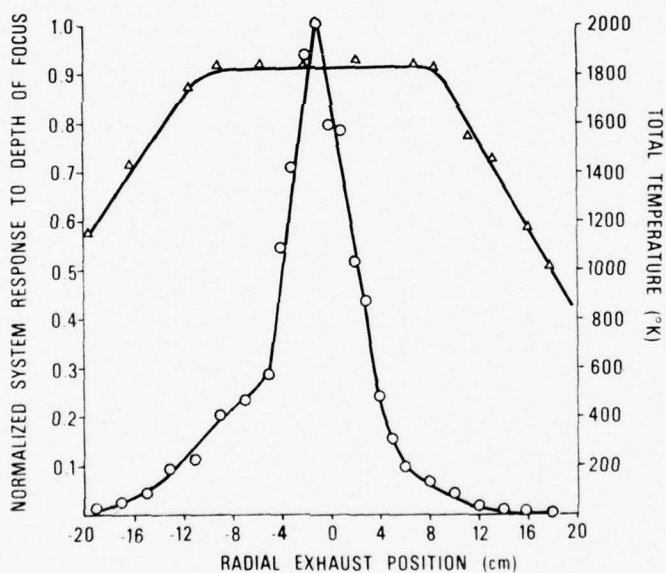


Figure 5. Measured radial response of the Raman transceiver (circles, left axis) compared to the radial temperature profile (triangles, right axis) reported by Lyon, et al. [3] 1.14 m from the plane of the exit nozzle.

3.3.1.3 The electronics

A block diagram of the electronics subsystem is given in figure 6. The subsystem was separated from the transceiver by about 15 m of cable and was located in the control room next to the test cell. As shown in figure 6, the system was completely controlled by the Nova computer. Three different signals were recorded for each laser pulse. The data signal from the PMT, which was synchronous with the laser pulse and carried the Raman signal, was recorded first followed by a recording of the laser power signal which came from the photodiode. After 600 μ s from each laser pulse, the signal from the PMT was again sampled to determine the non-laser-induced background signal. This sequence was repeated for the number of laser pulses programmed. The three signals were accumulated in the computer during this signal-acquisition time. At the end of this period, the accumulated background signal was subtracted from the accumulated data signal and the result was divided by the normalized value of the integrated laser power during the period. This net signal as well as the three raw signals were recorded on punched paper tape for subsequent analysis. After this process was completed, the spectrometer was stepped to the next programmed wavelength and the sequence was repeated.

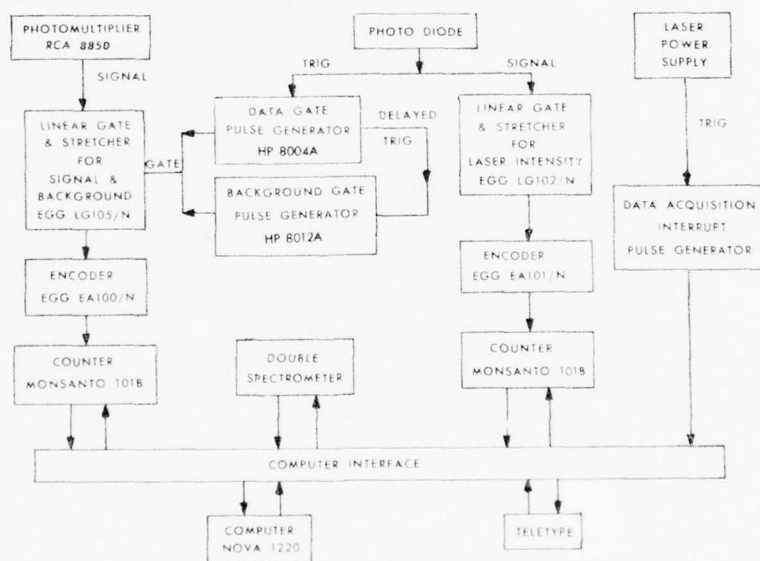


Figure 6. Raman electronics subsystem.

3.3.1.4 Signal detection

Signal detection using a linear-gate-and-stretcher circuit is an analog method (versus pulse counting) in that the pulses from the detector are integrated in real time. The output of this circuit is a relatively long pulse ($\sim 3 \mu$ s) whose amplitude is linearly related to the total electric charge received at the input. Since the anode current in a PMT or a photodiode is proportional to the number of photons incident on the photocathode

per second, integrating the anode pulse gives a signal proportional to the number of photons detected. The pulses from the PMT were about 20 ns in width across their base. A 20 ns gate signal was applied to the linear gate module attached to the PMT, and its time delay was adjusted to be synchronous with the room-air nitrogen (N_2) Raman signal. In a similar manner, a gate signal delayed by 600 μ s was applied to the module in order to sample the non-laser-induced background signal.

This gated current-integrating detection scheme had the advantage of a low duty cycle, namely 5×10^{-6} for our case, which suppressed signals that arose from ambient sources such as room lights, combustion plume radiation, etc. A second advantage came from the discrimination against fluorescence processes which had lifetimes equal to or greater than about 10 ns. Although many of the processes occurring in combustion zones appear to have lifetimes shorter than 10 ns, we have found that there is almost always some fluorescence emission present beyond 10 ns from the laser-pulse peak.

The main disadvantage of this detection technique is that the limit on the dynamic range of signal measurement is set by the linear-gate-and-stretcher module. The module used with the PMT was specified to have a linear range of at least 3 to 100 pico-Coulombs (pC). This required that the voltage applied to the PMT be adjusted so that the maximum anticipated signal did not exceed the 100 pC value. As shown in figure 6, the output of the module was sent to an encoder which produced a burst of 40 MHz pulses. The number of pulses in the burst were proportional to the input pulse amplitude. The counter recorded the number of pulses and sent the value to the computer. Our concern was that the entire signal detection and recording scheme was linear over the largest possible range. Calibration measurements were made with the linear gate, encoder, and counter combination using attenuated test pulses into the linear gate as well as with the complete detection system using attenuating optical (neutral density) filters taken while sitting on a peak of the room-air N_2 Raman line. These measurements showed that the response was linear to within ± 1 percent over a range of at least 50 to one, with signals down by a factor of 100 being usefully detected. This was precisely the range needed in our studies to record the Raman spectrum of N_2 with the engine at "Military" power. At this power, the signal dynamic range was the largest of all the observed spectra due to the very low laser-induced background.

3.3.2 Spontaneous Raman scattering

In the simplest terms, Raman scattering arises from the modulation of an incident electromagnetic wave by the temporal fluctuations of the dielectric constant of the medium being probed. This modulation produces the "side bands" which are electromagnetic emissions that are shifted in frequency in a symmetric manner above and below the frequency of the incident wave as illustrated in figure 7(a). In the case of a simple diatomic gas, the dielectric constant depends on the electric polarizability of its molecules. As a molecule vibrates and rotates, its polarizability oscillates at frequencies which are characteristic of the vibrational and rotational states that can be occupied by that molecule. The

relative intensities of the side bands are determined by the populations of these states which in turn are governed by the rules of quantum mechanics and the temperature of the medium. The scattered light intensity is linearly dependent on the intensity of the incident light and, in general, occurs in all directions from the scattering medium. These features are characteristic of spontaneous scattering. In the two following sections, the Raman scattering from diatomic molecules and the manner in which it depends on temperature are briefly reviewed.

3.3.2.1 The Raman spectrum of a diatomic molecule

The theory of Raman spectra in general as well as of diatomic molecules in particular has been well documented [26,27,28]. Furthermore, the theory has been reviewed a number of times in publications concerned with Raman thermometry [5,6,7,8,11]. Therefore, we will only outline those features of the theory which clarify the rationale and methods used to obtain the Raman temperatures.

As shown in figure 7(a), the Raman emissions shifted to frequencies higher than the incident laser frequency form the anti-Stokes spectrum, while those shifted lower are called the Stokes spectrum. In addition to the Raman spectra, a medium will scatter the incident light without any shift of frequency. This is called Rayleigh scattering; however, in many measurement circumstances, additional unshifted light is scattered by various sizes and types of particles (e.g., soot) in the medium and, as such come under the topic of Mie or Tyndall scattering [29]. To characterize the strength of spontaneous Raman emissions, it is noted that Rayleigh scattering from a pure gas is generally not visible (i.e., a bright beam of light viewed from the side on a dark, clear night cannot be seen). The Raman emissions from N_2 gas are on the order of a thousand times weaker than its Rayleigh scattering. Thus, the need for high-power lasers and sophisticated detection equipment is clearly dictated.

In figure 7(b), a portion of the energy level scheme of a diatomic molecule is schematically represented. The vibrational energy levels labeled with the quantum number v show a decreasing spacing with increasing energy. The quantum mechanical selection rules require that if the vibrational state of the molecule changes, it can only do so if the change in v is by one unit, that is, $\Delta v = \pm 1$. In addition, in any vibrational state a molecule can have rotational energy specified by the quantum number J . The rule governing changes in rotational energy which appear in the Raman spectrum is $\Delta J = 0, \pm 2$. In figure 7(b), only six of the many possible transitions are shown all of which have $\Delta J = 0$. For example, in the transition labeled "0," the molecule is excited into the first vibrational level ($v = 1$) by the incident laser light of frequency L with the Stokes Raman light appearing at "0" in figure 7(a). Thus, with the inclusion of all the permitted lines, it can be seen that the position, density, and spread of the lines in the Raman spectrum is determined by the energy level scheme of the molecule.

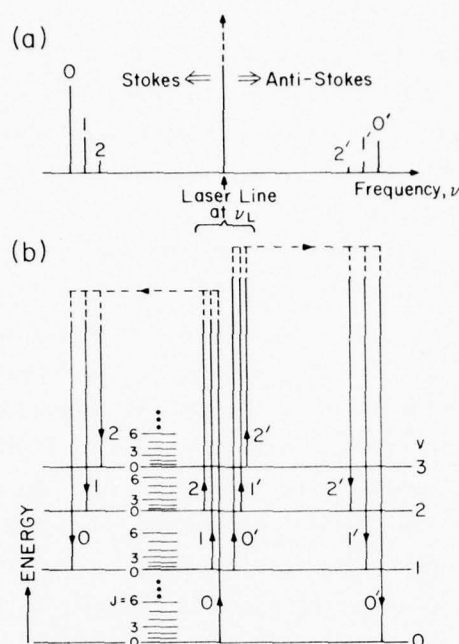


Figure 7. (a) Simplified Raman spectrum. (b) Schematic representation of the energy levels and selected Q branch transitions of a diatomic molecule.

The vibrational-rotational Raman spectrum of a diatomic molecule is divided into three branches of spectra. The group of lines for which $\Delta J = 0$, a small portion of which is shown in figure 7, is called the Q branch. On either side of the Q branch are broad (20 to 40 Å wide) groups of weak lines which result from a change in the rotational energy given by $\Delta J = \pm 2$. The band on the high-frequency side of the Q branch is called the O branch ($\Delta J = -2$) with the remaining band being the S branch ($\Delta J = +2$). Generally, the intensities of these two branches are about two orders of magnitude weaker than the peak of the Q branch [8]. Because of the relatively low intensity of these branches, they are often neglected for high temperature measurement purposes [30,31]; however, since our studies included measurements of temperatures below ~ 900 K, we calculated the contributions of these branches to the Raman spectra.

3.3.2.2 Temperature dependence

Raman scattered light is directly proportional to the concentration of molecules in the observed volume. Because of the unequal spacing of the vibrational energy levels, as illustrated in figure 7(b), the Q branch spectrum is made up of one, two, or more bands or peaks corresponding to the initial energy levels of the transitions responsible for the bands. The relative intensity of a band depends on the fraction of the observed molecules present in the initial level of the band (i.e., the population). This fraction depends on the temperature. As the temperature increases, the population of the higher levels ($v > 0$

in figure 7(b)) increases at the expense of the lowest level ($v = 0$). Thus, the corresponding bands of lines of which two are represented by the single lines labeled "1" and "2" in figure 7(a), will become more intense relative to "band 0." For this reason, these bands are commonly called "hot bands." As a convenience, we shall refer to band "0" as the "main peak" since it is commonly the strongest feature in the Raman spectra of diatomic molecules for temperatures less than 3000 K.

We performed temperature measurements by making use of the fact that the intensity envelope of the Stokes Q branch provides a unique signature for every temperature. Typical Stokes Raman spectra (as a function of wavelength, not frequency) calculated for N_2 gas are given in figure 8. The laser wavelength used for these spectra was 3371 Å. Clearly, as the temperature increases, the intensity of the hot band labeled $v = 1$ relative to the main peak labeled $v = 0$ also increases. A finite spectral width of the laser line plus a wide slit setting of the spectrometer were assumed in order to obtain the trapezoidal slit function shown in the figure. This slit function integrates or smooths out the contributions from the individual Q branch lines described above. It should be noted that these spectra have their peak intensities normalized to unity to provide for a convenient format. In practice there is a decrease in the intensity of the main peak with increasing temperature, not only due to shifts of energy-level populations, but also due to a loss of gas density as given by the gas law.

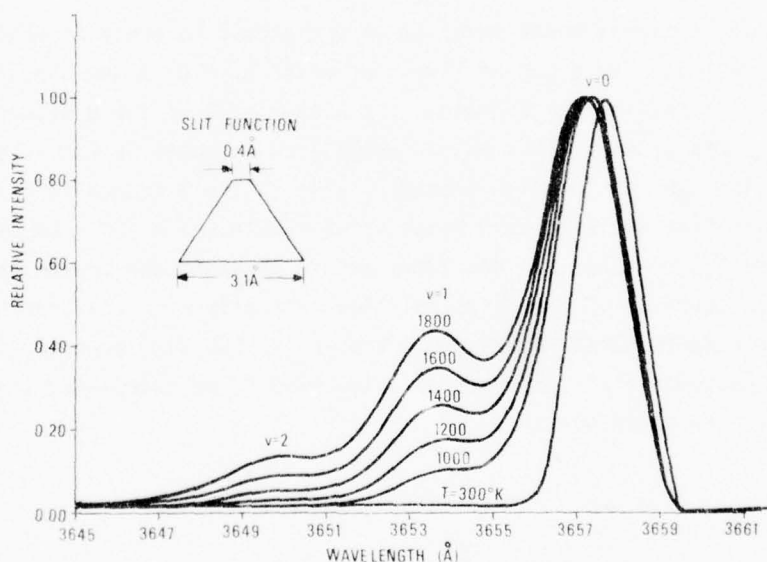


Figure 8. Calculated Stokes Q branch spectra of N_2 on a normalized intensity scale for 3371 Å excitation and a trapezoidal slit function.

A second approach to temperature measurement uses the result that as the higher vibrational levels become occupied with increasing temperature, the anti-Stokes spectrum ($\Delta v = -1$) becomes more intense. Thus, the temperature can be calculated from the ratio of the total anti-Stokes intensity to the total Stokes intensity. However, in the studies reported here, the engine-induced vibration of the spectrometer prevented the use of the first-order gratings needed to record the anti-Stokes spectrum.

In addition to Raman spectra involving both vibrational and rotational transitions, pure rotational Raman can be observed wherein only $\Delta J = \pm 2$ and $\Delta v = 0$. In this case, a very closely spaced array of lines appear on both sides and in the immediate vicinity of the laser line. Although, the pattern and intensity envelope of these groups of lines are temperature dependent, this region is occupied by pure rotational Raman spectra of all molecular gases. It is possible to pick out specific rotational lines for temperature measurement [12] providing that the spectral line width of the laser is sufficiently narrow. In these studies, the line width of the nitrogen laser was about 1.0 Å which is larger than the spacing of the Raman lines in the pure rotational spectrum of N_2 gas. Thus, it was not possible to resolve this spectrum in this work.

3.3.3 Calculation of Raman temperature

The primary fact used in attempting to make remote temperature measurements in a gaseous atmosphere using any particular Raman technique is that the strength, shape, and extent of the Raman spectrum of a gas in equilibrium is unique for any given temperature. This is the case for pure rotational Raman scattering as well as for vibrational-rotational Raman scattering regardless of whether one of the complicated coherent Raman techniques is used or the simple spontaneous Raman technique used in these studies is chosen. Thus, if the spectral shape can be sufficiently resolved or if it can be sampled in such a way as to detect the features which are most temperature sensitive, then a temperature can be deduced.

Regardless of the approach chosen, it is absolutely essential that some means be provided to distinguish between the portion of the observed signal that is due to the desired Raman scattering and that which arises from other effects such as fluorescence, radiation from hot particles (i.e., soot), and other spurious sources. This is probably the single most significant impediment to making accurate measurements using a Raman technique. This is true for both the spontaneous Raman techniques as well as for the coherent Raman techniques such as coherent anti-Stokes Raman scattering (CARS) spectroscopy wherein the onset of additional Raman and other interfering phenomena produce "background" signal levels for which an accounting must be made [32].

The merits of one approach compared to another is not of concern here except that it is suggested that such comparisons deal in "trade-offs." That is, to gain an advantage in one area, a loss of something invariably arises in another area.

The following three sections outline the method of calculating the theoretical Raman spectra, the procedure used to fit the theoretical spectra to the experimental spectra to obtain temperatures, and the method of determining certain important parameters.

3.3.3.1 Calculation of Raman spectra

In the studies presented here, the Stokes vibrational-rotational Raman spectrum of the N_2 gas present in the combustion plume of the engine was scanned and recorded, point by point. The strength of this approach is in the complete theoretical description of the spontaneous Raman scattering of N_2 that is available (see Section 3.3.2.1). That is, we can calculate the spectrum quite accurately for any temperature. The weakness of this approach is that the observed zone must remain in a steady-state for a time period long enough to permit the spectrum to be scanned. In these studies, this period was usually five to eight minutes. Experience with this engine indicated that this time period was sufficiently short to permit the steady-state assumption to be reasonably valid. Thus, the approach used here was to find the temperature for which the calculated spectrum gave the "best fit" to the observed spectrum.

The observed wavelength of a Stokes Raman line, λ_r , due to an incident laser beam of wavelength λ_L can be written as

$$\lambda_r = (\lambda_L^{-1} - \bar{\nu}_r)^{-1} \quad (12)$$

$$\text{with } \bar{\nu}_r = [E(v', J') - E(v, J)]/hc, \quad (13)$$

where $E(v', J')$ and $E(v, J)$ are, respectively, the energies of the final and initial states of the transition (see fig. 7), h is Planck's constant, c is the speed of light, and $\bar{\nu}_r$ is in units of cm^{-1} . The energies are made up of a sum of the vibrational and rotational contributions [26,27,28]. The first and second order terms of the vibrational part plus the first order term of the rotational energy were found to give sufficient accuracy ($\sim 0.02 \text{ \AA}$) for these calculations.

The Raman scattering efficiency, ϵ , can be defined as the observed photoelectron count rate, N_R , divided by the incident laser power, P , (photons/s). For a given scattering geometry and a scattering molecule in a state given by J and v , the efficiency becomes

$$\epsilon \equiv N_R/P \propto n \eta'(\lambda_r) S_{JJ'}(v+1)\lambda_r^{-4}, \quad (14)$$

where J' is the final rotational state quantum number, n is the population of molecules in the state given by v and J , $\eta'(\lambda_r)$ is the quantum efficiency of the detection system at λ_r , and $S_{JJ'}$ is the rotational strength factor [26]. The strength factor is a function of J and it derives from three expressions, one each for the 0 branch, ($\Delta J = -2$), the Q branch, ($\Delta J = 0$), and the S branch, ($\Delta J = +2$). For a simple homonuclear, diatomic molecule, these expressions depend only on the polarizations of the incident and scattered light and on the nuclear spin. These expressions and their use are given in references [26,27,28].

Assuming that the observed medium is in thermal equilibrium, the molecular population n in the initial level of a transition is related to the concentration of the molecular species, n_0 , being probed through a Boltzmann factor. We have

$$n \propto n_0 (2J+1) \exp[-1.43879E(v,J)/T], \quad (15)$$

where $E(v, J)$ is the energy of the level in cm^{-1} measured relative to the $v = 0, J = 0$ level, and T is the absolute temperature in K. By accounting for various characteristics of the experimental setup, the intensity profile of a Raman spectrum was calculated for a specific temperature using eqs. (14) and (15) and compared to the observed spectrum. An iterative procedure was used to find the best match-up between the observed and calculated spectra thereby providing the temperature.

3.3.3.2 Computer fitting procedure

The technique used to determine the "best fit" is the method of non-linear least squares and comes under the general name of multiple regression analysis. The measure of goodness of fit used is the quantity chi-square given by

$$\chi^2 = \sum_{i=1}^N [y_i - y(\lambda_i)]^2 / \sigma_i^2, \quad (16)$$

where σ_i^2 are the variances in the observed data values y_i , $y(\lambda_i)$ are the calculated values of the Raman spectrum at the wavelengths λ_i , and N is the number of spectral positions recorded. In general, the observed spectrum depends on a set of parameters any subset of which can become free variables in any particular sequence of measurements. For the measurements reported here, the free parameters were temperature, the background signal level and slope, and the wavelength correction. A computer program was developed which minimized χ^2 with respect to the chosen set of parameters by an iterative search process. All that was required was that a set of reasonable starting values be provided. The program determined the best fit and generated standard errors for each fitted parameter. These errors were derived from calculations that effectively characterized the size and shape of the minimum in the hyper-surface that was defined by the functional dependence of χ^2 on the free parameters. Hence, the errors in effect specify how well-defined the minimum was with respect to the corresponding parameter.

One of the more interesting problems that arose in the search for an efficient least-squares fitting computer routine [34] was that certain parameters when made free showed a high degree of correlation. For example, the correlation coefficient between the laser-induced background and the temperature was typically between 0.4 and 0.7. Some fitting routines were found to be unable to find the best fit with such correlations. The program used in this work was derived from the program CURFIT [33]. Its speed and accuracy in handling correlated parameters when used with a CDC 6600 computer has been satisfactory to date.

The digital data values recorded during a measurement were on an arbitrary scale set by the apparatus as described in Section 3.3.1.4. In order, to make the calculations of χ^2 and

the parameter errors numerically correct, it was necessary to determine the average number of observed counts per photoelectron. Weak processes such as light scattering follow Poisson statistics [33], wherein the variance of the count value is equal to the count value. It was found for the PMT voltages used, about 250 counts corresponded to one photoelectron. Since the dynamic range of our detection apparatus was about 1250 observed counts per laser pulse, we observed up to five photoelectrons from each laser pulse. If the combined efficiency of the optics, spectrometer, and PMT was 10 percent, then this amounts to a maximum of 50 scattered photons per laser pulse.

The spectrum calculations and the computer fits were performed on the photoelectron values of the data. This insured that the variances in eq. (16) were statistically related to the data values. Since the variances weight the individual observed calculated differences in eq. (16), their values determine the magnitude of χ^2 which, in turn, fixes the magnitudes of the parameter errors. The value of χ^2 reflects both the degree of agreement between the functional forms of the calculated and observed spectra and the amount of fluctuation or noise in the data. A useful quantity is the reduced chi-square, χ_r^2 , which is χ^2 divided by the number of degrees of freedom (N minus the number of free parameters). The ideal value for χ_r^2 is 1.0; however, in practice, values < 1.5 are acceptable [33]. Except for (1) the low temperature (<1000 K) spectra where the approximations in the slit function were visible in the fit, and (2) the spectra having high, and therefore noisy, backgrounds, the χ_r^2 values obtained satisfied this criterion. With one exception, the χ_r^2 values for all the Raman fits reported here were <2.0.

3.3.3.3 Determination of fixed parameters

In order to perform the computer fit described in the previous section, it was necessary to computationally duplicate the integrating effect of the wide spectrometer slits used plus the ~ 1 Å width of the incident laser light on the dense line spectrum described in Section 3.3.2. This was done by determining the effective overall slit function. This function had to be known in order that the theoretical spectrum determined for a minimum χ_r^2 was calculated under conditions that had a one-to-one correspondence to the conditions under which the experimental spectrum was obtained.

There are several approaches to determining the slit function; however, because of its large width relative to the spacing of the individual lines in the N_2 Raman spectrum, it was possible to greatly simplify the required calculations by approximating the effective slit function as a trapezoid such as shown in figure 8 where the top and bottom dimensions were determined operationally. This was accomplished by fitting the parameters of the trapezoidal slit function to the Raman spectrum of N_2 in room-temperature air using the same slit settings that were used with the engine measurements. The N_2 Raman transitions at room temperature ranges up to $J=15$ to 20 in the Q branch which spans a range of less than 0.1 Å with 3371 Å excitation. Thus, the observed shape of the room-temperature Raman Q branch "line" is, in effect, the effective slit function.

The spectrometer was operated in third order with entrance/middle/exit slit dimensions of 1.0 mm/1.5 mm/1.0 mm. The trapezoidal slit function fitted to the room temperature data had a slit-bottom half width of $1.481 \pm 0.026 \text{ \AA}$ and a slit top-to-bottom width ratio (ST/BWR) of 0.121 ± 0.038 . This gave a full width at half-maximum (FWHM) of $1.660 \pm 0.062 \text{ \AA}$.

The importance of the careful determination of a valid effective slit function can be seen in a study [35] of the dependence of the fitted temperature on the two slit parameters with all other parameters held fixed. It was found that the temperature shifted up about 2.5 K for a 10 percent increase in ST/BWR while a downward shift of about 31 K occurred for a 10 percent increase in the FWHM. Clearly, the opportunities for accumulation of systematic errors are significant in a circumstance such as this one where a number of parameters are correlated. The point, of course, is that there are many "good" fits possible to a given set of data depending on which parameters are permitted to be free. Therefore, to obtain the "correct" fit, it is necessary to minimize the number of free parameters while choosing values for the fixed parameters that can be justified on physical grounds (i.e., on measurements).

As the result of the sensitivity to the slit parameters, an additional complication was brought on by the intense vibrations induced in the spectrometer by the engine as discussed in Section 5. The observed value of FWHM increased by ~5 percent while ST/BWR decreased by ~20 percent when the engine power was increased from the minimum afterburning (A/B) condition to the maximum A/B condition. From the above-mentioned study [35], both of these changes would shift the fitted temperature upwards if constant slit parameters equal to the room-temperature values were used. The shift was found to be ~20 K. The slit parameters were varied in a linear way with engine A/B power between the minimum and maximum A/B power values in order to correct for this bias.

For the most part, the scattering by a diatomic molecule is isotropic (*viz.*, the so-called "trace" scattering). That is, the scattering follows the electric dipole induced by the oscillating electric field (i.e., the polarization) of the incident wave. The intensity due to trace scattering I_T is the primary contribution to the Q branch. Due to the molecule's non-spherical shape, there is also an anisotropic part to the polarizability which not only contributes a small amount to the Q branch intensity but also determines the strength of the O and S branches. This anisotropic part produces a scattering intensity I_A that contains a portion which is polarized perpendicular to the incident polarization. Thus, the total intensity of the Q branch can be operationally defined as $I_T + bI_A$ where b is a small fraction which accounts for the polarization properties of the optical system (*viz.*, the laser beam and the spectrometer).

Ordinarily, it is sufficient to calculate only the Q branch contributions [30,31]; however, in our case it was found necessary to deal with an additional feature. Scans of the scattered laser light at 3371 \AA (Rayleigh scattering) revealed that the laser emission included a weak "hot-band-type" line at about 3367 \AA . The strength of this "spurious" emission line was about 2 percent of the "Rayleigh" peak. Since the Raman scattering from this peak nearly coincides with the first hot band in the N_2 Raman spectrum of the 3371 \AA

laser line, it was necessary to measure it accurately and to include it in the calculations. This was accomplished by recording the N_2 Raman spectrum of room air over large portions of the O and S branches as well as the Q branch. A signal range of over 1000:1 was recorded by operating the PMT at two voltages and recording the three branches using overlapping spectra. The calculated spectrum, including the spurious line, was fitted to this observed spectrum. The fractional contribution of I_A specified by b , the spurious line height, and the line's position were made free parameters along with the slit parameters. By means of a series of fittings, the best fit of these parameters was obtained. The value of b was found to be 0.174 ± 0.016 with the spurious line shifted down by $4.713 \pm 0.036 \text{ \AA}$ with a strength ratio relative to the main line of 0.0203 ± 0.0012 . The value of b is acceptably close to the value of 0.156 predicted for unpolarized laser light and polarization insensitive detection [27,36].

A linear background was added to the calculated spectrum described above. The parameters for this background were the intercept at 3657 \AA and the slope. These two parameters, the temperature, and a wavelength correction parameter were made free parameters in the fitting procedure. All the calculations included the O and S branch contributions, the strengths of which relative to the Q branch were fixed by the constant b . However, several of these calculations were repeated with $b=0$, and it was found that the fitted background increased slightly while the fitted temperature decreased. The temperature decrease ranged from about 0.8 percent at $\sim 800 \text{ K}$ to 0.2 percent at $\sim 1600 \text{ K}$. These results suggest that in many cases the anisotropic part of scattering can be neglected.

5.2 Raman data

Examples of the recorded Raman spectra are presented in figures 11 and 12. The data in figure 11 are plotted on logarithmic scales in order to reveal the character of the low data values on either side of the main peak. Note the beginning of the O and S branches in the "Military" scan and the absence of these features in the low afterburner (A/B) spectrum. In figure 12, the data are plotted on linear scales. The A/B data shown in figure 11 were included to aid comparisons between the three power conditions. The onset of the second hot band is seen in the 4000 lb/hr A/B spectrum. The noise due to the high background in the 1775 lb/hr data (nearly three times the Raman hot band) compared to the 4000 lb/hr data is clearly evident. The fit of the calculated curves shown in the two figures are typical of all the Raman data reported here.

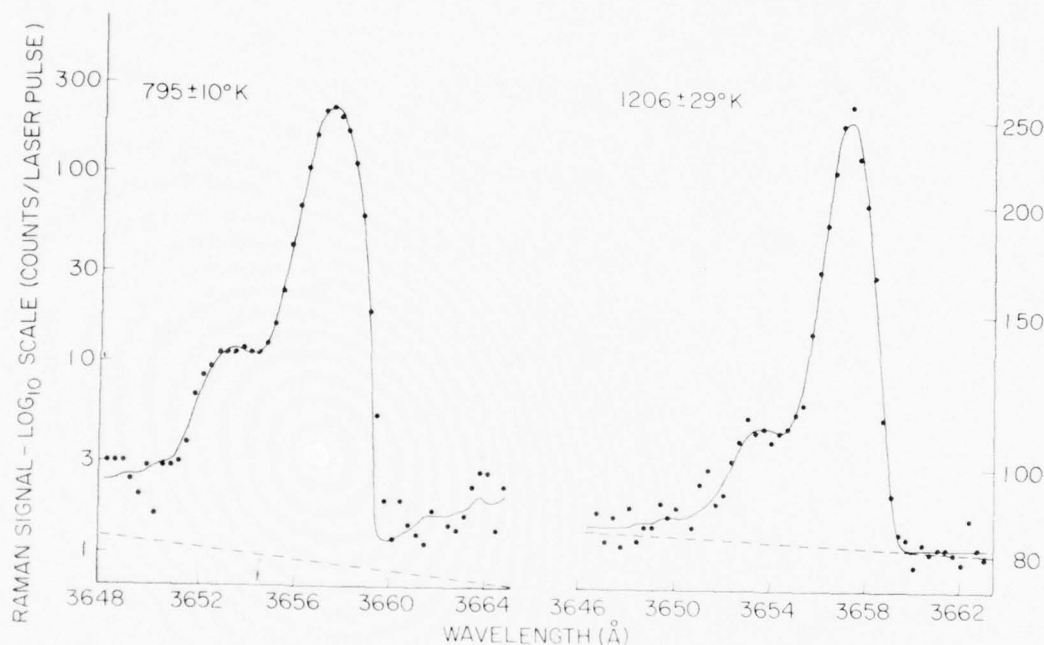


Figure 11. Observed (points) and fitted theoretical (solid lines) spectra of the N_2 Q branch Raman transitions on logarithmic scales for the Military (left) and 1775 lbs/hr afterburner power (right) conditions of the J85-5 engine obtained in March 1977.

The July data are presented in table II along with the temperatures measured simultaneously with the gas sampling probe and reported in table I. The March data are given in table III. The engine F/A ratios given in table III permit a comparison of the Raman temperature with the gas-sampling-probe temperatures obtained from the July tests.

TABLE I
ENGINE AND GAS SAMPLING DATA COLLECTED AT NEARLY THE SAME TIME AS THE RAMAN DATA IN TABLE II.

Test Conditions	Data Point	Inlet Temp (°K)	Ambient Pressure (Atms)	Mach No.	Gamma	Engine F/A	CO ₂ (A)	CO (PPM)	THC (PPM)	Local F/A	Comb. Eff.	Probe Temp (°K)	Static Engine Temp Rise (°K)
Military (1 S.D.)	T1A/07/13/77 3 Data Points	298	0.980	1.0	1.326 ±.001	0.0178 ±.0003	3.48 ±.05	615 ±8	45 ±6	0.0169 ±.0002	0.990 ±.001	974 ±11	837 ±10 539 ±6
*Military (1 S.D.)	T1/07/14/77 3 Data Points	299	0.980	1.0	1.324 ±.001	0.0177 ±.0003	3.54 ±.05	620 ±8	50 ±6	0.0171 ±.0002	0.990 ±.001	987 ±11	849 ±10 546 ±6
*1000 Lbs A/B (1 S.D.)	T2/07/14/77 7 Data Points	300	0.960	1.0	1.310 ±.003	0.0250 ±.0003	4.8 ±0.4	2395 ±292	2251 ±94	0.0250 ±.0016	0.929 ±.009	1196 ±50	1036 ±46 733 ±49
2000 Lbs A/B (1 S.D.)	T3B/07/12/77 5 Data Points	302	0.974	1.0	1.294 ±.009	0.0317 ±.0002	6.29 ±.02	2650 ±119	1650 ±108	0.0316 ±.001	0.952 ±.004	1419 ±32	1237 ±29 1118 ±33
2000 Lbs A/B (1 S.D.)	T3B/07/13/77 5 Data Points	298	0.978	1.0	1.292 ±.009	0.0319 ±.0002	6.01 ±.02	2560 ±119	1664 ±108	0.0303 ±.001	0.956 ±.004	1379 ±32	1200 ±29 1077 ±33
3000 Lbs A/B (1 S.D.)	T3A/07/11/77 4 Data Points	301	0.975	1.0	1.271 ±.003	0.0384 ±.0004	8.1 ±0.1	1550 ±31	205 ±18	0.0386 ±.0006	0.988 ±.001	1676 ±20	1476 ±18 1375 ±16
3000 Lbs A/B (1 S.D.)	T3B/07/11/77 4 Data Points	299	0.975	1.0	1.274 ±.003	0.0384 ±.0004	7.9 ±0.1	1625 ±31	210 ±18	0.0377 ±.0006	0.988 ±.001	1646 ±20	1448 ±18 1347 ±16
4000 Lbs A/B (1 S.D.)	T2A/07/11/77 4 Data Points	297	0.975	1.0	1.248 ±.002	0.0451 ±.0006	9.8 ±.12	1050 ±73	48 ±7	0.0456 ±.0005	0.994 ±.001	1884 ±17	1676 ±16 1586 ±14
4000 Lbs A/B (1 S.D.)	T2B/07/11/77 4 Data Points	298	0.975	1.0	1.251 ±.002	0.0450 ±.0006	9.6 ±.12	1035 ±73	32 ±7	0.0447 ±.0005	0.995 ±.001	1860 ±17	1653 ±16 1355 ±14
*4000 Lbs A/B (1 S.D.)	T4A/07/13/77 4 Data Points	298	0.978	1.0	1.252 ±.002	0.0451 ±.0006	9.4 ±.12	1130 ±73	37 ±7	0.0454 ±.0005	0.995 ±.001	1882 ±17	1674 ±16 1581 ±14
*4000 Lbs A/B (1 S.D.)	T4B/07/13/77 4 Data Points	298	0.978	1.0	1.252 ±.002	0.0451 ±.0006	9.4 ±.12	1130 ±73	37 ±7	0.0454 ±.0005	0.994 ±.001	1882 ±17	1674 ±12 1581 ±14
Max A/B (1 S.D.)	T6B/07/14/77 10 Data Points	304	0.980	1.0	1.232 ±.006	0.0521 ±.0007	10.7 ±0.4	2350 ±124	16 ±16	0.0504 ±.002	0.990 ±.001	2009 ±48	1800 ±47 1704 ±49
Max A/B (1 S.D.)	T5A/07/13/77 10 Data Points	299	0.978	1.0	1.231 ±.006	0.0519 ±.0007	10.8 ±0.4	2300 ±124	21 ±16	0.0507 ±.002	0.990 ±.001	2014 ±48	1805 ±47 1715 ±49
Max A/B (1 S.D.)	T1A/07/12/77 10 Data Points	299	0.974	1.0	1.230 ±.006	0.0517 ±.0007	10.9 ±0.4	2450 ±124	15 ±16	0.0510 ±.002	0.990 ±.001	2021 ±48	1812 ±47 1721 ±49

*Average gas sampling results over a three day period used for these data points. Problems with gas sampling equipment prevented simultaneous measurement with Raman.

TABLE II. Summary of Raman Data from July, 1977 Tests.

Test Conditions ^a	Run/Date	Engine F/A ^b	Probe Stat ^c Temp (°K)	Raman Temp (°K)	Slit Function (Å)	Raman Signal ^d			Background Signal ^d			No. of Points in Scan
						Hot Bd	Main Pk	(c/p)	Hot Bd	Main Pk	Slope (c/p/Å)	
Military (1 S.D.)	T1A/07/13/77	0.0178 ± 0.0003	837 ± 10	798 ± 12	0.18/1.48	8.2	180.9	2.7	2.6 ± 1.1	-0.02 ± 0.02	0.1	61
Military (1 S.D.)	T1/07/14/77	0.0177 ± 0.0003	849 ± 10	813 ± 12	0.18/1.48	10.3	186.2	2.4	2.1 ± 1.1	-0.11 ± 0.02	0.1	61
1000 Lbs A/B (1 S.D.)	T2/07/14/77	0.0250 ± 0.0003	1036 ± 46	1074 ± 37	0.15/1.54	16.4	133.4	86.6	83.2 ± 1.6	-0.88 ± 0.08	0.1	61
2000 Lbs A/B (1 S.D.)	T3B/07/12/77	0.0317 ± 0.0002	1236 ± 29	1381 ± 34	0.15/1.55	27.9	118.6	48.5	45.9 ± 1.1	-0.70 ± 0.14	0.5	39
2000 Lbs A/B (1 S.D.)	T3B/07/13/77	0.0319 ± 0.0002	1200 ± 29	1196 ± 33	0.15/1.55	26.3	116.2	63.2	60.9 ± 1.5	-0.62 ± 0.07	0.4	61
3000 Lbs A/B (1 S.D.)	T3A/07/11/77	0.0384 ± 0.0004	1476 ± 18	1475 ± 20	0.14/1.57	28.1	110.9	7.7	8.3 ± 1.2	0.15 ± 0.03	0.7	61
3000 Lbs A/B (1 S.D.)	T3B/07/11/77	0.0384 ± 0.0004	1448 ± 18	1407 ± 18	0.14/1.59	33.7	147.7	11.1	11.7 ± 1.6	0.15 ± 0.07	0.7	40
4000 Lbs A/B (1 S.D.)	T2A/07/11/77	0.0451 ± 0.0006	1676 ± 16	1525 ± 32	0.13/1.59	39.8	136.8	5.4	6.1 ± 2.4	0.16 ± 0.22	0.9	36
4000 Lbs A/B (1 S.D.)	T2B/07/11/77	0.0450 ± 0.0006	1653 ± 16	1680 ± 17	0.13/1.59	51.5	146.5	2.3	2.6 ± 1.2	0.08 ± 0.05	0.9	45
4000 Lbs A/B (1 S.D.)	T4A/07/13/77	0.0451 ± 0.0006	1674 ± 16	1641 ± 20	0.13/1.59	36.2	100.8	2.7	2.7 ± 1.2	0.01 ± 0.03	1.5	61
4000 Lbs A/B (1 S.D.)	T4B/07/13/77	0.0451 ± 0.0006	1674 ± 12	1690 ± 18	0.13/1.59	52.0	125.1	3.5	3.2 ± 1.2	-0.07 ± 0.03	1.5	61
Max A/B (1 S.D.)	T6B/07/14/77	0.0521 ± 0.0007	1800 ± 47	1818 ± 71	0.12/1.61	23.8	62.3	47.6	44.9 ± 1.8	-0.74 ± 0.13	9.1	43
Max A/B (1 S.D.)	T5A/07/13/77	0.0519 ± 0.0007	1805 ± 47	1809 ± 28	0.12/1.61	47.1	104.3	4.2	5.6 ± 1.5	0.36 ± 0.15	7.4	37
Max A/B (1 S.D.)	T1A/07/12/77	0.0517 ± 0.0007	1812 ± 47	1748 ± 33	0.12/1.61	31.8	87.8	6.4	8.5 ± 1.3	0.53 ± 0.13	5.3	37

^aAfter burner (A/B) fuel flow in lbs per hour. Standard deviations (S.D.) for the Raman data are the uncertainties obtained from the fitting procedure. See text.

^bEngine and probe data given in Table I.

^cParameters are for the trapezoidal slit function used in the fitting procedure. First number is top half width and second is bottom half width. See text.

^dSignal values are given in "counts per (laser) pulse" (c/p) where the counts are not photoelectrons but are on a convenient charge-digitizing scale which depends on the photomultiplier tube (PMT) voltage. The PMT voltage was adjusted to match the dynamic range of the linear gate with the observed signal range for each run. The PMT voltages ranged between 2260 and 2560 V. The peak of the (first) "hot" band (Bd) is at 3653.8 Å and the main peak (Pk) is at 3657.4 Å with the laser excitation at 3371 Å used in these studies.

^eNumber of spectral positions recorded where the spacing was 0.3 Å. The signal was recorded for 2000 laser pulses at each position.

TABLE III. Summary of Raman Data from March, 1977 Tests.

Test Condition ^a	Run/Date	Engine F/A/B	Raman Temp (°K)	Slit ^c Function (Å)	Raman Signal ^d		Background Signal ^d			No. of Points in Scan
					Hot Bd (c/p)	Main Pk (c/p)	Hot Bd (c/p)	Main Pk (c/p)	Slope (c/p/Å)	
Military (1 S.D.)	FLA/03/30/77	0.0179	816 ±12	0.18/1.48	9.9	216.4	1.0	0.9 ±.1	-0.03 ±.03	46
Military (1 S.D.)	FLB/03/30/77	0.0179	795 ±10	0.18/1.48	10.3	222.7	1.0	0.9 ±.1	-0.03 ±.02	51
1775 lbs A/B (1 S.D.)	FLA/03/29/77	0.0300	1130 ±33	0.15/1.55	29.4	184.1	84.6	83.3 ±.9	-0.38 ±.12	51
1775 lbs A/B (1 S.D.)	FLB/03/29/77	0.0303	1181 ±27	0.15/1.55	30.6	172.3	81.3	80.2 ±.7	-0.32 ±.10	51
1775 lbs A/B (1 S.D.)	FLC/03/29/77	0.0301	1206 ±29	0.15/1.55	29.2	179.0	82.4	81.5 ±.8	-0.25 ±.11	51
2600 lbs A/B (1 S.D.)	F2A/03/29/77	0.0358	1299 ±36	0.14/1.57	31.8	150.5	47.1	46.7 ±.8	-0.12 ±.12	50
2600 lbs A/B (1 S.D.)	F2B/03/29/77	0.0357	1333 ±24	0.14/1.57	38.6	150.0	46.1	45.3 ±.5	-0.23 ±.06	61
2600 lbs A/B (1 S.D.)	F2C/03/29/77	0.0355	1350 ±29	0.14/1.57	35.8	151.1	44.4	43.8 ±.6	-0.15 ±.08	61
3450 lbs A/B (1 S.D.)	F2A/03/30/77	0.0417	1481 ±25	0.13/1.58	35.1	114.3	16.6	16.2 ±.4	-0.09 ±.05	57
3450 lbs A/B (1 S.D.)	F2B/03/30/77	0.0415	1438 ±28	0.13/1.58	29.4	114.8	16.9	16.5 ±.4	-0.10 ±.06	56
4000 lbs A/B (1 S.D.)	F2/03/21/77	0.0446	1591 ±22	0.13/1.59	32.8	95.6	9.4	9.2 ±.3	-0.04 ±.04	51
4000 lbs A/B (1 S.D.)	F2/03/24/77	0.0450	1521 ±21	0.13/1.59	22.1	68.3	11.3	11.1 ±.2	-0.05 ±.03	61

^aAfter burner (A/B) fuel flow in lbs per hour. Standard deviations (S.D.) for the Raman data are the uncertainties obtained from the fitting procedure. See text.

^bEngine data can be derived from Table I.

^cParameters are for the trapezoidal slit function used in the fitting procedure. First number is top half width and second is bottom half width. See text.

^dSignal values are given in "counts per (laser) pulse" (c/p), where the counts are not photoelectrons but are on a convenient charge-digitizing scale which depends on the photomultiplier tube (PMT) voltage. The PMT voltage was 2400 V for all runs except "Military," which used 2350 V giving a gain reduction to about 79% of the 2400 V value. The peak of the (fit) "Hot" band (Bd) is at 3653.8 Å and the main peak (Pk) is at 3657.4 Å with the laser excitation at 3371 Å used in these studies.

^eNumber of spectral positions recorded where the spacing was 0.3 Å. The signal was recorded for 2000 laser pulses at each position except for Max A/B which was recorded for 4000 pulses and at 250 pps.

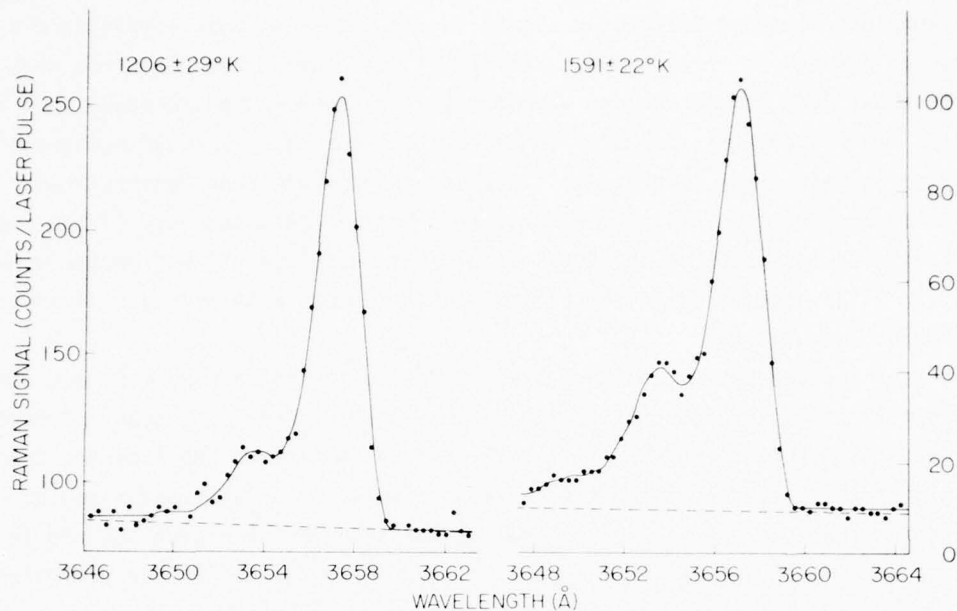


Figure 12. Observed (points) and fitted theoretical (solid lines) spectra of the N_2 Q branch Raman transitions on linear scales for the 1775 lbs/hr (left) and 4000 lbs/hr (right) afterburner power conditions of the J85-5 engine obtained in March 1977.

5.2.1 Background signals

The Raman temperature values and the fitting errors obtained from the March and July tests were in good accord with each other and with the gas sampling probe data. However, the similarity ends there. As table III shows, the March data has a well-defined trend in the laser-induced background signals and slopes. This is consistent with the uninterrupted sequence in which ten out of the twelve runs were carried out. In the July tests, a large variability in the background signals and slopes was recorded. Some of these features are apparent in table II. For example, the background signal drops sharply and the slope reverses sign at the 3000 lb/hr A/B condition. Also, run T6B/07/14/77 shows an extraordinarily high background relative to the Raman hot band signal, especially for the Max A/B condition. High backgrounds occurred at other engine conditions too, but the data were too noisy to give viable fits. There is no clear basis for understanding why the two tests had such a different character. The gas sampling probe data did not have any characteristics which could account for these differences. Although speculations can be made to explain the data, it is suffice here to suggest that the laser-induced background signal carries information concerning the engine operation which is not commonly accessible.

The laser-induced background signal was the most intense at low afterburning (A/B) conditions and decreased rapidly as the A/B power was increased. For example, as the fuel flow to the afterburner was increased from 2000 lb/hr to 3000 lb/hr, table II shows that

the ratio of the laser-induced-background signal to the Raman-hot-band signal decreased from about two to about 0.3. From table I, the total hydrocarbon concentration also decreased from about 1600 ppm to 200 ppm with the static temperature increased from about 1200 to 1400 K. We believe this behavior signifies that the laser-induced background signals observed in this study were due to fluorescence from unburned hydrocarbons. Laser-induced soot incandescence was unlikely because this engine generated very little soot [3]. Also, the laser intensity in the focal volume was quite low which from the work of Eckbreth, et al. [11] suggests that soot incandescence did not make strong contributions to the backgrounds in our runs.

The non-laser-induced background signal was essentially constant during each scan. The values given in tables II and III resulted from averaging over each scan. Presumably, this signal comes from the luminosity of the plume since it follows the expected trend. Namely, the higher the temperature the greater is the emission at short wavelengths, and hence, the greater the non-laser-induced signal in the 3646-3664 Å region scanned in these studies. Again, the March values were larger, by about a factor of two for equivalent conditions, than the July values for no apparent reason.

5.2.2 Inaccurate background measurements

A precise determination of the laser-induced background levels on both sides of the spectrum was important for all A/B conditions. Without adequate pinning of the background on both sides of the spectrum, the apparent strength of the hot band can vary widely, easily ± 30 percent. This occurs when the computer search fits a background that is shifted either too high or too low. When this happens, there is a negatively correlated shift in the fitted temperature. The result is that the fitted temperature is in error by as much as 10 percent. An example of this effect is the T2A/07/11/77 run in table II. The fitted temperature is clearly 10 percent low while the laser-induced background is about a factor of two higher than the other values at the 4000 lb/hr A/B condition. In addition, the standard deviation (S.D.) values for the background signal and slope are very high. This scan was incomplete in that it was short (36 points), and it was cut off before the high wavelength background was scanned. Thus, by comparisons with the other data, it is apparent that the low temperature and its high standard deviation (S.D.) as well as the unusual background parameter and S.D. values resulted from a lack of well defined background data on both sides of the Raman spectrum. This run was retained in the data set to provide an illustration of this problem area.

Another likely, but somewhat more subtle example of the problem of pinning the background is run T3B/07/12/77 in table II. None of the measured or fitted values for this run by themselves suggest a problem. However, only 39 points were used in the scan. This would not be a problem if the background signal was small, as in the last two Max A/B runs in the table. It is evident from the other data that the fitted temperature is 10 percent too high. As it turned out, only two background data points were obtained on the high wavelength side of the Raman spectrum with four points on the low side. With so few

points, the background signal was inadequately determined. Although a good fit was obtained, the fitted temperature was incorrect because the statistical fluctuations in the background signal were not averaged out over a sufficient number of points.

5.2.3 Error analysis

The errors in the Raman temperatures were mainly comprised of contributions from the measuring apparatus and from the analysis of the data. The errors in the measured variables, signal strength and wavelength, were quite small. The wavelength errors were generally within $\pm 0.05 \text{ \AA}$, and therefore, were negligible because of the wide slits used in these studies. The performance and use of the detection apparatus is discussed in Section 3.3.1.4. Clearly, a nonlinearity in the response of the apparatus would introduce a bias error in the fitted temperature. The response became slightly nonlinear below about 25 counts/pulse (c/p) such that the measured value was high. This increased the recorded weak background levels obtained with the Military engine condition thereby lowering the recorded strength of the weak hot band. This shifted the fitted temperatures low for the Military condition. Comparison of these temperatures with the probe values in table II shows a shift of about 4 percent. For the remaining runs, this nonlinearity introduced only slight errors in the fitted background signals and did not affect significantly the temperatures because of the high background or hot band signals, or both.

There were two kinds of errors in the analysis of the data. There were bias errors that arose in the fitting procedure which resulted from various approximations that were made to simplify the analysis of the data and bias errors that could occur due to the large Raman scattering volume. Also, there were the errors due to the statistical fluctuations in the data. The bias errors in the fitting procedure and the scattering volume are described in Sections 3.3.3 and 3.3.1.2. If these bias errors were adequately considered in our computations, and if the theoretical description of the N_2 Raman spectrum used in this work was sufficiently accurate, then the fitting errors in the temperature given in tables II and III for the A/B power conditions characterize the accuracy of this approach to Raman thermometry.

One half or more of the temperature fitting error for an A/B condition was due to the noise associated with the background. A dramatic example of this is the first Max A/B run in table II (TGB/07/14/77). This run had a laser-induced background that was about 10 times higher than the remaining Max A/B runs which more than doubled the S.D. in the temperature fit.

This dependence of the fitting error on the background was revealed in a more general way by using the fact that the hot-band-to-main-peak ratio was a linear function of temperature [37] for our choice of slit function. Thus, if V is this ratio, then

$$V = m(T - T_0), \quad (17)$$

where m is the slope and T_0 is the temperature intercept. From eq. (17), the temperature error is given by

$$\sigma_T = (\sigma_V/V) (T - T_0). \quad (18)$$

By applying eq. (18) to the March data in table III and adjusting the calculation to make σ_T on the average equal to the fitting errors in table III, the contributions of the background to the temperature errors were revealed. The results of these calculations are shown in figure 13. These curves are presented only to illustrate this characteristic dependence of the temperature error on the background signals. Since the signal-to-noise ratio is proportional to the square root of the time interval over which the signal is recorded, then a longer scan time will give a smaller error. However, the probed medium must remain steady during this longer scan. In our case, this meant that the engine performance had to be repeatable throughout the test sequence. We found it difficult to achieve this in blocks of time greater than four days. Thus, our scan times were indirectly influenced by the constraints set by the number of runs planned and the number of days available for the runs.

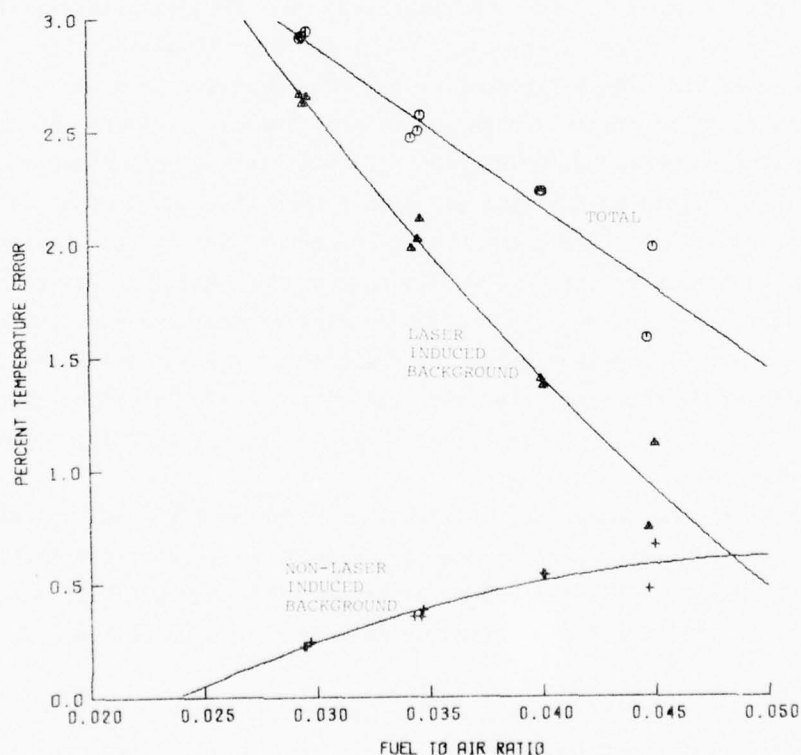


Figure 13. Temperature error analysis of the March 1977 Raman data calculated from the linear dependence of the first-hot-band-to-main-peak ratio on the temperature for the ten afterburner conditions. The curves are best fits to the data points shown.

5.2.4 Vibration problem

Initially, the plans were to record both the Stokes and anti-Stokes spectra and to obtain the temperature from these measurements. The spectrometer was equipped with first-order gratings blazed at 3000 \AA and calibrated. The Raman spectra of N_2 occur at 3658 and 3125 \AA for an excitation wavelength of 3371 \AA . However, as the engine power was increased, the Stokes and anti-Stokes spectra of N_2 dropped in intensity and broadened in wavelength. To identify the problem, the spectrum of a mercury lamp placed on the table supporting the spectrometer was recorded for different engine operating conditions. As the engine power was increased, vibration of the linkage between the two gratings of the spectrometer also increased causing the gratings to vibrate about their rotational axes. This caused the image on the third (output) slit to sweep back and forth creating the observed effect. Every effort was made to reduce the vibration of the spectrometer but it was to no avail.

The recorded spectra of the 3125 \AA line of mercury as affected by this vibration are shown in figure 14 (a), (b), and (c). Because the spacing between the main peak of the N_2 Stokes spectrum and the first hot band is 3.6 \AA , it was desirable to use slit widths that give a spectral resolution of 2.0 \AA or less. With the first order gratings, this corresponded to $333\text{ }\mu\text{m}$ wide slits. However, judging from the amount of engine-induced broadening shown in figure 14 (c), the effective amplitude of the vibration at the exit slit was between 100 and $200\text{ }\mu\text{m}$. This loss of spectral resolution made it untenable for us to proceed with the first-order gratings.

The solution to the vibration problem was to change to third order gratings. This permitted the slits to be increased by a factor of three to $1000\text{ }\mu\text{m}$ thereby greatly reducing the influence of the vibration. However, because of the 3333 \AA blaze of these gratings, only the Stokes spectrum could be efficiently recorded which meant that the temperature had to be extracted from the profile of this spectrum. The spectra of the 3125 \AA line of mercury using the third-order gratings are shown in figure 14 (d), (e), and (f) as a function of engine power. Clearly, the vibration-induced broadening is quite small compared to figure 14 (c). The effect of this residual broadening and the procedure followed to correct for it are described in Section 3.3.3.3.

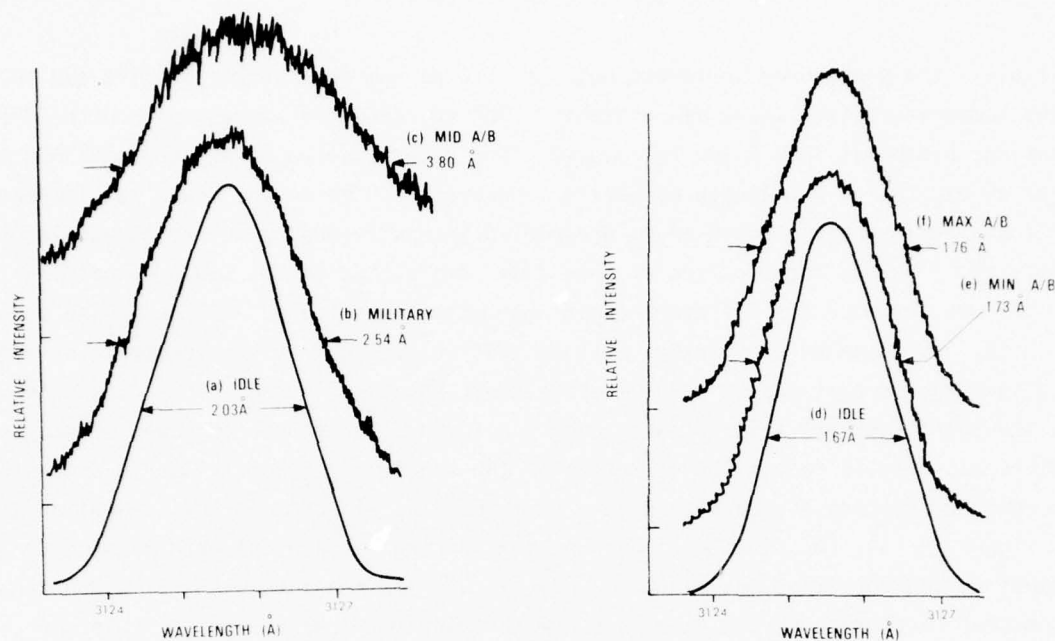


Figure 14. Spectral line shapes of the 3125 Å line from a mercury lamp resulting from engine-induced vibrations. The upper curves, (a), (b), and (c), were obtained with the first order gratings and 333 μm /500 μm /333 μm slits. The lower curves, (d), (e), and (f), were obtained with the third order gratings and 1000 μm /1500 μm /1000 μm slits. The measured full widths at half maximum are given for each curve.

6. Summary and Conclusions

The objective of this study was to assess the feasibility of using spontaneous Raman scattering to measure temperatures in the plume of an afterburning J85-5 turbojet engine. This assessment required Raman spectral measurements of sufficiently good quality to permit temperature determinations and confirmation that the temperatures were correct within reasonable error limits. Our basic approach was to use gas sampling as a standard technique to be compared with the Raman technique. Simultaneous gas sampling and Raman measurements were made at about the same time and axial location in the plume (114 cm from nozzle exit plane) and for different engine afterburning conditions. Additional gas sampling measurements were made later in the test program and thermocouple measurements were also made. The simultaneous measurements were directly compared. All the measurements

were then compared by plotting temperature rise versus engine fuel-air ratio. The conclusions from these measurements are summarized below:

(1) Our gas sampling measurements and those made by Lyon, et al. [3], for nearly the same test conditions, agreed within an experimental error of less than 5 percent. This established our confidence for using gas sampling as a standard technique.

(2) Raman N_2 Q branch spectra were obtained with sufficient resolution to permit temperature measurements over the entire operating range of the afterburner. The temperatures were determined by fitting theoretical spectral profiles to experimental data. This technique for obtaining temperatures provided all the information essential for estimating the probable errors associated with the Raman temperature measurements.

(3) The error in the Raman temperatures estimated from the spectral-profile fitting procedure varied between about 1 percent and 4 percent depending on test conditions. These errors may be a little low but appear reasonable based on the comparisons with other techniques.

(4) Simultaneous Raman and gas sampling temperatures agreed within experimental error of about 3 percent.

(5) Engine static temperature rise was measured by Raman, gas sampling, and thermocouple techniques over an engine F/A ratio range of 0.017 to 0.052. A plot of these data versus engine F/A ratio showed that Raman and gas sampling measurements agreed within an experimental error of less than 5 percent. The thermocouple measurements were in agreement up to a F/A ratio of 0.045. At higher F/A ratios, the thermocouple measurements were significantly below the temperatures measured by the other techniques. We believe that this occurred because the thermocouple junction was cooled when it was bent towards the cooled tip of the probe by the high gas velocities.

(6) The non-laser-induced background was not a serious problem for these experiments because of the low duty cycle (5×10^{-6}) provided by the 20 ns time-gated detection electronics.

(7) The laser-induced background was the most serious Raman-related problem encountered during the test program. It was the primary factor that determined the accuracy of the temperature measurements. We believe that the background was due to fluorescence from unburned hydrocarbons similar to that observed by Leonard [8] and could have been influenced by the plume temperature as suggested by Bailly, et al. [9].

The uncertain nature of the laser-induced background raises questions about whether our Raman system could be used to measure temperatures at other locations within the afterburner plume. According to the gas sampling measurements made by Lyon, et al. [3], the total hydrocarbon concentrations can be as high as 6000 ppm at the engine exit plane and the static temperatures are just under 1300 K. Under these conditions, we would expect a strong laser-induced background signal. Additional experiments are needed to determine whether Raman temperature measurements can be made in this environment.

The authors gratefully acknowledge the effort and dedication of Mr. P. R. Hemmer who assembled and developed the Raman computer fitting routine. Special appreciation is extended to Mr. T. H. Hemmer for his assistance in the July, 1977 tests and for performing the computer analyses of the Raman data presented in this paper. The authors thank Dr. J. Ay for his valued assistance in setting up and performing the early measurements in this program and for preparing several figures presented in this paper.

The authors would like to express their appreciation to Mr. L. Angello, Mr. R. Whitlock, and Mr. J. Carnes for operating and maintaining the engine during the experiments and Mr. R. Allen, Mr. T. Campbell, and Mr. J. Malone for calibrating and operating the various instruments associated with the test cell. Special acknowledgments are given to Dr. T. Rosfjord for developing the theory used to calculate temperatures from emissions measurements and Mr. S. Farenbach and Mr. B. Eresman for writing the computer codes for making the calculations. The authors would also like to thank Mr. F. Voll and Mr. R. Hornbuckle for assisting in the data reduction and Mr. R. Bradley for aiding in plotting various data. Special appreciation is extended to Mr. G. Glawe at NASA Lewis for providing the thermocouple probe used in this study, to Mr. T. Lyon for his discussions about their probe measurements, and to Dr. Marshall Lapp for sharing the results of his N₂ Raman calculations with us.

References

- [1] Temperature, Its Measurement and Control in Science and Industry, Vol. III, Part 2 (Reinhold, New York, 1962).
- [2] Procedure for the Continuous Sampling and Measurement of Gaseous Emissions from Aircraft Turbine Engines, Society of Automotive Engineers, Aerospace Recommended Practices No. 1256 (Oct. 1971).
- [3] Lyon, T. F., Calley, W. C., Kenworth, J. J., and Bahr, D. W., Development of Emissions Measurement Techniques for Afterburning Turbine Engines, AFAPL-TR-75-52 (1975).
- [4] Samulson, G. S. and Harmen, J. N., Chemical transformation of nitrogen oxides while sampling combustion products, Air Pollution Control Association, 27, 648-655 (July 7, 1977).
- [5] Lapp, M. and Penney, C. M., eds., Laser Raman Gas Diagnostics (Plenum Press, New York, 1974).
- [6] Lapp, M. and Penney, C.M., Raman measurements on flames, in Advances in Infrared and Raman Spectroscopy, J. H. Clark and R. E. Hester, eds. (Heyden and Son Ltd., London, 1977).
- [7] Lederman, S., The use of laser Raman diagnostics in flow fields and combustion, Prog. Energy Combust. Sci. 3, 1-34 (1977).
- [8] Leonard, D. A., Field Tests of a Laser Raman Measurement System for Aircraft Engine Exhaust Emissions, AFAPL-TR-74-100 (Oct. 1974).

- [9] Bailly, R., Pealat, M., and Taran, J. P. E., *Opt. Comm.* 17, [1], 6873 (April 1976).
- [10] Setchell, R. E. and Aeschliman, D. P., Fluorescence Interferences in Raman Scattering from Combustion Products, Sandia Laboratories Energy Report SAND76-8705 (Feb. 1978).
- [11] Eckbreth, A. C., Applicability of Laser Raman Scattering Diagnostic Techniques to Practical Combustion Systems, Project SQUID Technical Report UTRC4PU (Oct. 1976); also Eckbreth, A. C., Bonczyk, P. A., and Verdick, J. F., Practical considerations for laser light scattering diagnostics, The Winter Annual Meeting of the American Society of Mechanical Engineers, Atlanta, Georgia, November 27-December 2, 1977, Session 4A, in Gas Turbine and Combustion Fuels Technology, E. K. Bastress, ed.
- [12] Williams, W. D., Powell, H. M., McCay, T. D., Jones, J. H. and McGuire, R. L., Exhaust plume gas dynamic and radiation measurements on a 500 LBF thrust liquid rocket engine at simulated flight conditions, Part II: Laser Raman/Mass Spectrometer Diagnostics, AEDC-TR-78-17 (May 1978).
- [13] Goulard, R., ed., Combustion Measurements: Modern Techniques and Instrumentation (Hemisphere Publishing and Co., Washington, D.C., 1976)
- [14] North, J., Callaghan, E., and Lanzo, D., Investigation of Field and Velocity Profiles of an Afterburning Engine, NACA-RM-E54G07 (1954).
- [15] Scadron, D., and Warshawsky, I., Experimental Determination of Time Constants and Nusselt Numbers for Bare-Wire Thermocouples in High-Velocity Air Streams and Analytical Approximation of Conduction and Radiation Errors, NACA-TN-2599 (1952).
- [16] Scadron, D., Warshawsky, I., and Gettelman, C. D., Thermocouples for jet-engine gas temperature measurement, *Prac. Instr. Soc. Am.*, Paper No. 52123, 7, 142-148 (1952).
- [17] Glawe, G. E., Simmons, F. S., and Stickney, F. M., Radiation and Recovery Corrections and Time Constants of Several Chromel-Alumel Thermocouple Probes in High-Temperature, High-Velocity Gas Streams, NACA-TN-3766 (1956).
- [18] Williamson, R. C. and Stanforth, C. M., Measurements of Jet Engine Combustion Temperature by the Use of Thermocouples and Gas Analysis, SAE Paper 690433 (1969).
- [19] Glawe, G. E. and Shepard, C. E., Some Effects of Exposure to Exhaust-Gas Streams on Emittance and Thermoelectric Power of Bare-Wire Platinum Rhodium-Platinum Thermocouples, NACA-TN-3253 (1954).
- [20] Baumeister, T. and Marks, L. S., eds., Standard Handbook for Mechanical Engineers, Seventh Edition (McGraw-Hill, New York, 1967).
- [21] Gordon, S. and McBride, B. J., Computer Program for Calculation of Complex Chemical Equilibrium Compositions, Rocket Performance, Incident and Referenced Shocks, and Chapman Jouquet Detonations, NASA Special Publication, 273 (1971).
- [22] U.S. Environmental Protection Agency, Control of air pollution from aircraft and aircraft engines, *Federal Register*, 38, [136] (July 17, 1973).
- [23] Blazowski, W. S., and Henderson, R. E., A Review of Turbopropulsion Combustion, AFAPL-TR-77-41 (June 1977).
- [24] VanWylen, G. J., and Sonntag, R. E., in Fundamentals of Statistical Thermodynamics (Wiley, New York, 1965).

- [25] Rosfjord, T. J., Efficiency Determined from Exhaust Measurements, Internal Air Force Aero Propulsion Laboratory Paper.
- [26] Herzberg, G., Molecular Spectra and Molecular Structure, I. Spectra of Diatomic Molecules (D. Van Nostrand Co., New York, 1950).
- [27] Widhopf, G. F. and Lederman, S., Species Concentrations Measurements Utilizing Raman Scattering of a Laser Beam, Polytechnic Institute of Brooklyn, PIBAL Report No. 69-46 (November 1969).
- [28] Koningstein, J. A., in Introduction to the Theory of the Raman Effect (Reidel Publishing Co., Dordrecht, Holland, 1972).
- [29] Van De Hulst, H. C., in Light Scattering by Small Particles (Wiley, New York, 1957).
- [30] Lapp, M., Penney, C. M., and St. Peters, R. L., Laser Raman Probe for Flame Temperature, Project Squid Technical Report GE-1-PU (April 1973).
- [31] Lapp, M., Goldman, L. M., and Penney, C. M., Raman scattering from flames, *Science*, 175, 1112-1115 (1972).
- [32] Roh, W. B., Coherent Anti-Stokes Raman Scattering of Molecular Gases," AFAPL-TR-77-47, (August 1977).
- [33] Bevington, P. R., in Data Reduction and Error Analysis for the Physical Sciences (McGraw-Hill, New York, 1969).
- [34] Hemmer, P. R., Yaney, P. P., and Roquemore, W. M., Computer fits of calculated Raman spectra of N_2 to observed spectra, *Bull. Am. Phys. Soc.* 22, 1039 (1977).
- [35] Hemmer, T. H., Yaney, P. P., and Hemmer, P. R., Effect of variations in instrument function on the temperature calculated from the Raman spectrum of N_2 , *Bull. Am. Phys. Soc.* 23, 162 (1978).
- [36] Gilson, T. R., Hendra, P. J., Laser Raman Spectroscopy (Wiley-Interscience, New York, 1970).
- [37] Yaney, P. P., Hemmer, P. R., Hemmer, T. H., and Roquemore, W. M., Determination of temperatures in the combustion zone of a J85-5 jet engine using the laser-excited vibrational-rotational Raman spectrum of nitrogen, in Thirty-Third Annual Molecular Spectroscopy Symposium (Ohio State University, June, 1976); also Ay, J., Roquemore, W. M., Yaney, P. P., and Hemmer, P. R., Raman measurements in the J85-5 afterburning turbojet engine plume, The Winter Annual Meeting of the American Society of Mechanical Engineers, Atlanta, Georgia, November 27-December 2, 1977, postdeadline paper, Session 4A.
- [38] Voll, F. and Eresman, B., C-Stand Stationary Turbojet Engine Test Facility and Data Acquisition and Data Reduction, AFAPL-SFF-TM-77-24 (1977).
- [39] Lyon, T. F., Colley, W. C., Kenworth, J. J. and Baker, D. W., Development of Emissions Measurement Techniques for Afterburning Turbine Engines, Supplement 1-Engine Emissions Test Data, AFAPL-TR-75-52-Supplement 1 (Oct. 1975).

APPENDIX B

COMBUSTION DIAGNOSTICS USING A
PULSED-LASER RAMAN SPECTROSCOPY SYSTEM

INTERIM REPORT

COMBUSTION DIAGNOSTICS USING A PULSED-LASER RAMAN
SPECTROSCOPY SYSTEM

UNIVERSITY OF DAYTON RESEARCH INSTITUTE
300 COLLEGE PARK AVENUE
DAYTON, OHIO 45469

JANUARY 1979

INTERIM REPORT

Approved for public release; distribution unlimited

AIR FORCE AERO PROPULSION LABORATORY
AIR FORCE WRIGHT AERONAUTICAL LABORATORIES
AIR FORCE SYSTEMS COMMAND
WRIGHT-PATTERSON AIR FORCE BASE, OHIO 45433

TABLE OF CONTENTS

SECTION	PAGE
1 INTRODUCTION	54
2 SYSTEM PERFORMANCE	58
2.1 Modified Laser	58
2.2 Optics Configuration	60
2.3 Optics Table	66
3 MEASUREMENTS	72
3.1 Raman Thermometry Techniques	72
3.2 Raman Measurements	82
3.3 Measurements of Background Spectra	103
4 CONCLUSIONS	115
5 RECOMMENDATIONS	120
5.1 Modification of Current LARS System	120
5.2 Modifications to Provide For "Instantaneous" Measurements	122
5.3 Modification to Improve Background Discrimination Capability	122
REFERENCES	124
APPENDIX	126

LIST OF ILLUSTRATIONS

FIGURE		PAGE
1	Block Diagram of the Modified-LARS System Showing the Principal Subsystems.	55
2	Oscilloscope Trace of the 3371-A Laser Pulse with the Unstable Resonator Installed.	61
3	Optical Arrangement and Sample Volume Used in the Transceiver Unit of the Modified-LARS System.	62
4	A Typical Set of Dimensions for the Transceiver Optics Shown in Figure 3.	64
5	A Cross-Sectional View of the Combustion Tunnel Showing the Paths of the Optical Beams Through the Tunnel Windows.	67
6	A Portion of the Floor Plan of Room 20 in Building 18 of AFAPL Showing a Typical Position of the Transceiver Unit at the first Optical Port of the Combustion Tunnel.	70
7	Calculated Stokes Q-Branch Spectra of N ₂ for 3371 A Excitation and an Arbitrary Trapezoidal Slit Function.	79
8	Measured Temperature Profile of a Horizontal, Pre-Mixed, Acetylene-Air Flame with an Argon Sheath Produced by two Concentric Capillary Burners.	86
9	Scan of the Region Occupied by the Stokes Q-Branch Spectrum of N ₂ during the Run at 1935 on 6 July 78 reported in Tables 3 and 4.	98
10	Laser-Induced Background Spectra Observed with Natural-Gas (Methane) Fuel at 1646 on 28 July 1978.	107
11	Laser-Induced Background Spectrum Observed with Propane Fuel at 2042 on 27 July 1978.	111
12	Non-Laser-Induced Background (Emission) Spectrum Observed with Natural-Gas (Methane) Fuel at 1759 on 7 July 1978.	113

LIST OF TABLES

TABLE		PAGE
1	Optical Components Used in the Modified-LARS System	65
2	Transverse Temperature Profile of a Horizontal-Mounted, Air-Acetylene Capillary Burner (Argon Separated) Obtained from Four-Wavelength Raman Measurements	85
3	Combustion Tunnel Temperatures with Natural-Gas Fuel Obtained from Computer Fitted Raman Scans	89
4	Raman Data for Combustion Tunnel Runs Given in Table 3	90
5	Combustion Tunnel Temperatures with Natural-Gas Fuel Obtained from Four-Wavelength Raman Measurements Taken on 5 July 1978	91
6	Raman Data for Combustion Tunnel Runs of 5 July 1978 Given in Table 5	92
7	Combustion Tunnel Temperatures with Natural-Gas Fuel Obtained from Six-Wavelength Raman Measurements Taken on 6 July 1978	93
8	Raman Data for Combustion Tunnel Runs of 6 July 1978 Given in Table 7	94
9	Combustion Tunnel Temperatures with Natural-Gas Fuel Obtained from Six-Wavelength Raman Measurements Taken on 24 July 1978	95
10	Raman Data for Combustion Tunnel Runs of 24 July 1978 Given in Table 9	96
11	Run Conditions for the Background Spectra Given in Figures 10, 11, and 12	109

SUMMARY

This interim report consists of a review of the performance of a recently-modified laser Raman scattering (LARS) system and the presentation of the results of temperature measurements carried out using the system. A pulsed nitrogen-gas laser with an unstable resonator provided 165 mW of average power into a 10 nsec pulse at 250 pps. The detection of the spontaneous Raman signal was by means of a double spectrometer, an 8850 photomultiplier tube (PMT), and gated (20 nsec) current integration of the PMT pulses. The digitized signals and the control functions were handled by a dedicated minicomputer. The entire optical system was mounted on an 8-inch-thick, research grade optics table 145 cm square. The height of the table was remotely controlled via the computer programming to permit profile measurements to be carried out. In the right-angle (90°) scattering configuration, sample volumes as small as 2 mm square by about 0.4 mm thick approximately 30 cm from the system were achieved. Stability and resetability of the vertical position of the table was in the range of ± 0.1 to 0.2 mm.

The measurements were made on a pre-mixed flame from a capillary burner using air-acetylene and air-propane mixtures and on a turbulent diffusion flame in a 10-inch diameter combustion tunnel using various air flow rates with natural gas (methane) and propane fuels. The temperatures were calculated by the computer-fit method and the N-wavelength method. In the computer-fit method, the theoretical spectrum corresponding to a specific temperature was found which best fit (via chi-square minimization) the continuous-step scan of the Stokes Q-branch spectrum of N_2 from the flame. The N-wavelength method used the fact that the ratio of the first-hot-band intensity to the intensity of the main peak is a linear function of temperature. Thus, a minimum of four measurements, two to determine the background and two

to fix the total intensities at the wavelengths of the first hot band and the main peak, were sufficient to calculate the temperature.

Profile measurements made on the capillary flames gave temperatures up to $1860^{\circ}\text{K} \pm 4.2\%$ with propane and $2200^{\circ}\text{K} \pm 9.1\%$ with acetylene. The acetylene flame produced a laser-induced background that was about twice the Raman hot-band intensity while the background from the propane flame was considerably less.

Forty-eight sets of Raman data were taken over a wide range of operating conditions of the combustion tunnel. Both methods were used to calculate the temperatures. The temperatures ranged from 1000 to over 2000°K with an average Poisson standard deviation for 21 of the measurements of about 4%. The remaining uncertainties averaged 18% ranging from 8 to as high as 95% depending on the level of the laser-induced background. This background was determined to be due to fluorescence with an approximate lifetime of 20 nsec. Temperature measurements were made in highly turbulent regions by using 20 mm-long sample volumes and long (10 to 16 minute) measurement times. Temperatures were successfully determined for relatively fuel-rich conditions in which the background was almost ten times more intense than the Raman hot-band intensity. Typical scans of the laser-induced and the non-laser-induced background spectra are presented and analyzed. Recommendations for future studies with the LARS system which cover a wide range of topics are also offered.

SECTION 1

INTRODUCTION

The original laser Raman scattering (LARS) system was developed by AVCO Everett Research Laboratory on Air Force Contract No. F33615-71-C-1875. The system was initially designed for making field measurements of emissions in jet engine exhausts.¹ Some modifications to the LARS system were made by Computer Genetics Corporation on Air Force Contract No. F33615-74-C-2023. The purpose of the modifications were to improve the combustion diagnostic capabilities of the LARS system.²

The main objectives of the current program were: (1) to make LARS measurements on the combustion plumes of an after-burning J85-5 turbojet engine and various other combustors, (2) to implement modifications of the LARS system to permit computer control of the vertical position of the sampled volume, (3) to modify and update the performance of the system to permit measurements in the AFAPL combustion tunnel facility, and (4) to make measurements in that facility using the modified LARS system. The purpose of this interim report is to present the results of the preliminary measurements made on the combustion tunnel using the modified LARS system.

The modified LARS system consists of five subsystems. These are the optics table, the laser, the signal detection apparatus, the signal processing apparatus, and the computer. The interconnections between these subsystems are illustrated in Figure 1. The optics table supports the laser head and the signal detection apparatus the combination of which makes up the optical transceiver unit that is located at the measurement site. The signal processing apparatus and the computer, the latter of which includes the

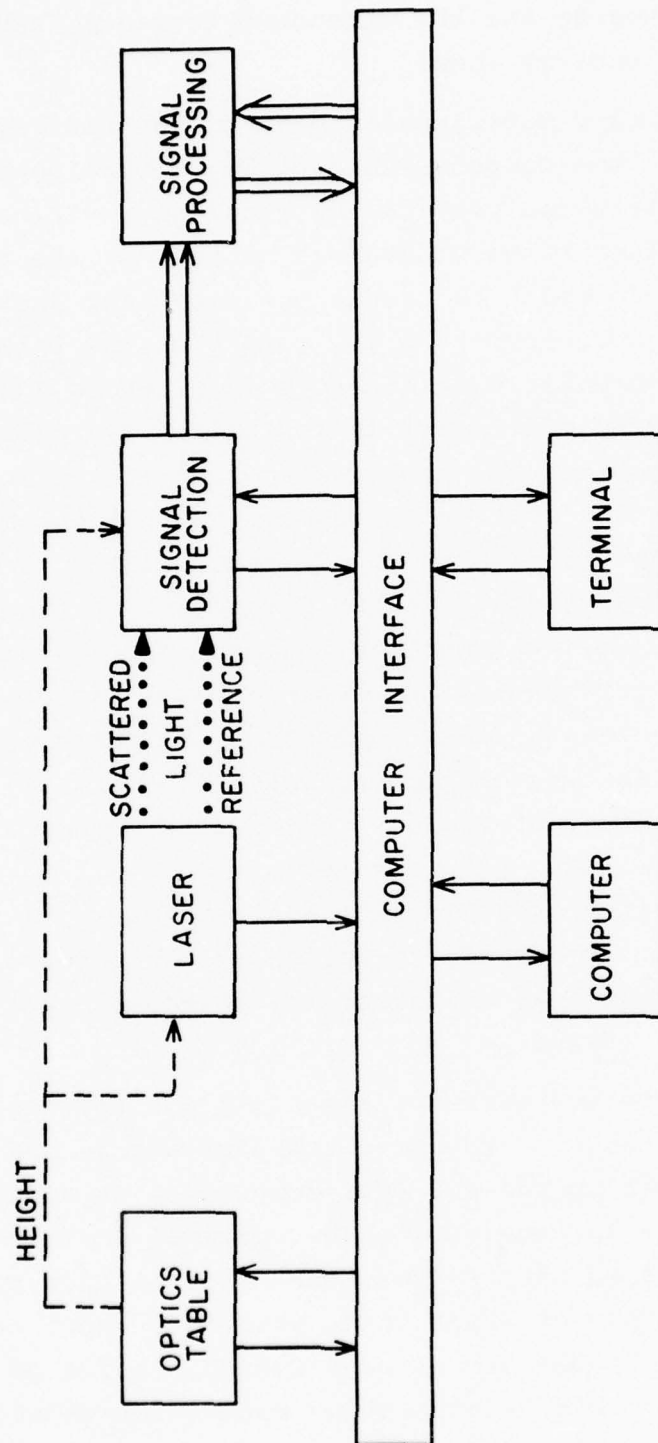


Figure 1. Block Diagram of the Modified-LARS System Showing the Principal Subsystems.

interface boards and the attendant terminal, are located in the nearby control room.

The primary modification made on the LARS system was the addition of the computer-controlled, vibration-protected optics table which permits the vertical position of the sampled volume to be programmed as part of the data-taking sequence. In order to handle the resulting increased programming requirements, the memory of the Data General Nova 1220 computer was increased from 16K to 32K words. Other hardware modifications include: (1) redesign of the laser-beam optics and the light-collecting optics for operation in the 90° scattering geometry with the combustion tunnel, (2) installation of the Tektronix 4010 CRT terminal, (3) installation of an unstable resonant cavity in the AVCO nitrogen laser, (4) installation of an optical encoder in the SPEX spectrometer and wavelength-position counter with initial-wavelength preset switches, (5) installation of an automatic laser-wavelength-actuated shutter, (6) modification of the computer interface with the SPEX Compudrive unit to reduce the minimum step size from 1 Å to 0.1 Å, and (7) other changes/additions such as the addition of a preamp to the photomultiplier output, re-packaging the interrupt pulse generator, and improvement of the performance of the spectrometer drive.

Extensive software modifications and additions were also implemented both in the Nova computer and in the data analysis programs used in the CDC 6600 computer. In addition to the new programming required by the vertical positioning feature of the modified LARS system, the original code was modified to provide initial laser power printout, input of the ratio of the data-to-background gate widths, choice of photon-counting or current-integration modes, and closed-loop control of the spectrometer wavelength. Among the significant improvements made in the data analysis code was the

inclusion of the measured laser emission spectrum, the use of an operationally determined instrument function, and the use of a chi-square minimization program to determine the best-fit temperature and the fitting errors.

The modified LARS system was moved into Room 20 of Building 18 of the Air Force Aero Propulsion Laboratory (AFAPL) on 13 June 1978. It was operational with the combustion tunnel by 30 June. The objectives of this report are: (a) to characterize the performance of the modified system, (b) to present the results of the preliminary measurements made with the modified system on the combustion tunnel, and (c) to make recommendations regarding the operation of the modified system. Hereafter, the use of the term "LARS system" or "system" will refer to the modified-LARS system.

SECTION 2

SYSTEM PERFORMANCE

The performance aspects of interest in this report are those which are involved with the modifications and additions that directly influence the measurements made with the system in the combustion tunnel facility. This includes the modified laser, the optics, and the optics table. Distinction is made here between the features and parameters which characterize, in general, the flexibility and capability of the system and the capability of the system to provide measurements on specific combustion environments. The performance of the system with various combustors is the subject of Section 3.

2.1 MODIFIED LASER

In a laser light-scattering experiment it is desirable to minimize the volume of the sampled region without sacrificing any available light. A small volume permits the measurement of the profile of a parameter, such as temperature, across some region. In the 90° scattering geometry of interest here, the minimum size of the sampled volume in two of the three dimensions for a given optical configuration is determined by the angular divergence of the laser beam. The AVCO C5000 pulsed, nitrogen-gas laser used in this work had a near-field beam consisting primarily of two very narrow, bright lines of light separated by 3.2 mm and 50 mm in length. Its far-field pattern consisted of a complex array of parallel "lines" of light having an overall measured half-angle divergence of approximately 1.2 mr by 10.4 mr. Actually, at least one of these "lines" extended to almost twice the 10.4 mr value. Although most of the light was contained within this 10.4 mr dimension, this feature of the beam greatly complicated the shape of the sample volume defined by the focused beam. The size of the

focused beam is essentially determined by the beam divergence, the aperture of the focusing lens, and the distance of the lens from the sample volume. The sample volume in the 90° geometry is defined by the dimensions of the cross-sectional area of the focused beam and the length of the beam that is selected by the collecting (i.e., receiving) optics. The aperture size and the lens-to-focus distance is fixed by the design of the combustion tunnel. Calculations showed that with the AVCO laser as described above, the sample volume would extend along the axis of observation as much as 8 mm. Since the radius of the proposed center body of the combustor was only 70 mm, this 8-mm size would not permit the spatial resolution of the profile of a measured parameter that would be needed to characterize a complex combustion environment.

The spatial resolution was enhanced by modifying the laser. The non-resonant, transverse-excited laser cavity of the AVCO laser was made resonant in the long dimension of the beam by the addition of two cylindrical mirrors which formed an unstable resonator.³ The resonator is of the Cassegrain design which introduces in the near field a dark region in the central region of the beam due to the "secondary" mirror. The far-field pattern is now confined to a well-defined, narrow rectangular area with a half-angle divergence of about 0.2 mr by 4.7 mr. This modification of the laser produces a focused beam with a long dimension observed to be no greater than 2 mm and a narrow dimension which was found to be completely within 0.4 mm as determined by direct observation of the dependence of a Raman signal on the width of the spectrometer entrance slit.

The addition of the unstable resonator to the laser also increased the available power from the laser and slightly changed the character of the light pulse. Before the modification, about 95 mW of average power was measured near a

focus using a Scientech power meter with the laser at 80 kV, 44 mA, and 250 pps. With the unstable resonator installed and adjusted, the power at the same location and under the same conditions was about 165 mW. Figure 2 shows an oscilloscope trace of the laser pulse obtained using a high-speed photodiode. Without the resonator, the pulse was roughly Gaussian-shaped having a width of 11 nsec to 12 nsec at half maximum. With the resonator, the pulse appears, in Figure 2, to be slightly more triangular in shape with a width between 10 nsec and 11 nsec.

2.2 OPTICS CONFIGURATION

The layout of the laser and the optical components used to obtain the 90° scattering geometry with the combustion tunnel is shown in Figure 3. Optical access to the combustion environment is provided by two optical-grade-fused-quartz, 1.0-in thick windows which have clear apertures of 76 mm (3.0 in) by 305 mm (12 in). The positions of the laser and the laser-beam input lens L1 were chosen so that the long dimension of the beam just filled the 76-mm (3.0 in) diameter of the laser-beam output lens L2. The focal length of lens L2 was chosen as short as possible to minimize the sample volume while permitting vertical translation of the volume across the 25.4-cm-diameter (10 in) combustor pipe. Because of the complicated spatial pattern produced by the laser, an aperture is provided which can be used to shape the focused beam in the sample volume. This aperture, when used, becomes the object of lens L2 and can be used to reduce the ΔX dimension of the sample volume. Of course, there is a corresponding loss of available laser power when the aperture is used for this purpose. The lens L2 can be stopped down by two independently-adjustable aperture masks parallel to the long dimension of the window to prevent vignetting of the laser beam during remote operation. This

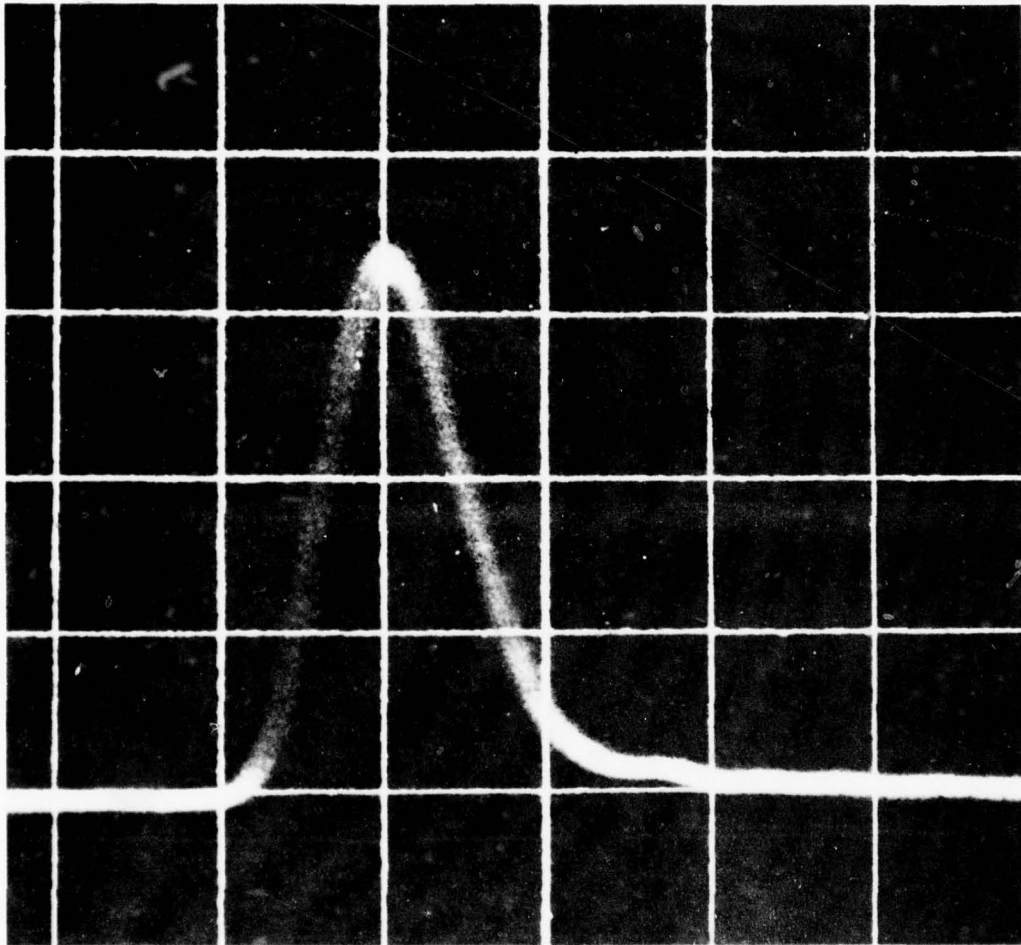


Figure 2. Oscilloscope Trace of the 3371-Å Laser Pulse with the Unstable Resonator Installed. (An ITT F4000 photodiode at 500 V was used. The AVCO C5000 nitrogen laser was operated with 8.0 kV at 44 mA and 250 pps giving 165 mW average power. Horizontal and vertical scales are respectively 10 nsec/div and 1.0 volt/div [into 50 Ω]).

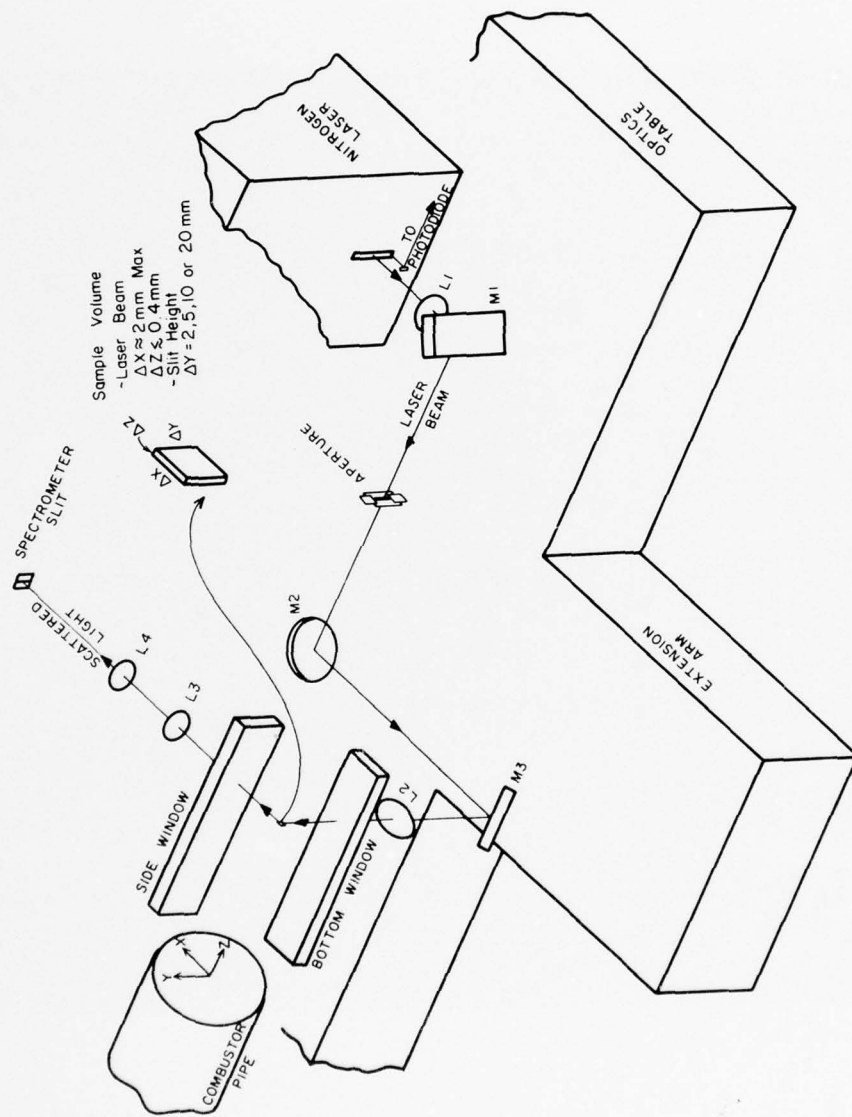


Figure 3. Optical Arrangement and Sample Volume Used in the Transceiver Unit of the Modified-LARS System. (The "combustor pipe" and the windows are parts of the combustion tunnel.)

feature is particularly useful when a region off the combustor axis is to be probed. Again, laser power is sacrificed when these masks are used.

The scattered-light collecting lens L3 has its focal point located at the sample volume. The resulting parallel beam is picked up by focusing lens L4 which images the light collected from the sample volume onto the spectrometer entrance slit. Thus, any X-axis translation of the sample volume, such as in off-axis measurements, can be followed simply by an adjustment of lens L3 along its axis. Lens L3 also is fitted with aperture masks similar to those on lens L2 which can be used to prevent vignetting of the top and bottom edges of the collected cone of light during remote operation.

A typical set of dimensions for the optics shown in Figure 3 are given in Figure 4. The aperture is shown shifted towards L1 somewhat from the focal point of L1. This was observed to be a point where the laser beam formed the smallest "image." This required that lens L2 be shifted slightly towards the window with the result being that the sample volume dimension ΔX was slightly smaller than the anticipated value. A list of the optical components shown in Figures 3 and 4 is given in Table 1. At present, the four lenses are not anti-reflection coated. As a result, 25% of the available light at the entrance slit is lost to reflections. If the windows are included, then about 35% of the available light is lost to surface reflections from the uncoated optics.

The region that can be probed by the optical arrangement shown in Figures 3 and 4 is somewhat restricted by the narrow aperture of the windows. The limits on the vertical (Y-axis) translation of the sample volume are determined by where the top and bottom edges of the side window cut into (vignette) the cone of light collected by the lens L3. With

TABLE 1. OPTICAL COMPONENTS USED IN THE MODIFIED-LARS SYSTEM

Lenses--Optical-Grade Fused Quartz, Uncoated

<u>Component</u>	<u>Label</u>	<u>Description</u>
Laser-beam input lens	L1	Two element (on hand) f.l. = 375 mm at 3371 Å diameter = 67 mm
Laser-beam output lens	L2	Bi-convex (Special Optics) f.l. = 219 mm at 3371 Å diameter = 76 mm
Collecting lens	L3 }	Bi-convex (Melles Griot) f.l. = 291 mm at 3658 Å diameter = 50 mm
Focusing lens	L4 }	

Mirrors--Planar, First-Surface Aluminum, Enhanced at 3371 Å

<u>Component</u>	<u>Label</u>	<u>Description</u>
First laser-beam mirror	M1	70 mm X 150 mm 20 mm thick
Second laser-beam mirror	M2	100 mm diameter 20 mm thick
Third laser-beam mirror	M3	114 mm diameter 20 mm thick

no reduction in the aperture of L3, the vertical range is about ± 23.5 mm. This range can be extended to about ± 27.5 mm by reducing the vertical aperture of L3 to 35 mm which results in a reduction of the signal by about 17%. The limits on the transverse (X-axis) position of the sample volume are determined by the long dimension of the laser beam at the bottom window. This dimension is about 36 mm which leaves about a ± 20 -mm range along the X axis. Although this range can be increased by shortening the long dimension of the beam with the aperture masks on lens L2, the loss in available laser power could be significant. No matter how small the apertures on L2 and L3 are made, the limits on the area that can be probed are ultimately fixed by the 76-mm (3-in) width of the two windows. The area that is accessible without use of the apertures is illustrated in Figure 5. The accessible area can be increased somewhat over that shown by using scattering angles other than 90° .

2.3 OPTICS TABLE

The main optics table which supports the optics, laser and spectrometer, is a research grade, steel honeycomb table fabricated by the Newport Research Corporation (NRC). The 8-in-thick table was cut to special dimensions of 145 x 145 cm for this application. The table incorporates a 3/16-inch-thick top surface of ferromagnetic stainless steel drilled and tapped for 1/4-20 screws on one-inch centers.

The table was modified at the University so that the extension arm shown in Figure 3 could be added to one side and vertical posts to support the spectrometer table could be mounted on another side. The platform which supports the spectrometer was made from a standard 2-1/4-inch-thick, honeycomb breadboard table fabricated by NRC. This 3x4-foot table includes a 1/8-inch-thick, ferromagnetic stainless-steel top surface drilled and tapped on 1-inch

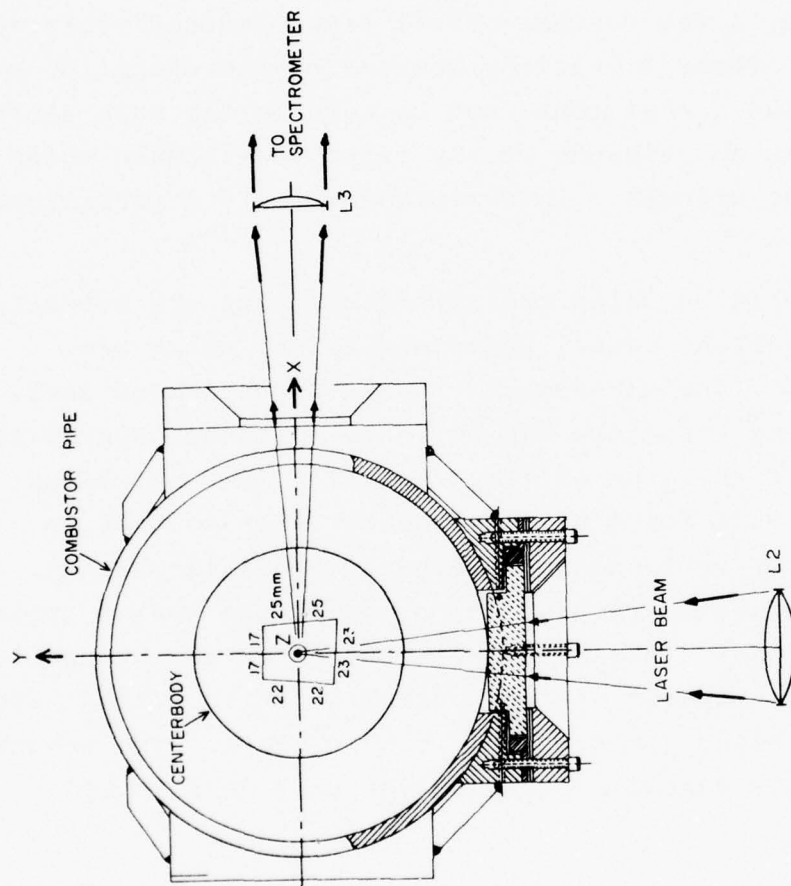


Figure 5. A Cross-Sectional View of the Combustion Tunnel Showing the Paths of the Optical Beams Through the Tunnel Windows. (The four-sided dimensioned figure around the Z axis is the area accessible to 90° scattering as determined by the beam dimensions and the window widths.)

centers for 1/4-20 screws. The magnetic surface on this table as well as on the main table is used to support the optical components with magnetic bases.

The main optics table is supported and isolated from floor-induced vibrations by four air-filled elastomer mounts. These mounts behave normally like air springs having a natural frequency of approximately 3 Hz and transmit only a few percent of all floor-induced vibrations above 3 Hz. Floor vibrations created by the operation of the combustion tunnel could not be felt on the main table and there was no evidence of any vibration-induced noise in any of the signals. This represents only a preliminary assessment.

The mounts on which the main table sits are supported by two angle-iron frames, upper and lower, which are separated by a 4000-lb-capacity hydraulic scissors jack. The supporting structure was designed to occupy approximately one half the area of the original LARS transceiver unit, to provide for mobility, and to allow for 610 mm (24 inches) of vertical adjustment in operating height. The upper frame carries the isolation mounts and optics table. The lower frame supports the scissors jack, the hydraulic system, and a portion of the controls. It is fitted with casters, leveling jacks, and lifting eyelets. The weight of the completely assembled transceiver unit is 1588 kg (3500 lbs).

The hydraulic system for the scissors jack is controlled by a Moog servo controller. The controller can be operated either automatically through the computer, or manually by a switch attached to the transceiver. A pair of rotary potentiometer-type feedback transducers are used to provide vertical and horizontal displacement information to the operator on the relative position of the sample volume with respect to the combustor. The outputs of these transducers

are digitized in tenths of a millimeter and displayed on two meters at the operator's station. The output of the vertical transducer also goes to the servo controller where it controls the automatic up/down scan of the scissors jack. Limit switches have been provided to control scan movements to within the limits of the vertical transducer. The maximum vertical range permitted by a given positioning of the transducer housing is 127 mm (5 in).

The main criteria for characterizing the performance of the automatic control of the table height are stability, repeatability, and accuracy. Preliminary observations indicated that short term (minutes) stability was ± 0.1 mm with long term (hours) stability being about ± 0.2 mm. The repeatability depends on whether the position is approached with the table rising or lowering. Generally, better control has been observed when the servo is driven to a position (i.e. rising) rather than going to that position by reducing the volume of oil in the hydraulic cylinder (i.e. lowering). Repeatability was usually better than ± 0.2 mm when rising and about twice that value when lowering. The accuracy depends for the most part on the calibration circuits in the control unit. If a calibration curve (meter reading versus relative table position) was determined at the beginning of a run sequence, it was generally observed that the calibrations should be checked once a week. Within a week of operation, the calibration was observed to hold within a range of about 0.3 mm.

The importance of these criteria depends on the size of the sample volume and the steadiness of the combustion environment being probed. In the preliminary measurements presented in this report, the flame was not only unsteady, on the scale of many millimeters in many cases, but it was also usually quite asymmetric. Since measurements made with a 2-mm-high slit did not yield analyzable data, a 10-mm or

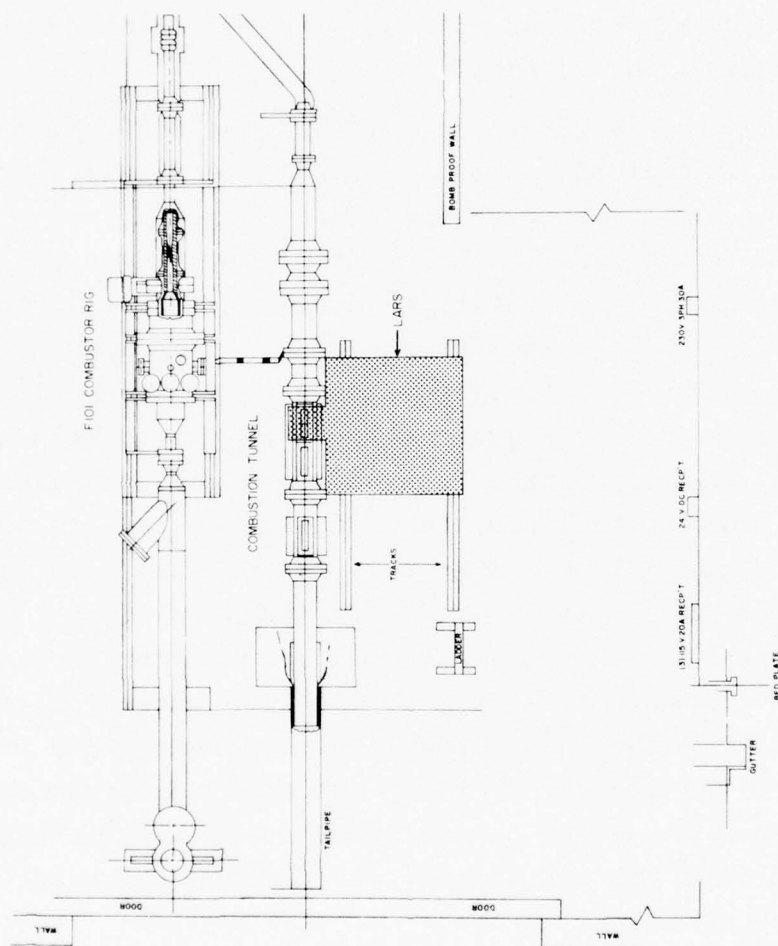


Figure 6. A Portion of the Floor Plan of Room 20 in Building 18 of AFAPL Showing a Typical Position of the Transceiver Unit at the first Optical Port of the Combustion Tunnel. (The tracks are 305-cm [10-ft] long.)

20-mm high slit was used. This dimension is sufficiently large compared to the above-cited uncertainties to make them of only minor importance to these measurements.

A typical position of the transceiver at the first window location is illustrated in Figure 6. Two sets of wheels are provided for rolling the transceiver. One set has solid rubber-band tires which were used to move the unit through the building from the unloading area to the combustion tunnel test cell in Building 18. The other set are grooved steel wheels that can roll on a track. The transceiver was fitted with these grooved wheels after it was positioned at the combustor and set on two parallel, 305-cm (10-ft) long tracks as shown in Figure 6. The tracks were positioned so that the transceiver could be moved parallel to the combustor axis. The movement of the transceiver on the tracks was easily accomplished by one person.

SECTION 3 MEASUREMENTS

Extensive Raman measurements were carried out on the plume of an afterburning J85-5 turbojet engine with the LARS system as originally designed.⁴ Extensive upgrading of the system performance was accomplished and completely new data-handling and analysis procedures for obtaining precise Raman temperatures were developed in the course of this work. Following the completion of the J85 measurements, the modifications discussed in Section 1 and 2 were implemented. Three types of measurement efforts have been carried out with the LARS system following the completion of the modifications. The first measurement efforts were made at the University of Dayton on a premixed flame from a capillary burner. After the LARS system was put into operation at the AFAPL combustion-tunnel facility, two basic types of measurement activities were carried out. These were temperature measurements obtained from Raman data and various measurements of the background spectra observed from the turbulent diffusion flame of the tunnel. These three efforts are reported in this section. In addition, the two methods used to calculate the temperature from Raman data are reviewed.

3.1 RAMAN THERMOMETRY TECHNIQUES

The approach to obtaining temperature measurements from Raman spectra used in these studies is based on resolving the spectral profile of the Stokes Q-branch Raman spectrum (i.e., the vibrational spectrum) of the nitrogen gas (N_2) in the combustion environment. It is assumed that the N_2 molecules being observed behave as non-interacting molecular probes in thermal equilibrium with their surroundings. To date this assumption appears valid. A brief review of the theory underlying this approach as well as a listing of

references on the subject has been given by Roquemore and Yaney.⁴ The two methods of utilizing the Stokes Q-branch spectral profile used in this work are discussed in the following sections. An effort was made to observe the anti-Stokes Q-branch spectrum of N_2 in the combustion tunnel. At best, the maximum Raman signal was about 30% of the background signal and the signal levels in general were about a factor of six smaller than the Stokes signals. No further anti-Stokes studies were pursued.

3.1.1 Computer-Fit Method

This method uses a chi-square (χ^2) minimization procedure to find the temperature for which the theoretical spectral profile best fits the experimental data. The data are in the form of a 40 to 60 equal-step wavelength scan of the Stokes N_2 spectrum centered about the first hot band at about 3653.8 Å. Although details concerning the method used have been covered by Roquemore and Yaney,⁴ it is useful to discuss certain aspects of the method here. The normal procedure for obtaining a fit is to first determine the effective instrument or slit function. This is done by fitting the slit parameters to a scan of a room-temperature spectrum of N_2 . These parameters account for the spectral width of the spectrometer slit settings and the spectral function of the laser output. This has to be done for each combination of slit settings and grating order used. The effective slit function is approximated in the calculations by a trapezoid given by the slit-bottom half-width (SBHW) and the slit top-to-bottom width ratio (STBWR) parameters. The full width at half maximum (FWHM) of the resulting effective spectral passband is given by $FWHM = SBHW(1 + STBWR)$. With the slit parameters determined, the temperature, the height and slope of the background, and a wavelength correction factor are fitted to the data. It is possible to include the slit parameters in the fitting

procedure; however, when the data are noisy, this occasionally results in totally unreasonable slit parameters which raises the question of the validity of the temperature fit.

The quantity χ^2 used here is the sum of the squares of the differences between the signal data and the theoretical values weighted (divided) by the variances of the data with the summation taken over all the scan steps. The computer code determines the parameter values which minimizes χ^2 . A useful criterion is the value of the reduced chi-square χ_r^2 which is χ^2 divided by the number of degrees of freedom in the fit. This number is simply the number of data values (steps) less the number of parameters fitted. The value of χ_r^2 is ideally one when the theoretical function is that function contained in the experimental data and when the variances used in calculating χ^2 totally account for the noise in the data. Deviations from either of these conditions will make $\chi_r^2 > 1.0$.

In most of the data presented in this report, the noise level was quite high and was not completely accounted for in the variance values used. Generally, the variances used were determined from Poisson statistics where the variance equals the photoelectron count. The recorded datum values were not photoelectron counts but were digital counts on a scale determined by the charge-digitizing instrumentation to which the 8850 photomultiplier tube (PMT) was connected. The observed count depended on the PMT voltage; however, studies of the observed count statistics for a known source indicated that one photoelectron on the average was equal to about 250 observed counts. This factor was used to convert all observed data to photoelectron counts from which the variances and χ_r^2 values were determined. Thus, the goodness of the fit is reasonably given by how close χ_r^2 is to unity.

In the computed-fitted combustion-tunnel data presented in this report, $\chi_r^2 \geq 3.0$. Two conditions were observed which contributed to these large values of χ_r^2 . First of all, it was discovered that the mercury-vapor lamps used to light the room housing the combustion tunnel introduced a spurious spectrum in the observed data. This condition existed during the runs of 30 June through 18 July 1978. The runs prior to 18 July were carried out using the third-order spectrum. A Corning CS7-54 ultraviolet-transmitting, visible-blocking filter was used to remove the low-order spectra in these runs; however, the spurious spectrum was apparently due to some accidental specular reflection of the near-ultraviolet emission lines of the mercury vapor. After 6 July, the first order spectrum was used. Although the intensities of the spurious features were reduced, they were still observed. After 18 July the room lights were turned off during the times when Raman data was recorded and the spurious spectrum was no longer observed.

The second condition contributing to large χ_r^2 values was the apparent unsteadiness of the combustion zone in the tunnel. Specifically, the flame almost always appeared visually to be asymmetrical and to rotate or fluctuate around or about the axis of the combustor pipe. The unsteadiness was so large that, coupled with the high laser-induced background, it was not possible to use a 2 mm slit height on the spectrometer due to the large excursions observed in the data. The circumstance was greatly alleviated by using 10-mm and 20-mm slit heights. Such large spatial extents over an unsteady combustion region raises the question of the meaning of the resulting temperature fits. An optimistic speculation would be that they represent some sort of average temperature.

The computer code also generates the standard deviations (SD's) in the values of the parameters fitted at the χ_r^2

minimum.⁵ The relationship between χ_r^2 and the SD's is not simple. For example, the spurious spectrum discussed above will make χ_r^2 large because this spectrum is not included in the theoretical spectrum being fitted to the data. On the one hand, the dependence of χ_r^2 on temperature may be quite sharp giving a small temperature SD. On the other hand, a large noise level would not only increase χ_r^2 but also the SD values of the fitted parameters. These features in the fits to the data are discussed in Section 3.2.2.

It is of particular interest to determine how the laser-induced and non-laser-induced backgrounds contribute to the temperature SD. As is discussed in the next section, the ratio, V , of the hot-band Raman signal to the main-peak Raman signal is a linear function of temperature between about 1000 and 3000°K for the effective slit functions used in these studies.⁴ Thus, it is possible, assuming Poisson statistics, to calculate a temperature SD value and the contributions of the two backgrounds to this value. The ratio of this SD value to the computer-generated temperature SD can be used to scale the background contributions to the computer result. It was found that this scale factor was about $\sqrt{6}$ which suggests that the computer fit is approximately equivalent to six independent temperature measurements using the four-wavelength method described in the next section. It must be recognized that this calculation gives only an approximate measure of the background contributions to the temperature SD since any extraneous source of temperature uncertainty will be absorbed, at least in part, into the background values determined in this manner. What this scheme does provide is a reasonably self-consistent basis for comparing Raman temperature measurements using different methods.

An example of a typical computer fitting is given in the Appendix. The run was on 26 July 1978 at the time of

2143 (9:43 pm). The raw data is prepared for the fitting program called TEMP by the program DATIN. DATIN formats the raw data, adds all the parameters which define the experimental conditions (e.g., diffraction order), specifies which parameters are to be fitted, and provides starting values for these parameters. This is the first listing given in the Appendix and represents the input to TEMP. The output of TEMP is provided in tabular and graphical forms. The second listing in the Appendix is the final results of the fit followed by the tabulated experimental and calculated (i.e., fitted) datum values. These values are presented both in the form of digital counts per laser pulse and in the form normalized to the maximum of the calculated spectrum. The background fitted to the data and the datum SD values used in calculating χ_r^2 called ERRORS in the table are also given. The third listing includes two graphs of the data given in the previous table. The first graph has a linear data scale (ordinate) while the second graph has a logarithmic scale. Three curves are plotted in each graph. The experimental data is labelled E, the calculated spectrum is labelled C, and the calculated background is labelled B.

3.1.2 N-Wavelength Method

The Stokes Q-branch Raman spectra of N_2 calculated for six temperatures are shown in Figure 7. These spectra show how the intensity of the first hot band ($v = 1$) increases with temperature relative to the main-peak intensity ($v = 0$). The ratio, V , of the intensities ($v = 1$ to $v = 0$) is a linear function of the temperature, T , over the range of about 1000 to nearly 3000°K. The actual range, the degree of linearity, and the particular slope and intercept values depend on the effective slit function and its FWHM value. These values can be easily obtained from a set of spectra calculated with a specific slit function. The primary obstacle in using this relationship is in determining

the portion of the signals recorded at the hot band and main peak wavelengths that are due only to the Raman spectrum. That is, the background values at these wavelengths must be deduced.

Basically, the N-wavelength ($N-\lambda$) method is based on the assumption that the background values at the $v = 0$ and $v = 1$ wavelengths can be found by fitting a smooth curve to background values measured on the two sides of the spectra shown in Figure 7. Two values of the $N-\lambda$ measurements are taken at the $v = 0$ and $v = 1$ wavelengths. This is generally at or near 3657.4 and 3653.8 Å, respectively, for an incident laser wavelength of 3371 Å. If the background curve is assumed linear, then only two additional measurements will fix the background values at these two wavelengths by linear interpolation. These two additional measurements must be made sufficiently distant from the Raman spectrum such that no part of the effective slit function includes or overlaps this spectrum. Thus, measurements of the signals at four wavelengths can determine a value of V and hence T . This is the $4-\lambda$ method.

Referring to Figure 7, it is clear that the background measurements should be made at >3660 and <3647 Å. The spacing between the main peak and the first hot band is approximately 3.6 Å. It was found convenient to step in intervals of 3.6 Å with the first value at 3646.6 Å and the last (i.e., fourth) value at 3661.0 Å. The value at the second hot band ($v = 2$) was not used. Since the SBHW was usually less than 1.6 Å, the choice of 3.6 Å steps insured that the background measurements did not include the Raman Q-branch spectrum. However, such measurements do include the O- and S-branch spectra (due to vibrational-rotational transitions) which extend many angstroms on both sides of the Q branch. Since these spectra are usually on the order of only 1 to 3% of the Q-branch intensities we have

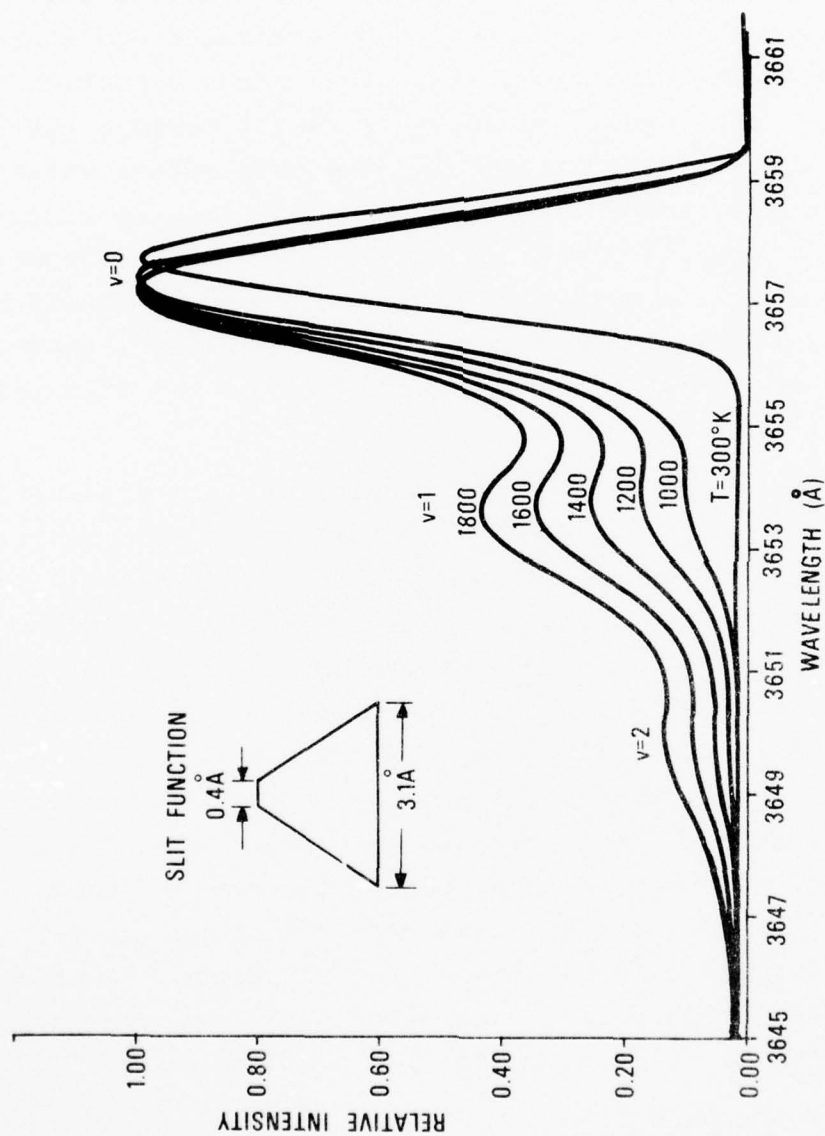


Figure 7. Calculated Stokes Q-Branch Spectra of N₂ for 3371 Å Excitation and an Arbitrary Trapezoidal Slit Function. (The spectra are plotted on a scale for which the intensity of each main peak ($v=0$) is normalized to unity. Figure taken from Reference No. 4.)

neglected their influence on the $N-\lambda$ data presented in the following sections.

The analyses presented in this report using the $N-\lambda$ method for run dates through 18 July contain a bias due to the spurious spectrum mentioned in the previous section. The magnitude of this bias cannot be estimated and there is reason to believe that there were run-to-run variations in the magnitude. Nevertheless, it is fairly certain that the bias had the effect of increasing the temperature values calculated from the data. This is because the spurious spectrum introduced a peak in the vicinity of the first hot band. Thus, the accuracy of these measurements cannot be specified; however, the measurements do provide a test of the technique and they can be examined from the standpoint of reproducibility.

The $4-\lambda$ method is clearly the simplest of a number of variations that can be used which fall within the generic class of the $N-\lambda$ method of temperature measurements. One variation used here involved making four measurements of the background, two on each side of the Raman spectrum. Again, the 3.6 \AA interval was used. The averages of the two pairs of measurements were first calculated. These values, assuming a linear background gave background values at the mean wavelengths of the corresponding measurements. These two sets of values were then used to compute the background values at the hot band and main peak following the $4-\lambda$ method. This is referred to as the $6-\lambda$ method. Basically, this approach reduces the uncertainties in the background measurements by $\sqrt{2}$ assuming Poisson statistics.

3.1.3 Error Analysis

The computer-fit method provides uncertainties in the fitted parameters as part of the fitting code.⁵ The $N-\lambda$ method can be analyzed in a straightforward way if Poisson statistics are used. This analysis provides an additional

feature in that it can give the contributions to the temperature uncertainty which arise from the laser-induced background, B' , and the non-laser-induced background, B'' . As described in Section 3.1.1, this analysis can also be applied to the computer-fitted results to give the corresponding breakdown in the sources of temperature error in those measurements.

The temperature, T , is related to the hot-band-to-main-peak Raman signal ratio, V , by

$$T = T_0 + mV \quad (1)$$

where T_0 is the temperature intercept at $V = 0$ and m is the slope. The temperature SD, σ_T , is given by

$$\sigma_T = \{\sigma_0^2 + (mV)^2 [(\sigma_V/V)^2 + (\sigma_m/m)^2]\}^{\frac{1}{2}} \quad (2)$$

where σ_0 , σ_V , and σ_m are the SD's respectively in T_0 , V , and m . Generally, σ_0 and σ_m range between 0.5 and 1.0% of T_0 and m , respectively, and, as such, represent upper limits to the accuracy of the N- λ method. The main source of uncertainty is σ_V which can be written, assuming Poisson statistics, as

$$\sigma_V/V = [(R_1 + 2B_1)/R_1^2 + (R_0 + 2B_0)/R_0^2]^{\frac{1}{2}} \quad (3)$$

where R and B respectively identify the Raman and background signals, and the subscripts 1 and 0 respectively identify the hot band and main peak values. The factor two multiplying the background arises from the fact that the Raman part of the signal can only be obtained by first subtracting the background from the observed datum. The background values are the sums of the two background sources, thus

$$B_1 = B_1' + B_1'' \quad \text{and} \quad B_0 = B_0' + B_0'' \quad (4)$$

In actuality, the non-laser-induced background is measured separately, 0.6 msec after each laser pulse, and is usually only a small fraction of the laser-induced value. Thus, those parts in Equation (3) which arise from the two backgrounds can be separated out and their contributions to σ_T can be calculated.

3.2 RAMAN MEASUREMENTS

The LARS system was checked out using a pre-mixed flame from a capillary burner. The measurement effort was limited being intended only to demonstrate the operation of the system. The results are summarized here to illustrate a typical temperature-profile measurement.

After the system was moved to the combustion tunnel facility at the AFAPL, a wide range of Raman measurements were carried out. The data and results from these measurements are presented here in tabular form. Because of the unsteadiness of the flame, very few radial (i.e., transverse) profile data were obtained. Some effort was made to measure axial profiles; however, the main thrust of the studies was on the temperature-measurement capabilities as a function of the fuel and air flow rates.

3.2.1 Capillary Burner

The horizontally-mounted capillary burner used in these studies consisted of water-cooled inner and outer burners surrounded by an argon sheath.⁶ Both acetylene and propane fuels were used. The air-acetylene flame was 15 to 20 cm in length and orange in color while the air-propane flame was 2 to 4 cm in length but very clear and blue.

The measurements made on the air-propane flame were at about 1 cm from the burner face using a 5-mm-high slit.⁷ Continuous step-scans of the N_2 spectrum were made at

five vertical profile positions in the flame. The scans took 6.8 minutes each. The data were computer-fitted using the appropriate slit parameters. The temperature profile had a maximum of $1862^{\circ}\text{K} \pm 4.2\%$ at about 7 mm below the burner axis. The temperature dropped to $1270^{\circ}\text{K} \pm 2.4\%$ at 14 mm below the axis. On the axis the temperature was $1545^{\circ}\text{K} \pm 4.5\%$ but dropped sharply 7 mm above the axis to $523^{\circ}\text{K} \pm 3.4\%$. It increased to $1762^{\circ}\text{K} \pm 3.2\%$ at 14 mm above the axis. The χ_r^2 values for the fits were about 2.0 or less. The flame was rather structured due to the low flow rates that were required to obtain a blue flame. Also, there were additional contributions to this structure by the separately-controlled inner and outer parts of the burner. These features support the 523°K value given above which indicates that a relatively cold region was present in the flame. The maximum value reported above is consistent with the temperature expected for this burner under the given operating conditions.⁸ These measurements using propane fuel were carried out to insure that the excessive background signals experienced with acetylene were in no way due to a malfunction or misalignment in the LARS system.

The burner was operated primarily with acetylene fuel. The flame was characterized by a strong orange color which contributed not only a noticeable non-laser-induced background but also a very large laser-induced background. This orange color is apparently characteristic of phosphine which is a common impurity in commercial acetylene.⁹ Attempts were made to obtain a supply of the fuel with less impurities but these were of no avail. A trap could have been constructed which would have cleaned the fuel, but this was not done.⁹

Although the background signals were more than twice the strength of the hot band (i.e., the Raman signal at the peak of the first hot band), it was possible to perform pro-

file measurements by summing the signals over 10,000 laser pulses and using the $4-\lambda$ method.

The time to acquire the data for each temperature measurement was 2.7 minutes. The results of these measurements¹⁰ are summarized in Table 2. Because of the 10-mm slit height, the measurements at the +20-mm position include relatively cool air in a portion of the sample volume. The data show that both of the background-induced temperature error contributions form a well-defined profile across the flame which characterizes the fluorescence and self-luminosity of the flame. Although the temperature SD values are rather large, the temperature values are in good agreement with the expected values.^{8,11} The temperature results are presented in graphical form in Figure 8. The plot shows the center of the temperature profile to be lower than the centerline of the burner as was observed with the propane fuel. This could be due to a slight misalignment; however, it also may be due to an asymmetric flow of argon and the surrounding air around the flame due to its horizontal attitude. The effect of the inner and outer burners is clearly evident in the triple-peaked shape of the profile.

The constants of Equation (1) used to convert the ratio V to temperature in Table 2 were

$$\begin{aligned} T_0 &= 810.9^\circ\text{K} \pm 0.46\% & \text{and} \\ m &= 2415.6^\circ\text{K} \pm 0.35\%. \end{aligned} \quad (5)$$

These values were obtained from a least-squares fit to data acquired from 14 theoretical calculations of the Raman spectrum using the effective slit function defined by

$$\begin{aligned} \text{SBHW} &= 1.3541 \text{ \AA} & \text{and} \\ \text{STBWR} &= 0.04935. \end{aligned} \quad (6)$$

The range of the calculations covered from about 1300 to 2500°K. The slit function was fitted to a third-order,

TABLE 2. TRANSVERSE TEMPERATURE PROFILE OF A HORIZONTAL-MOUNTED, AIR-ACETYLENE CAPILLARY BURNER (ARGON SEPARATED) OBTAINED FROM FOUR-WAVELENGTH RAMAN MEASUREMENTS^a

Position (mm)	Signal ^c		Background ^{c,d}		Ratio ^e V	Temperature ^f		Bkgnd-Induced Temperature SDF	
	Main Peak (c/p)	Hot Band (c/p)	Laser- Induced (c/p)	Non- Laser (c/p)		(°K)	SD (%)	Laser- Induced (%)	Non- Laser (%)
+20	118.13	10.64	3.80	2.4	0.0598	955	1.5	1.0	0.6
+15	63.79	27.22	18.41	3.4	0.1942	1280	4.8	4.1	1.4
+10	52.78	40.04	26.75	5.9	0.5105	2044	7.1	5.9	2.3
+5	50.94	38.41	26.16	6.1	0.4944	2005	7.5	6.2	2.5
0	44.69	36.66	25.61	7.9	0.5792	2210	9.1	7.5	3.4
-5	44.27	34.80	22.74	8.3	0.5603	2164	7.9	6.3	3.1
-10	43.85	32.48	23.22	7.7	0.4487	1895	8.8	7.3	3.4
-15	40.22	29.31	15.98	3.2	0.5502	2140	6.1	4.8	1.8

^a The third order spectrum, a CS 7-54 filter, and slit FWHM = 1.42 Å were used with 10,000 laser pulses per measurement at 250 pps.

^b Measured along the vertical diameter about 40 mm from the burner face. Burner centerline at 0 mm and flame diameter about 40 mm. Position values below centerline are negative. Position resolution was $\Delta Y = 10$ mm.

^c Main peak and hot band values measured respectively at 3657 and 3654 Å. c/p = average digital counts per laser pulse.

^d Laser-induced background is average of values measured at 3660 and 3648 Å. Non-laser-induced background was measured 0.6 ms after each laser pulse. Value given was measured at hot band wavelength.

^e $V \equiv (\text{hot-band Raman signal})/(\text{main-peak Raman signal})$.

^f The SD values are the estimated standard deviations calculated using Poisson statistics. See text.

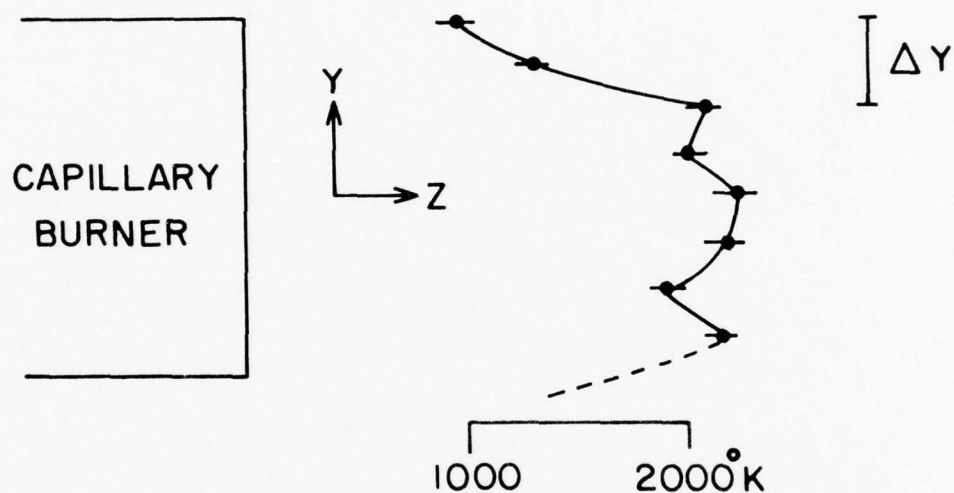


Figure 8. Measured Temperature Profile of a Horizontal, Pre-Mixed, Acetylene-Air Flame with an Argon Sheath Produced by Two Concentric Capillary Burners. (The resolution element, $\Delta Y = 10$ mm. The data are given in Table 2.)

room-temperature scan of the N_2 Raman spectrum using an entrance slit of 0.7 mm, a center slit of 1.0 mm, and an exit slit of 1.0 mm of the SPEX spectrometer. Actually, the entrance slit width was essentially source-limited since the image width at the entrance slit was about 0.4 mm.

3.2.2 Combustion Tunnel

The turbulent diffusion flame was produced using annular air flow around an 140-mm-diameter (5.5 in) cylindrical, bluff centerbody fitted with a 25.4-mm-diameter axial fuel tube. The centerbody was mounted on the axis of a 25.4-cm-diameter (10 in) pipe. During the period of about 29 June through 28 July 1978, various measurements were carried out on the operating tunnel. On at least eight of the days in this period, Raman measurements were attempted. Useful data were obtained on six of these days.

There were two significant obstacles to obtaining useful Raman data. These were a very large laser-induced background and an unsteady flame. The background is discussed in detail in Section 3.3. The unsteady flame resulted largely from an apparent lack of sufficient mixing of the fuel and air. This characteristic is related to the design of the centerbody and fuel tube. Although design changes were attempted by AFAPL personnel during the period of the Raman measurements, no significant change was made in the nature of the flame. Basically, the flame had a turbulent appearance, very coarse in texture, where the coarseness was due to fluctuating regions of yellow or orange color. At high fuel-to-air ratios the flame became quite orange-yellow in color and usually asymmetric in shape about the tunnel axis. At the leanest conditions with high air flow, the flame would extend beyond the second set of windows (~ 70 cm) and would tend to be more blue in color. At lower air flows, the flame would extend to the region between the first and second set of windows (~ 40 cm). The

coarse texture of the flame usually was on a scale of a few millimeters. This feature produced a fluctuation in the observed signals that made the 2-mm and 5-mm slit heights totally unusable. By using the 10-mm and 20-mm heights, these fluctuations were greatly reduced by the integration of the spatial variations over the slit length.

Generally, the background-to-Raman ratio, B/R, tended to follow the overall fuel-to-air ratio for a given position in the combustor. Similarly, the B/R was highest near the face of the centerbody and decreased as the distance from the face increased. Presumably, the hot, incompletely burned fuel was the primary source of the laser-induced background. Measurements were made on the air alone and on the un-ignited fuel alone. These measurements showed no evidence of the strong laser-induced background observed in the flame. The combination of a low-sooting fuel and a moderate-power laser beam (about 8 MW/cm^2 at focus) reduced the possibility of laser-induced incandescence of soot particles as a source of the background.

The fuel used was primarily natural gas (methane). However, a few measurements were carried out using propane. The propane flame gave a more steady flame and was less orange-yellow and more blue in color than the natural-gas flame. Correspondingly, the background level with propane was lower than with natural gas by about a factor of two. It was not possible to make detailed Raman measurements using the propane fuel due to an insufficient supply of the fuel.

Four sets of measurements are presented in Tables 3 through 10. Tables 3, 5, 7, and 9 give the combustion conditions provided by AFAPL, the positions of the sample volume, and the measured temperatures. For a given fuel, the equivalence ratio, ϕ , is directly proportional to the fuel-to-air ratio. Tables 4, 6, 7, and 10 give the Raman

TABLE 3. COMBUSTION TUNNEL TEMPERATURES WITH NATURAL-GAS FUEL OBTAINED FROM COMPUTER-FITTED RAMAN SCANS.

Date	Time	Fuel (lb/hr)	Air (lb/sec)	ϕ^a	Position ^b		Temperature ^c		Goodness ^d of Fit
					Axial (mm)	Radial (mm)	(°K)	SD (%)	
06/30/78	1826	9.84	4.965	0.0095	86	0	1579	6.7	7.1
	1859	9.51	4.962	0.0092	46	0	2186	1.9	31
	1924	10.11	4.939	0.0098	46	0	1835	4.9	11
	1945	10.31	4.938	0.0100	126	0	1412	2.8	3.0
07/05/78	2041	18.13	7.243	0.0120	35	0	2071	4.0	3.7
07/06/78	1935	16.39	7.207	0.0109	35	0	1721	3.1	14
07/18/78	1939	9.44	1.620	0.0280	175	0	1753 ^e	2.5	11
	2052	5.28	2.481	0.0102	175	0	1486 ^e	2.4	17
	2122	5.46	2.487	0.0105	175	0	no fit		----
07/24/78	1902	11.30	1.818	0.0298	175	0	1060	8.6	5.4
	1944	11.25	1.826	0.0296	175	-20	2230	2.9	9.4
	2120	7.19	2.526	0.0137	175	0	1092	2.3	8.4
	2208	6.71	2.521	0.0132	175	+20	1091	3.2	6.4
07/26/78	2143	7.63	3.609	0.0102	95	0	1195	5.9	3.0
	2215	7.58	3.638	0.0100	95	-8	1297	4.8	3.4

^a Equivalence ratio.

^b Axial position was measured along centerline and from the face of the centerbody. Radial position was measured up (+) or down (-) from the centerline. Centerbody diameter = 140 mm. Radial resolution, $\Delta Y = 10$ mm on 06/30/78, 07/05/78, and 07/06/78 with remainder at $\Delta Y = 20$ mm. See Figures 3 and 5.

^c The SD value is the standard deviation of the temperature fit. See Table 4 and text.

^d Reduced chi-square χ_r^2 of fit.

^e Slit parameters were included in the fitting procedure.

AD-A076 514

DAYTON UNIV OH RESEARCH INST
COMBUSTION DIAGNOSTICS USING LASER SPONTANEOUS-RAMAN SCATTERING--ETC(U)
APR 79 P P YANEY
F33615-76-C-2078

UNCLASSIFIED

AFAPL-TR-79-2035

NL

2 OF 2
ADA
076514



TABLE 4. RAMAN DATA FOR COMBUSTION TUNNEL RUNS GIVEN IN TABLE 3

Date	Time	PMT Voltage (kV)	Slit ^a FWHM (Å)	Signal ^b		Background ^b			Bkgnd-Induced Temp SD ^c		No. of Steps Scand
				Main Peak (c/p)	Hot Band (c/p)	Laser-Induced Main Pk (c/p)	Hot Bg (c/p)	Non- Laser (c/p)	Laser Induced (%)	Non- Laser (%)	
06/30/78	1826	1.95	1.42	68.3	56.3	41.2	43.2	2.2	6.1	0.8	42
	1859	1.95	1.42	72.3	50.3	11.7	20.3	1.7	1.3	0.2	46
	1924	1.95	1.42	77.1	65.6	48.8	49.5	1.7	4.5	0.4	51
	1945	2.00	1.42	52.9	25.5	16.8	17.2	2.5	2.4	0.5	51
07/05/78	2041	2.05	1.42	58.7	51.0	34.3	34.4	3.7	3.5	0.6	61
	1935	2.05	1.42	78.5	54.2	38.3	39.0	3.3	2.8	0.4	61
07/18/78	1939	2.05	2.21	68.9	47.7	30.4	31.0	1.0	e		51*
	2052	2.10	1.31	114.4	74.6	48.8	49.1	0.7	e		51
	2122	2.10	----	105.6	56.6	38.7	41.2	0.7	no fit		51
07/24/78	1902	2.10	1.64	153.0	122.3	117.8	116.6	1.2	8.5	0.5	61
	1944	2.10	1.64	138.6	107.5	85.2	84.3	1.0	2.7	0.2	81
	2120	2.10	1.64	94.0	35.8	25.9	26.0	0.7	2.0	0.2	95
	2208	2.10	1.64	92.9	44.2	31.2	31.8	0.7	2.8	0.2	51
07/26/78	2143	1.80	1.89	144.1	116.3	110.3	111.0	1.2	5.8	0.3	55*
	2215	1.80	1.89	113.9	85.8	74.8	76.8	1.1	4.6	0.3	39*

^a Slit height was 10 mm on 06/30/78, 07/05/78, and 07/06/78. Remainder was with 20 mm.

^b c/p = average digital counts per laser pulse.

^c Estimated standard deviations calculated using Poisson statistics. See text.

^d Wavelength steps were 0.3 Å. Third order spectrum was used on 06/30/78, 07/05/78, and 07/06/78. Remainder was first order. Number of laser pulses per step was 4000 at 250 pps except * = 8000 pulses. All third-order measurements were made using a CS 7-54 filter.

^e Computer-fitted slit parameters do not permit error analysis.

TABLE 5. COMBUSTION TUNNEL TEMPERATURES WITH NATURAL-GAS FUEL
OBTAINED FROM FOUR-WAVELENGTH RAMAN MEASUREMENTS TAKEN
ON 5 JULY 1978

Time	Fuel (lb/hr)	Air (lb/sec)	ϕ^a	Position ^b		Temperature ^c	
				Axial (mm)	Radial (mm)	(°K)	SD (%)
2110	18.10	7.232	0.0120	35	0	1984	17
2117	19.72	7.235	0.0131	35	0	1578	35
2121	21.75	7.234	0.0144	35	0	1811	30
2126	26.42	7.210	0.0176	35	0	1934	51
2130	24.32	7.223	0.0162	35	0	1581	39
2142	24.28	7.243	0.0161	105	0	1401	95
2146	21.98	7.264	0.0145	105	0	1320	29
2152	18.25	7.256	0.0121	105	0	1818	15
2206	18.12	7.237	0.0120	175	0	1369	7.1
2211	22.18	7.238	0.0147	175	0	1463	8.6
2215	23.77	7.236	0.0158	175	0	1813	11
2221	25.65	7.234	0.0170	175	0	1464	13

^a Equivalence ratio.

^b Axial position was measured along centerline and from the face of the centerbody. Radial position was measured up (+) or down (-) from the centerline. Centerbody diameter = 140 mm. Radial resolution, $\Delta Y = 10$ mm. See Figures 3 and 5.

^c The SD values are the estimated standard deviations calculated from the data using Poisson statistics. See Table 6 and text.

TABLE 6. RAMAN DATA FOR COMBUSTION TUNNEL RUNS OF 5 JULY 1978 GIVEN IN TABLE 5

Time	PMT Voltage (kV)	Signal ^a		Background ^a					Ratio ^b V	Bkgnd-Induced Temp SD ^c	
		Main Peak (c/p)	Hot Band (c/p)	Laser-Induced		Non- Laser (c/p)	Laser Induced (%)	Non- Laser (%)			
				Main Pk (c/p)	Hot Bd (c/p)						
2110	2.05	50.50	41.31	32.44	32.54	3.5	0.486	15.1	2.6		
2117	2.00	55.84	47.80	44.54	44.21	3.3	0.318	33	4.8		
2121	2.00	76.59	67.93	62.58	62.13	2.9	0.414	29	3.3		
2126	1.95	87.82	84.99	79.02	80.90	2.1	0.465	50	4.2		
2130	1.95	74.61	66.77	62.81	63.01	1.7	0.319	38	3.3		
2142	2.00	65.83	62.28	60.63	61.01	3.1	0.244	94	11		
2146	2.05	68.79	57.79	51.33	54.11	4.4	0.211	28	4.2		
2152	2.10	55.94	44.05	34.48	35.10	3.9	0.417	14	2.5		
2206	2.10	44.56	17.03	8.86	8.78	6.7	0.231	5.3	2.4		
2211	2.10	41.78	20.41	11.52	12.24	6.0	0.270	7.0	2.6		
2215	2.10	36.76	23.80	14.44	14.54	5.4	0.415	8.7	2.8		
2221	2.10	42.80	25.19	19.45	18.88	6.6	0.270	11.0	3.5		

^a Main peak and hot band values were measured respectively at 3657.4 Å and 3653.8 Å. Slit height = 10 mm and FWHM = 1.42 Å. Wavelength steps were 3.6 Å with 4000 laser pulses per step at 250 pps. The third-order spectrum was used with a CS 7-54 filter. c/p = average digital counts per laser pulse.

^b $V \equiv (\text{hot-band Raman signal})/(\text{main-peak Raman signal})$.

^c Estimated standard deviations calculated using Poisson statistics. See text.

TABLE 7. COMBUSTION TUNNEL TEMPERATURES WITH NATURAL-GAS FUEL OBTAINED FROM FOUR-WAVELENGTH RAMAN MEASUREMENTS TAKEN ON 6 JULY 1978

Time	Fuel (lb/hr)	Air (lb/sec)	ϕ^a	Position ^b		Temperature ^c	
				Axial (mm)	Radial (mm)	(°K)	SD (%)
1917	9.86	4.827	0.0098	35	0	2789	19
1921	10.52	4.820	0.0105	35	0	d	
1926	8.69	4.780	0.0087	35	0	1843	29
1957	9.23	4.858	0.0091	35	0	3097	11
2000	8.75	4.864	0.0086	35	0	1866	11
2028	8.81	4.858	0.0087	105	0	1254	12
2032	8.79	4.863	0.0087	105	0	1517	11
2038	10.22	4.856	0.0101	105	0	d	
2050	10.61	4.929	0.0103	175	0	1054	4.3
2053	10.59	4.849	0.0105	175	0	1016	5.2
2101	15.50	4.820	0.0154	175	0	1424	16
2103	15.60	4.844	0.0155	175	0	1583	14
2108	15.50	4.821	0.0154	175	0	2423	20
2113	15.33	4.816	0.0153	175	+20	d	
2149	9.78	3.604	0.0130	35	0	d	
2153	7.03	3.599	0.0094	35	0	d	
2157	5.76	3.603	0.0077	35	0	2372	18

^a Equivalence ratio.

^b Axial position was measured along centerline and from the face of the centerbody. Radial position was measured up (+) or down (-) from the centerline. Centerbody diameter = 140 mm. Radial resolution, $\Delta Y = 10$ mm. See Figure 3 and 5.

^c The SD values are the estimated standard deviations calculated from the data using Poisson statistics. See Table 8 and text.

^d No temperature calculation possible due to a weak Raman signal. See Table 8.

TABLE 8. RAMAN DATA FOR COMBUSTION TUNNEL RUNS OF 6 JULY 1978 GIVEN IN TABLE 7

Time	PMT Voltage (kV)	Signal ^a		Background ^a				Ratio ^b V	Bkgnd-Induced Temp SD ^c	
		Main Peak (c/p)	Hot Band (c/p)	Laser-Induced		Non- Laser (c/p)	Laser Induced (%)		Non- Laser (%)	
				Main Pk (c/p)	Hot Bd (c/p)					
1917	2.00	101.68	95.86	81.70	79.50	1.8	0.819	17.8	1.4	
1921	1.95	83.29	72.91	68.47	73.78	2.1	d	27	d	
1926	1.95	48.04	38.30	37.20	33.67	1.8	0.427		3.3	
1957	2.05	63.72	62.24	38.96	38.81	2.9	0.946	9.6	1.4	
2000	2.05	75.55	54.26	43.15	40.11	2.7	0.437	9.8	1.3	
2028	2.05	59.78	31.61	27.67	25.72	3.2	0.183	10.9	2.0	
2032	2.05	61.70	38.72	30.39	29.57	3.2	0.292	10.2	1.8	
2038	2.00	72.77	48.99	53.57	52.53	2.1	d		d	
2050	2.00	63.65	11.42	5.22	5.53	2.1	0.101	3.3	1.1	
2053	2.00	55.18	10.58	6.21	6.42	2.0	0.0850	4.4	1.3	
2101	2.00	60.68	42.89	36.44	36.74	3.3	0.254	15.5	2.4	
2103	2.00	58.72	43.48	33.50	35.42	2.4	0.320	13.3	1.8	
2108	2.00	53.56	49.00	38.92	39.23	2.6	0.667	18.1	2.5	
2113	1.95	98.00	87.28	91.32	88.12	1.5	d		d	
2149	1.80	214.74	243.44	223.62	216.55	0.5	e		e	
2153	2.00	131.45	115.95	124.51	138.24	2.2	e		e	
2157	2.05	77.69	58.93	59.79	47.36	2.3	0.646	17.1	1.9	

^a Main peak and hot band values were measured respectively at 3657.4 Å and 3653.8 Å. Slit height = 10 mm and FWHM = 1.42 Å. Wavelength steps were 3.6 Å with 4000 laser pulses per step at 250 pps. The third-order spectrum was used with a CS 7-54 filter. c/p = average digital counts per laser pulse.

^b V (hot-band Raman signal)/(main-peak Raman signal).

^c Estimated standard deviations calculated using Poisson statistics. See text.

^d No meaningful calculation possible due to a very weak Raman signal.

^e The Raman signal was too weak and the background too strong to permit a meaningful calculation.

TABLE 9. COMBUSTION TUNNEL TEMPERATURES WITH NATURAL-GAS FUEL
OBTAINED FROM SIX-WAVELENGTH RAMAN MEASUREMENTS TAKEN
ON 24 JULY 1978

Time	Fuel (lb/hr)	Air (lb/sec)	ϕ^a	Position ^b		Temperature ^c	
				Axial (mm)	Radial (mm)	(°K)	SD (%)
2030	11.32	1.814	0.0299	175	0	1340	4.3
2030+	11.32	1.814	0.0299	175	-20	1863	3.9
2107	6.82	2.528	0.0129	175	0	1211	2.0
2159	7.00	2.523	0.0133	175	0	1132	2.4

^a Equivalence ratio.

^b Axial position was measured along centerline and from the face of the centerbody. Radial position was measured up (+) or down (-) from the centerline. Centerbody diameter = 140 mm. Radial resolution, $\Delta Y = 20$ mm. See Figure 3 and 5.

^c The SD values are the estimated standard deviations calculated from the data using Poisson statistics. See Table 10 and text.

TABLE 10. RAMAN DATA FOR COMBUSTION TUNNEL RUNS OF 24 JULY 1978 GIVEN IN TABLE 9

Time	Signal ^a			Background ^a			Ratio ^b V	Bkgnd-Induced Temp SD ^c	
	Main Peak (c/p)	Hot Band (c/p)		Laser-Induced Main Pk (c/p)	Hot Bd (c/p)	Non- Laser (c/p)		Laser Induced (%)	Non- Laser (%)
2030	132.96	98.47		89.17	88.38	0.8	0.2304	4.0	0.3
2030+	120.50	98.51		83.15	81.79	0.9	0.4477	3.4	0.3
2107	97.95	40.25		27.26	27.77	0.9	0.1765	1.5	0.2
2159	75.87	31.19		23.42	23.65	0.7	0.1438	2.0	0.3

^a Main peak and hot band values were measured respectively at 3657.4 Å and 3653.8 Å. Slit height = 20 mm and FWHM = 1.64 Å. Wavelength steps were 3.6 Å with 25,000 laser pulses per step at 250 pps. The first-order spectrum was used. c/p = average digital counts per laser pulse.

^b V ≡ (hot-band Raman signal)/(main-peak Raman signal).

^c Estimated standard deviations calculated using Poisson statistics. See text.

data for the four sets of measurements. The signal and background values given in these latter tables for the main peak and hot band were measured respectively at 3657.4\AA and 3653.8\AA . The non-laser-induced background values resulted from additional measurements at each wavelength step made 0.6 msec after each laser pulse. The value given for a computer-fitted scan is the average over all the scan steps. In an N- λ measurement, the value given is the average of the two values recorded at the main-peak and hot-band wavelengths. These latter tables also include the breakdown in the contributions to the temperature error (SD) based on Poisson statistics as discussed in Section 3.1.3. Tables 3 and 4 give the data for the computer-fitted scans and Tables 5 through 10 give the data for the N- λ measurements.

It is useful to note that because of the accidental equality of the laser pulse repetition frequency (PRF) and the approximate digital counts per photoelectron at 250, the average digital counts-per-laser-pulse (c/p) values given for the Raman data in this report are approximately equal to the average photoelectron counts per second.

3.2.2.1 Computer-Fitted Measurements

Among the interesting features in the computer-fitted data given in Tables 3 and 4 is the generally low values for the temperature SD even in cases where χ_r^2 is very large. Although some of these small SD values certainly could be accidental, it is hard to see how the majority of them were accidentally low. As discussed in Section 3.1.1, the runs through 18 July include interferences from the mercury-vapor lamps used to light the room. These interferences are illustrated in Figure 9 which shows a chart recording of the scan taken at 1935 on 6 July. The mercury spectrum has strong lines at 3650, 3655, and 3663\AA . Features near these wavelengths are evident in Figure 9 when this recording is compared to the 1800°K spectrum in Figure 7. The presence

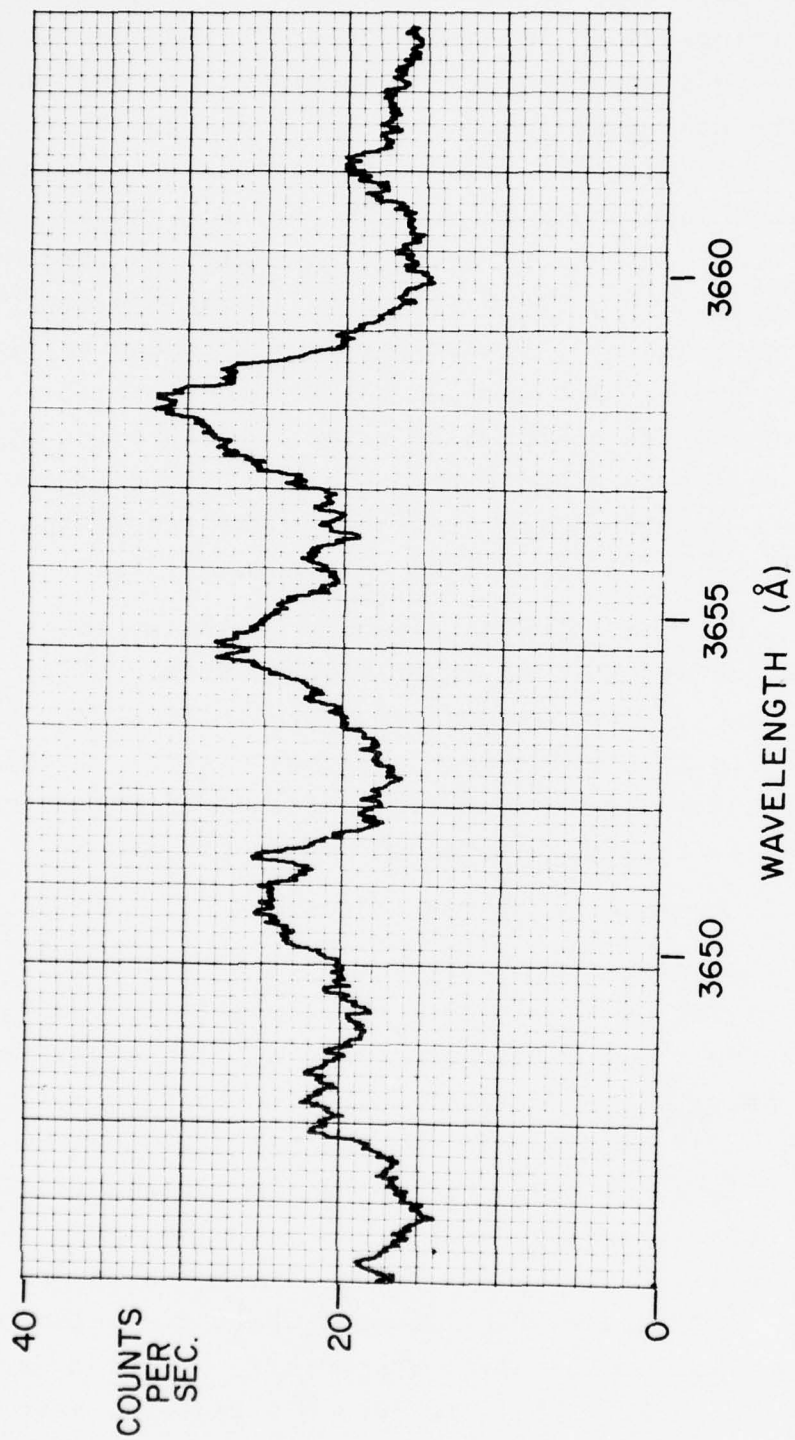


Figure 9. Scan of the Region Occupied by the Stokes Q-Branch Spectrum of N₂ during the Run at 1935 on 6 July 78 reported in Tables 3 and 4. (The spectrum shows interferences at or near 3650, 3655, and 3663 Å from the room mercury-vapor lamps.)

of this interfering spectrum clearly made the χ_r^2 high and it is probable that the interference introduced a systematic error in the fitted temperature. The extreme unsteadiness of the flame makes the estimation of the error impossible. This is evident in the 350°K difference between this scan and the scan taken at 2041 on 5 July which was made under similar conditions. This temperature difference is well outside the 136°K range defined by the SD values. Part of this difference could be due to the difference in value of ϕ . In any case, these temperatures are at least within the approximate upper limit of 2250°K for an ideal methane flame with a 300°K inlet temperature.¹²

Generally, the large values for χ_r^2 can be traced to the high noise level which arose from the high background signals and from the unsteadiness of the flame. This is particularly evident in the high χ_r^2 values for runs at 1944 and 2120 on 24 July. On these two runs, about 50% more steps were scanned than are needed to determine the background curve. Thus, the χ_r^2 was pushed up by the large number of noisy background data points. Interestingly, the temperature SD values did not suffer. The runs at 1902 and 1944 on this date as well as the run at 1939 on 18 July have the highest values of ϕ studied. As can be seen in the data for these dates, measurements were made only at the 175-mm axial position. The background level was too high at positions closer to the centerbody to permit detection of the N₂ Raman spectrum.

Most of the runs were plagued by the high ambient temperature and humidity conditions characteristic of July in Dayton, Ohio. The laser usually could not be operated for continuous periods when the temperature in the test cell was much over 27°C (80°F) because of insufficient capacity of the laser cooling unit. Long scans like at 2143 on 26 July which took almost 30 minutes were not often possible due to

the laser overheating. The problem was aggravated by the warming of the test cell due to the operation of the combustion tunnel. The humidity at times completely prevented any useful data being gathered due to condensation forming on the cool laser windows. Although jets of dry N_2 gas were used to prevent this problem from occurring, they were not adequate. This may have been the main contribution to the high χ_r^2 for the run at 1859 on 30 June when the available laser power dropped by almost 20% during the run. Although the recorded signal is normalized against laser power, the normalization did not adequately follow the spatial changes in the beam intensity caused by the fogging of the windows.

The initial Raman measurements made using the first-order spectrum occurred on 18 July. The first-order gratings were installed in the spectrometer in order to look at the anti-Stokes spectrum and to permit scanning the background spectra of the flame. (See Sections 3.1 and 3.3.) These data were computer-fitted with the slit parameters included in the fitting procedure. The run at 2122 was extremely noisy and could not be analyzed. The other two runs on 18 July also were very noisy which was partially the source of the large values obtained for χ_r^2 . The other main source of the high χ_r^2 values resulted from the inclusion of the slit parameters in the fit. Generally, the temperature SD as well as the χ_r^2 are increased when this is done. However, it has been found¹³ that the temperature does not usually differ significantly from the value obtained when the slit parameters are held fixed at their correct values.

The remaining first-order runs were fitted using slit parameters determined from room-temperature spectra. For 24 July, SBHW = 1.591 \AA and STBWR = 0.028; and for 26 July, SBHW = 1.862 \AA and STBWR = 0.0174. The three slits were each set at 0.33 mm in all first-order runs. The slit function for 26 July was different as the result of a minor

realignment of the final spectrometer mirror. The third-order slit parameters were those given in Equation (6).

3.2.2.2 N- λ Measurements

The twelve runs made on 5 July and summarized in Tables 5 and 6 used essentially the same relatively high air flow rate but the value of ϕ and the axial position were changed. These data are characterized not only by large B/R values but also by comparatively weak Raman signals. This latter feature, in particular, made the SD values unacceptably large. In fact, the temperatures show no meaningful correlation to ϕ or the position of the measurement. It is evident that the concentration of the N₂ probe molecule in the sample volume was quite low in these measurements. The data in Tables 5 and 6 illustrate a situation where the measurement parameters, in particular the number of laser pulses (i.e., the time duration of measurement), were not appropriate for the conditions being observed.

It is interesting to note that the poorest SD occurred at the highest ϕ value of the 105-mm-position data. Not only was the laser-induced SD almost twice as high as any of the remaining runs, but the non-laser-induced SD was 11%, over twice any of the other values. Clearly, the flame luminosity was quite high at this position.

Fourteen of the seventeen runs reported in Tables 7 and 8 for 6 July had the same air flow rate but at about two-thirds of the value used on 5 July. This allowed lower values of ϕ to be explored which resulted in generally lower SD values, particularly at the 35-mm and 105-mm axial positions. However, at this lower air flow rate there were cases when the Raman signal was quite weak thereby permitting the laser-induced background to dominate the observed spectrum. This situation gave rise to the five runs in Tables 7 and 8 wherein temperature measurements were not possible.

In order to characterize the reproducibility of the $N-\lambda$ method of temperature measurement, five runs were repeated during the 6 July studies. The clock times which identify these sets of measurements in Tables 7 and 8 are (1) 1917 and 1957, (2) 1926 and 2000, (3) 2028 and 2032, (4) 2050 and 2053, and (5) 2101, 2103, and 2108. In the first four sets the agreement is within the SD values. In the last set, the first two values are in good agreement but the third member is about 200°K outside one SD range. Since the SD values, 14 to 20% in the fifth set of runs, were calculated assuming Poisson statistics, they represent essentially the lowest possible uncertainties that can be expected for these measurements. (See Section 3.1.3.) The unsteadiness and the coarse turbulence of the flame which contributed an additional noise level to the signals is the probable cause of this discrepancy. Nevertheless, the overall reproducibility in these runs was quite reasonable considering the nature of the flame and the B/R values encountered. An indication of the bias discussed in Section 3.1.2 is seen in the first set of measurements identified above. These two values combine to give a weighted mean of $3012^{\circ}\text{K} \pm 9.5\%$. This value is well in excess of the estimated maximum theoretical temperature of 2250°K for this flame.¹²

Eight runs were made on 24 July. Four were computer-fitted and are reported in Tables 3 and 4. The other four are given in Tables 9 and 10. The objective was in part to make a preliminary comparison between the computer-fit method and the $N-\lambda$ method of temperature measurement. Only one pair of measurements, at 2120 and 2159, gave temperatures which agree within one SD range. However, this could be anticipated from the high values of χ_r^2 in Table 3 for 24 July. As all ready discussed, this situation indicates that there is some unknown feature or character in the data which is not included in the fitting procedure. Clearly, this increases the probability of systematic or

random shifts in the measured temperatures. Thus, the large value of χ_r^2 can be thought of as an accuracy indicator. When it is low, say 2.0, the measurement is probably accurate, and when it is high, i.e., 2.0, the measurement may have a systematic error of unknown magnitude and direction. This is another way of characterizing the presence of non-Poissonian noise in the data.

The parameters T_0 and m in Equation (1) used to calculate the temperatures and SD values in Tables 9 and 10 resulted from a least-squares fit to data obtained from 10 theoretical spectra calculated with the appropriate slit parameters. The temperature range of these spectra was about 1100 to 2500°K. The parameter values were $T_0 = 786.3^\circ\text{K} \pm 0.86\%$ and $m = 2404.6^\circ\text{K} \pm 0.76\%$.

3.3 MEASUREMENTS OF BACKGROUND SPECTRA

3.3.1 Origins of Background Signals

The non-Raman features in the observed signals can, in general, originate from three categories of sources. Those sources which occur, in one manner or another, as the result of the illumination of the sample volume by the laser beam are referred to as laser-excited sources. These sources usually arise from fluorescence or incandescence processes. Sources which exist in the sample volume independent of the laser beam can be classified as intrinsic emitters. Finally, there can be a source located outside of the sample volume which in some manner illuminates the entrance slit of the spectrometer to provide a totally spurious spectrum. An example of this last type of source is the mercury-vapor lamp discussed in Section 3.2.2.1 which superimposed the non-Raman features shown in Figure 9. Since this latter source can usually be completely eliminated by the experimenter, it need not be considered here.

For convenience, the two sources of interest are referred to as laser-induced and non-laser-induced backgrounds. However, it is to be noted that the sample volume is generally not the same for these two backgrounds. The 90° scattering geometry used in this work and described in Section 2.2 defines the sample volume shown in Figure 3 for the laser-induced background. This assumes that there are no significant contributions from reflections or spurious scattering of the laser beam. However, the sample volume for the non-laser-induced background is defined by the intersection of the acceptance solid angle of the collecting lens L3 and the volume of the emitting sources. In the case of the emission from the flame in the combustion tunnel, the sample volume would extend across the entire tunnel. Furthermore, any surfaces "seen" by lens L3 are potential sources of non-laser-induced backgrounds. The surfaces of the windows in the optical access ports of the tunnel are examples of this type of source. Actually the windows as well as the flame may contribute additional spectral features to the emission collected by L3 through absorption processes. For example, broad-band laser-induced emission from the small sample volume at the center of the tunnel would be a light source for exciting the absorption spectra of the molecular species that are present in the acceptance solid angle between the sample volume and the tunnel window.

3.3.2 Laser-Induced Background

The spectral character and intensity of the laser-induced background are governed primarily by: (1) the molecular constituents and their densities in the sample volume, (2) the wavelength of the emission, (3) the wavelength of the laser, (4) the temporal character of the laser excitation, e.g., the pulse length, and (5) the temporal character of the observation. The choice of fuel and the combustion

conditions determine (1). Assuming that Raman thermometry is to be used, then the emission wavelength is fixed by the choice of laser wavelength. Clearly, the capability of changing the laser wavelength would allow the possibility of reducing the laser-induced background by selecting the excitation wavelength. There are two basic types of non-Raman, laser-induced sources, namely fluorescent and incandescent. Eckbreth et al. have examined in detail laser modulated particulate incandescence particularly as it concerns Raman thermometry.¹⁴ In the studies reported here, incandescence did not appear to be a contributing factor. However, it is possible that Raman scattering from particles did make some contributions to the spectra observed under certain tunnel operating conditions. This would be another type of laser-induced background. Thus, if fluorescence is the primary source of the laser-induced background, then the temporal characteristics of the excitation and observation determine, to a large extent, the recorded background signal level.

The laser pulse used in these studies is shown in Figure 2. The detection apparatus used an RCA 8850 PMT connected through a fast-pulse pre-amplifier (gain = 10) to an EGG/ORTEC model LG105 gated current integrator. The output of the integrator was a 3 sec pulse whose amplitude was directly proportional to the area under the PMT pulse that occurred during the gate pulse. The amplitude of the 3 sec pulse was digitized on an arbitrary scale and sent to the computer. The gate pulse used in this work was about 20 nsec in width and was triggered at the laser PRF of 250 pps. The measured linearity of the complete detection system was within $\pm 1\%$ over a dynamic range of about 50 to 1. For this combination of laser and gate pulses, it can be shown¹⁴ that fluorescence species with lifetimes of about 120 nsec or greater will be effectively discriminated against. Background signals from fluorescence having a lifetime of

about 40 nsec will be reduced by about a factor of four with the current arrangement. Since the time scale of Raman scattering is in the sub-picosecond domain, the fluorescence discrimination capability is largely determined by the available apparatus.

Three approaches were taken towards characterizing the laser-induced background observed in these studies. (1) The background spectra detected through the gated-detection apparatus were recorded. (2) Spectra were obtained with the gate width reduced and with the time delay increased. (3) An effort was made to excite the fluorescence with a non-laser source. The latter effort was attempted in order to identify unambiguously the background as being due to fluorescence. A 75 watt, compact-arc, mercury-vapor lamp was set up and focused in the flame. Various combinations of filters were tried which changed the portion of the lamp spectrum incident on the observed volume. However, the only spectrum observed was that due to the intrinsic luminosity of the flame, namely the non-laser-induced spectrum. No change other than a slight increase in the broad, underlying band could be identified as being due to the mercury lamp.

The background spectrum of a natural-gas flame in the combustion tunnel induced by the 3371-Å laser is shown in Figure 10. The synchronized spectrum was taken with the normal gate width and gate delay time used to obtain Raman spectra. The gate delay was set by maximizing the Raman signal obtained from room-temperature N_2 . Thus, the gate time is synchronized with the arrival of the Raman signal at the gated integrator. The delayed spectrum was recorded with the gate delay time increased one gate width, namely about 20 nsec. A third spectrum was taken with the gate synchronized, but with a gate width of 10 nsec. This spectrum was essentially the same as the delayed spectrum shown in Figure 10 both in character and in amplitude.

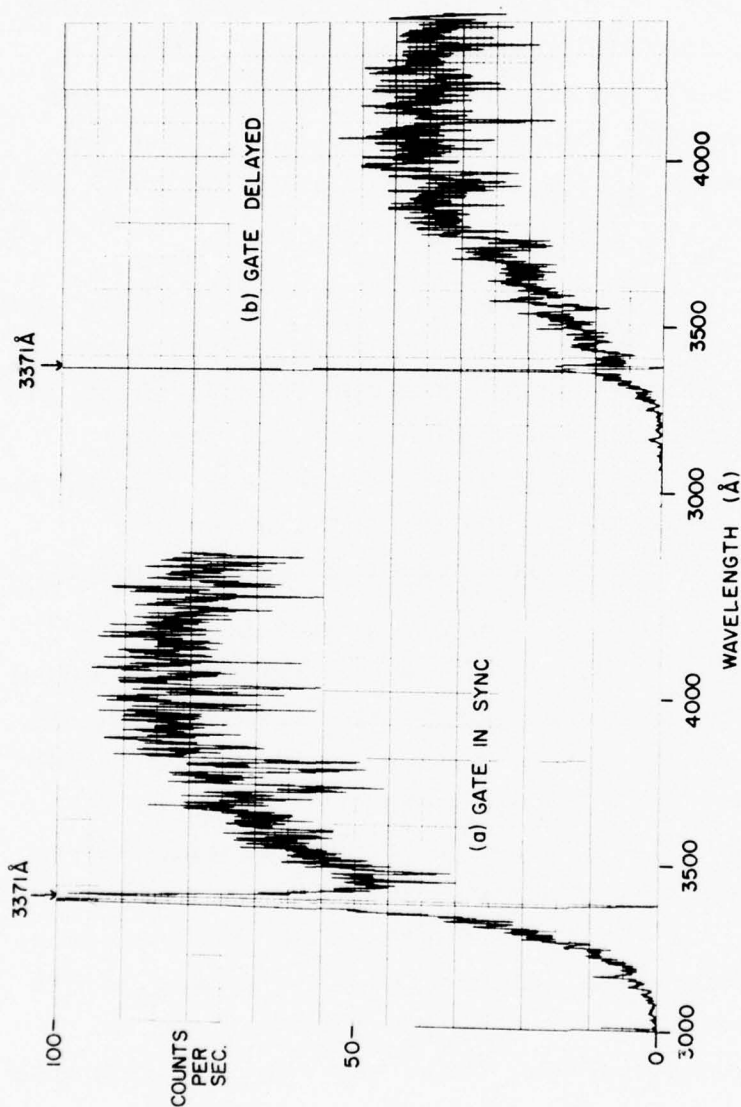


Figure 10. Laser-Induced Background Spectra Observed with Natural-Gas (Methane) Fuel at 1646 on 28 July 1978. (In spectrum (a) the 20-nsec wide detection gate was synchronous with the Raman (or laser) signal, and in (b) the gate was delayed 20 nsec. The spectra are uncorrected for system spectral responsivity and count saturation. Recorder time constant was 3 sec. The run conditions are given in Table 11.)

These spectra were recorded with an amplitude discriminator and ratemeter such that each anode pulse from the PMT above the dark-noise pulses produced a single count. In other words, the maximum count per laser pulse was one. Since the laser PRF was 250 pps, then the signal count rate recorded in this was cannot exceed 250 counts/sec (c/s). This characteristic is referred to as count saturation.¹⁶ The relationship between the true count rate, \dot{N}_{true} , and the observed count rate, \dot{N}_{obs} for a PRF of f is given by¹⁶

$$\dot{N}_{\text{true}} = f \ln[f/(f - \dot{N}_{\text{obs}})] \quad (7)$$

Applying Equation (7) to the spectra in Figure 10 shows that the true count rate at the maximum in the synchronized spectrum (viz., at about 4000 Å) is about 100 c/s while in the delayed spectrum count saturation accounts for only about a 10% reduction in the observed count rate. Thus, the difference in the shape of the broad bands in the two spectra can be attributed to the effect of count saturation.

The tunnel fuel and air flow rates used to obtain Figure 10 are given in Table 11. These conditions produced one of the more intense backgrounds. The Raman band N_2 is barely discernible in the synchronized spectrum. The drop in the amplitude of the delayed spectrum relative to the synchronized spectrum indicates a fluorescence lifetime on the order of 20 nsec. This behavior would not be expected if the background was due to laser-induced soot incandescence.¹³ Many of the absorption-like features did not appear in all three spectra indicating that they are probably due to intense temporal fluctuations. These fluctuations resulted from the highly turbulent and unsteady character of the flame for these combustion conditions. The ratemeter time constant of 3 sec used in these scans shows that these fluctuations were on a rather slow time scale. Another feature which occurred in all three spectra is the emission line at about 3160 Å. Its presence in the delayed spectrum

TABLE 11. RUN CONDITIONS FOR THE BACKGROUND SPECTRA GIVEN IN FIGURES 10, 11, AND 12

Date & Fuel	Time	Tunnel Conditions		Axial ^b Position (mm)	PMT Voltage (kV)	Slit Width ^c		Laser ^d Power (mW)
		Fuel (lb/hr)	Air (lb/sec)			Input (mm)	Spectral (Å)	
07/07/78 Methane	1759	18.10	4.818	0.0180	35	2.10	0.70	5.0
07/27/78 Propane	2042	8.53	3.61	0.0103	175	1.90	0.33	1.7
07/28/78 Methane	1646	8.37	1.814	0.0221	175	1.90	0.33	1.7
								130

^a Equivalence ratio.

^b Radial position = 0 for the three runs.

^c Slit height = 20 mm.

^d Estimated power of the 3371-Å laser beam at the sample volume.

strongly suggests that it is due to an anti-Stokes fluorescence process.

A final feature of interest occurs in the synchronized spectrum in Figure 10. This is the presence of a background signal on the anti-Stokes side of the laser line. Including a factor of two reduction due to the system spectral responsivity, the level of this background at the anti-Stokes N_2 wavelength (3125 \AA) is about a factor of 15 lower than the value at the Stokes N_2 wavelength (3658 \AA). However, the Raman intensity of this band is also lower, for example, by a factor of 7.6 for 1300°K . Thus, the Raman-to-background signal ratio would only double if the anti-Stokes Raman band of N_2 were scanned. Moreover, the recorded Raman signal would have to be increased by a factor between 5 and 10 to make up for the lower signal strength. This would be accomplished by either increased laser power or a longer time of signal accumulation at each wavelength step, or both. This analysis is consistent with the anti-Stokes measurements referred to at the beginning of Section 3.1.

The laser-induced background spectrum observed with propane fuel is given in Figure 11. The lower amplitude compared to the natural gas spectrum is probably due in part to the lower equivalence ratio, ϕ , used with the propane run. The large amplitude changes in the natural gas spectra which were apparently of temporal origin appear to be somewhat lessened with propane. Furthermore, there is evidently a characteristic spectrum above about 3700 \AA . Since the Raman band having the largest shift would be due to OH which would occur no higher than about 3850 \AA , then most of the features in Figure 11 must be due to fluorescence. The intrinsic emission spectrum of the flame was significantly attenuated by gated detection process. The anti-Stokes fluorescence line at about 3160 \AA which appeared in the natural-gas background spectra was somewhat stronger in the propane spectrum. This

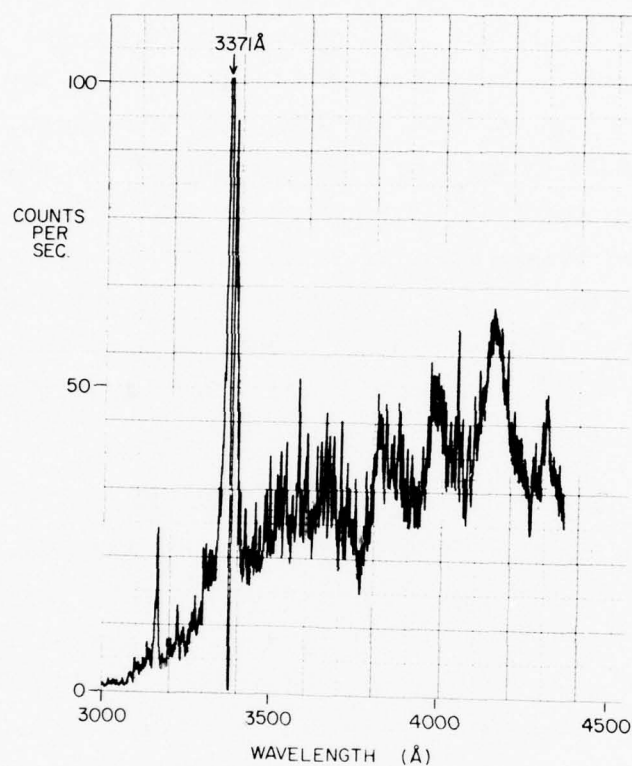


Figure 11. Laser-Induced Background Spectrum Observed with Propane Fuel at 2042 on 27 July 1978. (The spectrum is uncorrected for system spectral responsivity and count saturation. Recorder time constant was 3 sec. The run conditions are given in Table 11.)

suggests that the molecular species responsible for this line may also be in some way related to the source of the characteristic spectrum at longer wavelengths.

It is of interest to note in the propane spectrum that not only is the anti-Stokes background signal at 3125 \AA only about a factor of 3.5 smaller than the signal at 3658 \AA , but it is at least a factor of two larger than the value observed with natural gas. Thus for temperatures below about 2000°K , there would be little or nothing gained in using the anti-Stokes Raman band of N_2 instead of the Stokes band with a background spectrum like that given in Figure 11. Furthermore, the total dissimilarity of the background spectra obtained with the two fuels suggests that the choice of fuel as well as the combustion conditions may determine the effectiveness of a given measurement scheme.

3.3.3 Non-Laser-Induced Background

The background spectrum from the natural-gas flame recorded with the laser beam blocked from the sample volume is shown in Figure 12. By increasing the slit width and PMT voltage the sensitivity was increased by about a factor of 20 over the synchronized spectrum in Figure 10. The $3371\text{-}\text{\AA}$ line in the figure represents accidental leakage of the laser light.

The dominant spectral features in Figure 12 are the well-known emission bands of hydrocarbon flames.¹⁶ The following is a tabulation of these bands.

<u>Wavelength (\AA)</u>	<u>Species</u>
3063.6	OH Band head
3143	CH Systems
3900	
4315	
4737.1	
5129.3	C_2 --Members of the Swan system
5165.2	
5635.5	

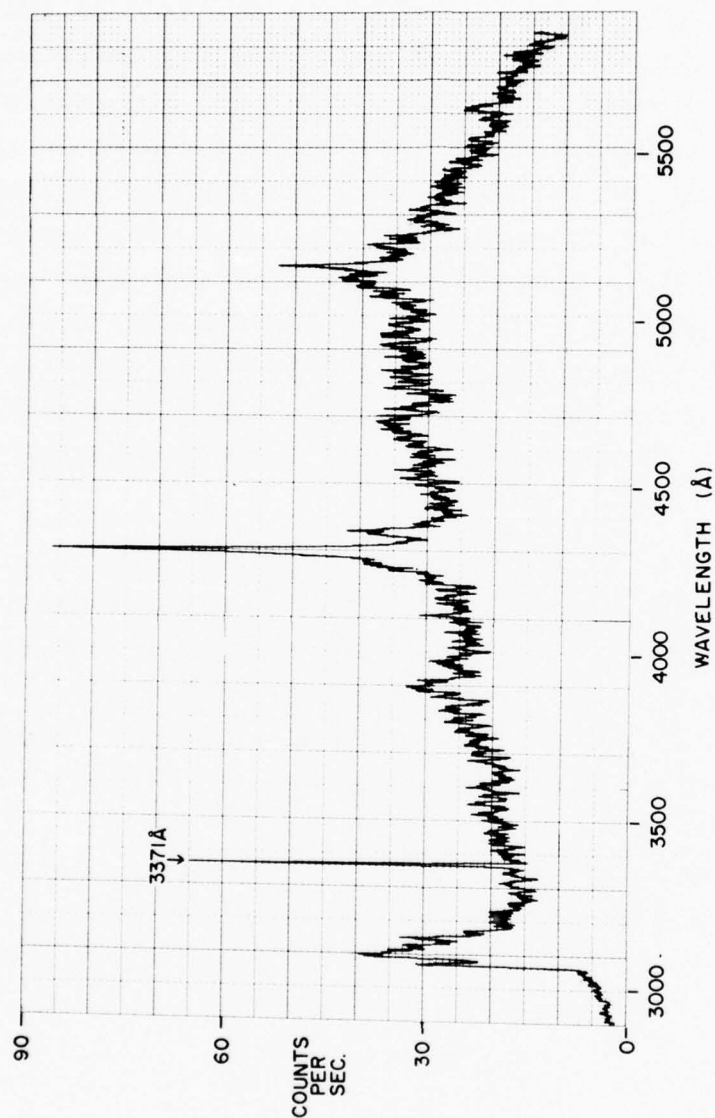


Figure 12. Non-Laser-Induced Background (Emission) Spectrum Observed with Natural-Gas (Methane) Fuel at 1759 on 7 July 1978. (The spectrum is uncorrected for system spectral responsivity and count saturation. Recorder time constant was 3 sec. The run conditions are given in Table 11.)

The background spectrum was also measured with the laser off and without gating using the discriminator and ratemeter method of recording the signal. The count rate was increased consistent with the increase of the duty cycle of detection to unity. Although the main features of the spectrum were the same as shown in Figure 12, there was one noticeable difference. In Figure 12, there are several regions of what appears to be periodic structures in the broadband portion of the spectrum. These structures were not detected in the non-gated spectra. They were apparently of temporal origin. Since the horizontal scan rate was about 100 sec per major division, the period of these peaks appears to range between about 8 and 16 seconds. This suggests that there was a stroboscopic effect associated with the laser PRF and some periodic temporal feature in the flame.

The intensity of the non-gated spectra apparently followed the visual appearance of the observed region in that it increased with increased brightness of that region. In addition to the conditions used to record Figure 12, the spectrum was also recorded for the following two conditions: fuel = 10.43 lb/hr, air = 3.573 lb/sec, $\phi = 0.0140$; and fuel = 8.17 lb/hr, air = 1.828 lb/sec, $\phi = 0.0217$. However, these spectra also showed that the ratios of the intensities of the spectral features due to the molecular species to the intensity of the broad, underlying band did not depend in an obvious way on the combustion conditions.

SECTION 4

CONCLUSIONS

The conclusions are divided into two parts. The first part addresses the performance of the LARS system while the second part is an assessment of the measurements made with the system on the combustion tunnel.

The design of the LARS system as modified during this program provides considerable flexibility for the optical arrangement and there is adequate surface area for accommodating a different laser or other apparatus needed in the future. The data acquisition and handling features of the system include the capability of performing numerous real-time functions in addition to the control activities. Essentially all of the design objectives for the modified system have been met. The results obtained from the right-angle (90°) scattering measurements on the capillary burner completely fulfilled expectations and provided a validation of the design philosophy. The Poisson errors in the temperature measurements made on the air-acetylene flame using the $4-\lambda$ method were between 5 and 9%. The fact that these temperature measurements were obtained with the Raman-to-total signal ratio around 30% (for the first hot band) in less than three minutes each shows that reasonable measurements are possible in practical combustion environments using the LARS system. Added to this result is the feature of the $4-\lambda$ ($N-\lambda$, in general) method wherein the temperature and uncertainty can be made available immediately upon completion of the signal measurements.

The mobility of the system and the general ease of transporting and positioning the transceiver unit was confirmed during the transfer of the system to Room 20, Building 18, of AFAPL. The vibration of the optics table which is supported by pneumatic mounts was well below the

level that would be detectable in the Raman signals for all run conditions of the combustion tunnel. Although preparations had been made to thermally isolate the system from the tunnel, it was found completely unnecessary due to the relatively low exterior temperature (about 150°C) of the combustor pipe.

Forty-eight sets of Raman data, taken over a wide range of operating conditions of the combustion tunnel, are analyzed and presented in this report. Another 20 or more sets of data were recorded, examined, and subsequently removed from further analysis for various reasons. In addition, about 20 scans of the background spectra from the flame of the combustion tunnel were recorded and studied. Of these spectra, four appear in the report. The overriding result of this measurement effort is that temperature measurements can be made on the combustion-tunnel flame using the LARS system in spite of the high fluorescence backgrounds and the highly turbulent nature of the flame.

The high backgrounds per se were not always the limiting factor in these measurements. For example, temperature uncertainties as low as 4% were obtained for measurements in which the Raman part of the total observed signal at the hot-band wavelength was only about 10%. This was accomplished by using long signal accumulations times (e.g., 100 sec) at each wavelength step and by making additional measurements on the background spectrum so as to increase the precision of the background determination. However, if, when the background level was high and either the fractional concentration of the N_2 probe molecule in the sample volume was much below average or the temporal fluctuations (e.g., due to turbulence) in the background were high, or both, then a meaningful measurement was not possible. Basically, the relative concentration must be high enough and the fluctuations small enough to permit an

unambiguous detection of the first hot band. In principle, if this band is detectable, then a temperature measurement is possible.

One of the main concerns about this circumstance is the meaning of a time-averaged temperature measurement. The difference between a two-minute and a ten-minute measurement is probably not significant in this regard. A longer time mainly puts more stringent demands on the constancy of the combustion conditions and the performance of the Raman apparatus. For example, the recurring obstacles to making long-time measurements experienced in these studies were the fogging of the laser windows due to high-humidity conditions and overheating of the laser due to the high ambient temperature in the environment of the LARS transceiver.

A preliminary computer study has been completed by Hemmer and Yaney¹⁸ which characterizes for constant density conditions the effect of a Gaussian (i.e., symmetric) distribution of temperatures existing in the sample volume on the apparent temperature obtained by fitting a theoretical spectrum to the composite Raman spectrum generated by the distribution. In the range of 1000 to 3000°K, the error in the average temperature introduced by measuring an average spectrum instead of determining the mean temperature from the distribution of many instantaneous measurements was 1% or less. This was calculated for a standard deviation in the temperature distribution of 200°K. With a mean temperature of 2000°K, a 400°K standard deviation introduced an error of less than 2% (downward). The study will be extended to include constant pressure conditions and asymmetrical distributions at a later date. Nevertheless, the results strongly suggest that if the combustion environment can be characterized by a well-defined temperature distribution function, then time-averaged measurements using Raman scattering are viable.

In the two cases in which Raman measurements were not possible, namely where the fractional N_2 concentration was unusually low and where the temporal fluctuations were excessive, are also circumstances where the question of the meaning of temperature must be raised. Presuming that the source of the fluorescence background was due to incompletely-burned hydrocarbon species, then the low number density of N_2 molecules relative to these species suggests that the amount of air available for combustion, and therefore the fractional oxygen concentration in the sample volume was specially low. This could be due to insufficient mixing of air with the fuel giving rise to regions wherein the concentration of partially oxidized fuel is high. Such regions would have relatively high chemical activity and would, therefore, be expected to be highly fluorescent. The meaning of temperature in a small, highly localized volume of such regions is not clear. In a similar sense, when turbulence or unsteadiness in the flame extends over spatial regions that are on the order of or larger than the dimensions of the sample volume, how is the temperature defined in the sample volume? The concern here is how these questions impact the combustor modeling activity with which the measurement activities must interface. This points to the need for a clarification of what constitutes meaningful temperature measurements in the various regions of a wide range of flame types. This need exists independent of whether the measurements are time averaged or instantaneous and should be addressed before an extensive measurement program is initiated.

Finally, it was shown that the $N-\lambda$ method of temperature measurement using the Stokes spectrum is an effective, rapid technique. The results presented in this report represent the first extensive application of the technique to a practical combustor. Interestingly, it was found that the background level in the N_2 anti-Stokes region was

too high to permit any use of this spectrum. The utility of the $N-\lambda$ method was revealed by the $6-\lambda$ measurements which gave an average temperature uncertainty from 10-minute scans comparable to the average of the uncertainties from the computer-fitted runs which took an average of 15 minutes each.

SECTION 5

RECOMMENDATIONS

The recommendations regarding future measurements on the combustion tunnel using Raman scattering concern two aspects of the activity. The first is simply a reiteration of the problem identified in Section 4. Namely, that the interrelationships between the character of the flame, the requirements for computer-modeling the flame, and the constraints attendant to the measurements on the flame be addressed before a new measurement program is started.

The second area of recommendations are concerned with the current LARS system. These recommendations are presented as three groups which can be implemented independently or in any combination. There are a number of variations or extensions within these groups, particularly the last two, which could also be recommended; however, the purpose here is not to provide an exhaustive list but rather to identify the areas where work is needed.

5.1 MODIFICATION OF CURRENT LARS SYSTEM

These recommendations assume that there will be no major changes in the current design of the system in the near future. The following list identifies the tasks that should be accomplished before a new measurement program is begun. The order of the tasks does not indicate priority.

- Investigate the system performance with the tunnel using different lasers that are available for short-term loan. A tunable dye laser would be particularly useful in characterizing the dependence on laser wavelength.
- Reduce the sensitivity of the laser to environmental temperature and humidity.

- Redesign the optics for the laser-power monitor to insure precise normalization of observed signal against changes in the laser-beam power.
- Obtain the necessary digital-to-analog converter and other instruments needed to provide a computer-independent chart recorder readout of the observed signals.
- Obtain a programmable pulse generator and tie it into the computer to permit rapid identification of fluorescence decay in the background signals.
- Provide for remote control of the axial position of the system.
- Examine the need for backscattering (180°) measurements in light of the review of the modeling requirements and the flame character and implement the needed changes, if any.
- Arrange to have the four lenses and the two combustor windows coated with appropriate (probably broadband) antireflection coatings.
- Update the software for the NOVA computer to permit $N-\lambda$ measurements and provide for direct readout of the average temperature and the appropriate error analysis.
- Provide for the storage of the data from the run in progress with all modes of readout available.
- Update the software to permit a permanent recording of the date, time of run, and all other data pertinent to the combustion tunnel and the LARS system in the data file.
- Determine the influence of the O and S branches of the Raman spectrum on $N-\lambda$ measurements made on the Q branch.

- Study the statistics of the measurements both experimentally and theoretically.
- Record and study the spectrum of the temporal fluctuations in order to minimize the interference from oscillations in the flame.

5.2 MODIFICATIONS TO PROVIDE FOR "INSTANTANEOUS" MEASUREMENTS

In this group it is recommended that the LARS system be upgraded to permit either (1) instantaneous 4- λ measurements or (2) instantaneous recording of the complete Raman spectrum of the molecule of interest. Measurements made in 1 sec or less are assumed to be "instantaneous." In (1), the current spectrometer would be converted to a four-channel, PMT-based polychromator while in (2), an optical multichannel analyzer would replace the PMT. Both would require extensive software development. Both could be used with the current laser but with the sacrifice of the instantaneous measurement capability. By replacing the current nitrogen laser with a laser having at least a factor of 10^3 more pulse energy should permit instantaneous measurements in the presence of weak or moderate backgrounds. Of course, laser-induced soot incandescence could be a factor with such a laser.¹⁴

5.3 MODIFICATION TO IMPROVE BACKGROUND DISCRIMINATION CAPABILITY

There are two parameters under the control of the experiments which can be changed in order to reduce the laser-induced background from a given flame, namely the width of the detection gate and the laser wavelength. The laser pulse width can be reduced so that a narrower detection gate pulse can be used. This would increase the discrimination against the fluorescence signals in the

background. For example, a 2 nsec gate pulse with a 1 nsec laser pulse would reduce the background contribution from a 20-nsec-lifetime fluorescence process by about a factor of 10 over the currently used 10-nsec laser and 20-nsec gate.¹⁵ The strength of the fluorescence also depends on the wavelength of the excitation. Often fluorescence is most intense with ultraviolet or near-ultraviolet excitation and weakens with increasing wavelength. However, increasing the wavelength, λ , of the laser reduces the Raman scattering efficiency by λ^4 and reduces the quantum efficiency of the photodetector. Thus, for this kind of fluorescence spectrum, there is a laser wavelength which optimizes the Raman-to-background signal ratio. The capability of achieving this optimization can be provided by a tunable dye laser. Hence, in this option it is recommended that the electronic detection apparatus be upgraded to permit gate pulses around 2 nsec to be used with a tunable dye laser having a pulse width of about 1 nsec. The required equipment is within the present state-of-the-art of the electronic and laser technologies.

SECTION 6

REFERENCES

1. D.A. Leonard, "Field Tests of a Laser Raman Measurement System for Aircraft Engine Exhaust Emissions," Final Technical Report No. AFAPL-TR-74-100 (AVCO Everett Research Laboratory, Inc., Everett, Mass., October, 1974).
2. D.A. Leonard and B. Caputo, "Development of a Raman System as a Combustion Diagnostic Tool," Final Technical Report AFAPL-TR-75-99 (Computer Genetics Corp., Wakefield, Mass., October, 1975); Interim Report, Task 19, Wright-Patterson Senior Investigator Program (Purdue University, West Lafayette, Ind., March 19, 1976).
3. The unstable resonator for the AVCO C5000 laser was purchased by AFAPL from the Computer Genetics Corp.
4. W.M. Roquemore and P.P. Yaney, "Comparison of Thermo-couple, Gas-Sampling, and Raman Measured Temperatures in an Afterburning Turbojet Engine Plume," presented at the 10th Materials Research Symposium on Characterization of High Temperature Vapors and Gases, National Bureau of Standards, September 18-22, 1978, Gaithersburg, Maryland (to be published).
5. P.R. Bevington, Data Reduction and Error Analysis for the Physical Sciences (McGraw-Hill, New York, 1969); program CURFIT.
6. The burner was provided on loan from the High Power Branch of AFAPL.
7. The settings of the flow gauges on the burner gas supply manifold were the following: inner, gas = 1.5, air = 6.5; outer, gas = 1.7; argon = 25. These scale readings give the ratios of the tube diameter to the float diameters as defined in the Handbook 10A9010, "Tri-Flat Variable Area Flowmeters," (Fischer and Porter Co., Warminster, Penn., 1964).
8. L.I. Boehman (private communication).
9. J.D. Winefordner (private communication).
10. The flow-gauge settings were the following: inner, gas = 1.9, air = 8.6; outer, gas = 4.4, air = 16.6; argon = 30. See Footnote No. 7.

REFERENCES (cont'd)

11. H. Haraguchi and J.D. Winefordner, "Flame Diagnostics: Local Temperature Profiles and Atomic Fluorescence Intensity Profiles in Air-Acetylene Flames," Appl. Spectrosc. 31, 195 (1977).
12. W. M. Roquemore (private communication).
13. P.P. Yaney, P.R. Hemmer, T.H. Hemmer, and W.M. Roquemore, "Determination of Temperatures in the Combustion Zone of a J 85-5 Jet Engine Using the Laser-Excited Vibrational-Rotational Raman Spectrum of Nitrogen," in Thirty-Third Annual Molecular Spectroscopy Symposium (Ohio State University, June 1978).
14. A.C. Eckbreth, "Applicability of Laser Raman Scattering Diagnostic Techniques to Practical Combustion Systems," Project SQUID Technical Report UTRC4PU (Oct. 1976); also A.C. Eckbreth, Laser Light Scattering Diagnostics, The Winter Annual Meeting of the American Society of Mechanical Engineers, Atlanta, Georgia,, November 27-December 2, 1977, Session 4A, in Gas Turbine and Combustion Fuels Technology, E.K. Bastress, ed.
15. P.P. Yaney, "Reduction of Fluorescence Background in Raman Spectra by the Pulsed Raman Techniques," J. Opt. Soc. Am. 62, 1297 (1972).
16. P.P. Yaney, "The Pulsed Laser and Gated Detection in Raman Spectroscopy--A Survey of the Spectra of Common Substances Including Studies of Absorbed Benzene," J. Raman Spectrosc. 5, 219 (1976).
17. A.G. Gaydon, The Spectroscopy of Flames (John Wiley and Sons, Inc., 1957).
18. T.H. Hemmer and P.P. Yaney, "Computer Study of Time-Averaged Temperature Measurements on Combustion Temperatures Obtained from Raman Spectra of N₂," Bull. Am. Phys. Soc. (to be published, 1979); a complete report is in preparation.

APPENDIX

TYPICAL COMPUTER PRINTOUT USING THE COMPUTER FIT METHOD

DIFFRACTION ORDER 1
 SIGNAL TO BACKGROUND GATE WIDTH RATIO .5273
 PULSES 8000 8000
 LAMBDA DATA CUMULATIVE DATA L-POWER S B

.2856490E+07

36485	900496	900496	1.0001	896156	8231
36488	919370	919370	1.0067	907985	11963
36491	911217	911217	1.0050	901978	9333
36494	871817	871817	1.0031	864314	5147
36497	880088	880088	.9981	876032	11848
36500	871379	871379	.9978	868684	8735
36503	904859	904859	1.0139	897187	7914
36506	970219	970219	1.0150	959906	11438
36509	863738	863738	.9998	864538	10189
36512	882629	882629	.9924	864183	9797
36515	889435	889435	.9914	892256	9203
36518	919829	919829	1.0140	911624	8683
36521	923160	923160	1.0181	910907	9418
36524	940503	940503	1.0271	929887	7612
36527	883546	883546	1.0251	856771	9994
36530	902772	902772	.9910	905724	8865
36533	886423	886423	.9837	895052	11304
36536	936126	936126	.9871	942567	17857
36539	932184	932184	.9906	935565	11267
36542	889938	889938	.9874	895746	11389
36545	906997	906997	.9808	919008	11684
36548	903265	903265	.9824	914635	9966
36551	920362	920362	.9901	925032	8511
36554	995392	995392	.9922	998925	8077
36557	914239	914239	.9912	918432	9117
36560	902524	902524	.9820	913438	11483
36563	917808	917808	.9798	932096	8611
36566	919421	919421	.9830	930656	8697
36569	895811	895811	.9874	901285	11156
36572	900166	900166	.9842	918361	12756
36575	917242	917242	.9821	928743	9717
36578	940605	940605	.9811	954790	7321
36581	899939	899939	.9848	919476	8130
36584	948618	948618	.9915	953562	7789
36587	907979	907979	.9859	916434	8471
36590	1001568	1001568	.9832	1013773	9195
36593	1121811	1121811	.9809	1136108	8521
36596	1032556	1032556	.9826	1045651	9677
36599	1059423	1059423	.9905	1164341	9850
36602	1145565	1145565	.9885	1193147	11771
36605	1120863	1120863	.9853	1131764	10878
36608	1104213	1104213	.9789	1123343	8865
36611	1059141	1059141	.9756	1080241	8972
36614	1127798	1127798	.9804	1143404	9187
36617	1034566	1034566	.9852	1044806	9905
36620	948231	948231	.9877	955326	8829
36623	906763	906763	.9851	914426	11327
36626	889320	889320	.9837	896994	9443
36629	861879	861879	.9872	868180	9125
36632	851273	851273	.9915	853790	8989
36635	857661	857661	.9930	859416	8081
36638	880921	880920	.9923	882909	8121
36641	911753	911753	.9912	914278	10463
36644	852127	852127	.9912	854411	11545
36647	886833	886838	.9969	883963	11654
0	953790	1153147	.9918	55	9534


```

CONTROL PARAMETERS FOR MINIMIZATION SUBROUTINE
NO.      NAME                                     VALUE
1  AFTER FINDING APPROX. MINIMA, STEP SIZES REDUCED BY 5.0 10
2  MARQUARDT PARAMETER                                .0 10
CONTROL PARAMETERS FOR RAMAN SUBROUTINE

NO.      NAME                                     VALUE
1  LEVEL OF OUTPUT          NORMAL                ,CODE: 3
2  MIN. FUNCTION (2*(DATA-CALC)/AVER. DIFF.)*2, CODE: -1
3  SCALE FACTOR             USING MAX. DATA VALUES ,CODE: -1
4  ASSUME WAVENUMBERS USED          N
5  ASSUME EQUAL WAVE-NUMBER/LENGTH INCREMENTS      Y
6  ACCURACY OF CALCULATIONS (COMPARED TO ONE)      .1E-13
7  FACTOR FOR SCALE MULT. CALC. (IF NEEDED)         .65

3 VARIABLE TYPES FOR SAMPLE: 0072678.12143.1800V.A.95.RC10
7 EXPERIMENTAL VARIABLES
NUMBER  NAME                                     VALUE          STD DEV      PRI.
1  TEMPERATURE                                1624.24771131   0.0000000000   4
2  WAVELENGTH CORRECTION                      2.9000000000   0.0000000000   1
3  LAMBDA 0                                    3370.63000000   0.0000000000   2
4  BACKGROUND INTERCEPT                    106.74029680    0.0000000000   2
5  BACKGROUND SLOPE                          -0.00134985     0.0000000000   3
6  BACKGROUND CURVATURE                      0.0000000000   0.0000000000   0
7  BACKGROUND FOCUS                          3656.60100000   0.0000000000   1

5 MORE EXPERIMENTAL VARIABLES
NUMBER  NAME                                     VALUE          STD DEV      PRI.
8  OVERALL SCALE FACTOR                      0.0000000000   0.0000000000   -1
9  SPHERICAL EMISSION SHIFT                  4.17260000     0.0355000000   0
10 SP. EMM. PEAK HEIGHT RATIO                0.02000000     0.0012000000   0
11 SLIT WIDTH HALF-WIDTH                     1.86200000     0.0000000000   0
12 SLIT TOP/WIDTH RATIO                      0.01740000     0.0000000000   0

6 NITROGEN VARIABLES
NUMBER  NAME                                     VALUE          STD DEV      PRI.
13 CROSS SECTION RATIO                       0.17360000     0.0156000000   0
14 WE                                          2359.61000000   0.0000000000   0
15 WEXE                                       14.45600000     0.0000000000   0
16 EE                                          2.01000000     0.0000000000   0
17 AE                                          0.01870000     0.0000000000   0
18 RELATIVE INTENSITY FOR N2                  1.00000000     0.0000000000   0

WHISQ = .39316028E+03
X(I)....
.29000000E+01 .34156895E+04 -.11195200E-11 .16242477E+04
DELTA X(I)....
.26258105E+00 .64940579E+02 .85486376E+11 .27261656E+13

X(I)....
.31625811E+11 .34156895E+04 -.11195200E-11 .16242477E+04

X(I)....
.26374189E+01 .34156895E+04 -.11195200E-11 .16242477E+04

X(I)....
.29000000E+01 .34156895E+04 -.11195200E-11 .16242477E+04

X(I)....
.29000000E+01 .33507489E+04 -.11195200E-11 .16242477E+04

X(I)....
.29000000E+01 .34156895E+04 .85374424E+11 .16242477E+04

X(I)....
.29000000E+01 .34156895E+04 -.85598328E+11 .16242477E+04

```


FINAL VALUES FOR PARAMETERS:

3 VARIABLE TYPES FOR SAMPLE: D072670.T2143.1800V.A095.RJ08

7 EXPERIMENTAL VARIABLES				
NUMBER	NAME	VALUE	STD DEV	PRI.
1	TEMPERATURE	1194.52459962	70.2721625357	4
2	WAVELENGTH CORRECTION	3.21132134	.0521344365	1
3	LAMBDA 0	3370.63200010	0.00000000	1
4	BACKGROUND INTERCEPT	110.28773795	.504211134	2
5	BACKGROUND SLOPE	-1.18295442	.059321721	3
6	BACKGROUND CURVATURE	0.00000000	0.00000000	0
7	BACKGROUND FOCUS	3656.63000000	0.00000000	0

5 MORE EXPERIMENTAL VARIABLES				
NUMBER	NAME	VALUE	STD DEV	PRI.
8	OVERALL SCALE FACTOR	298.41322248	0.00000000	-1
9	SPURIOUS EMISSION SHIFT	4.17260000	.035500000	2
10	SP. ENH. PEAK HEIGHT RATIO	.02031000	.00120000	1
11	SLIT BOTTOM HALF-WIDTH	1.86200000	.01000000	1
12	SLIT TOP/BOTTOM WIDTH RATIO	.91740000	0.00000000	1

6 NITROGEN VARIABLES				
NUMBER	NAME	VALUE	STD DEV	PRI.
13	CROSS SECTION RATIO	.17361000	.01561000	1
14	WE	2359.61000000	0.00000000	0
15	WEXE	14.45600000	0.00100000	0
16	BE	2.01000000	0.00000000	0
17	AE	.01870000	0.00000000	1
18	RELATIVE INTENSITY FOR N2	1.00000000	0.00000000	0

WAVELENGTH EXPR. CALC. ERRORS BKGR. EXPR. CALC. BKGR.
(ANGSTROMS) (COUNTS PER PULSE) (NORMALIZED)

3645.29	112.02	112.73	1.88	112.54	.7967	.8016	.8001
3645.59	113.51	112.68	1.39	112.44	.8072	.8014	.7937
3645.89	112.70	112.61	1.39	112.39	.8016	.8009	.7933
3646.19	108.04	112.56	1.35	112.33	.7684	.8006	.7949
3646.49	109.52	112.52	1.86	112.27	.7769	.8003	.7985
3646.79	108.59	112.47	1.85	112.22	.7723	.8000	.7931
3647.19	112.15	112.43	1.88	112.16	.7976	.7997	.7977
3647.39	119.59	112.41	1.95	112.10	.8534	.7995	.7973
3647.69	108.07	112.41	1.35	112.05	.7686	.7995	.7969
3647.99	110.52	112.39	1.97	111.99	.7061	.7993	.7965
3648.29	111.53	112.39	1.89	111.93	.7533	.7994	.7961
3648.59	113.55	112.41	1.90	111.87	.8105	.7995	.7957
3648.89	113.86	112.43	1.30	111.82	.8056	.7996	.7953
3649.19	116.24	112.43	1.91	111.76	.9267	.7997	.7949
3649.49	117.10	112.43	1.84	111.70	.7617	.7997	.7945
3649.79	113.22	112.45	1.39	111.65	.8052	.7998	.7941
3650.09	111.88	112.46	1.88	111.59	.7357	.7998	.7937
3650.39	117.02	112.46	1.93	111.53	.8380	.7999	.7933
3650.69	116.95	112.52	1.92	111.48	.8310	.8003	.7929
3650.99	111.37	112.66	1.88	111.42	.7964	.8013	.7925
3651.29	114.88	112.88	1.91	111.36	.8170	.8024	.7921
3651.59	114.33	113.19	1.37	111.31	.8132	.8051	.7917
3651.89	115.63	113.62	1.91	111.25	.8224	.8081	.7913
3652.19	124.87	114.18	1.96	111.19	.8801	.8121	.7919
3652.49	114.80	114.82	1.90	111.14	.8165	.8166	.7905
3652.79	114.18	115.38	1.90	111.08	.8121	.8206	.7901
3653.09	116.51	115.83	1.92	111.02	.8207	.8236	.7907
3653.39	116.33	116.14	1.92	110.97	.8274	.8260	.7893
3653.69	112.66	116.34	1.89	110.91	.8013	.8279	.7898
3653.99	113.55	116.41	1.90	110.85	.8076	.8279	.7894

3654.23	116.09	116.36	1.92	110.80	.8257	.8276	.7880
3654.53	119.35	116.55	1.94	110.74	.8489	.8291	.7876
3654.89	113.68	117.17	1.89	110.68	.8186	.8334	.7872
3655.19	119.20	118.32	1.94	110.63	.8478	.8420	.7868
3655.49	114.55	120.23	1.90	110.57	.8148	.8556	.7864
3655.79	126.72	123.17	2.00	110.51	.9113	.8761	.7861
3656.09	129.51	127.31	2.02	110.46	.9212	.9055	.7856
3656.39	130.71	132.16	2.13	110.40	.9256	.9400	.7852
3656.69	133.04	136.22	2.05	110.34	.9463	.9669	.7848
3656.99	144.14	139.15	2.13	110.29	1.0252	.9897	.7844
3657.29	141.47	140.60	2.11	110.23	1.0062	1.0000	.7840
3657.59	140.42	140.04	2.10	110.17	.9987	.996	.7836
3657.89	135.03	136.82	2.06	110.12	.9604	.9731	.7832
3658.19	130.43	130.95	2.03	110.06	.9276	.9314	.7828
3658.49	130.60	125.20	2.03	110.00	.9269	.8904	.7824
3658.79	119.42	121.01	1.94	109.95	.8493	.8535	.7820
3659.09	114.39	115.60	1.90	109.89	.8131	.8222	.7816
3659.39	112.37	112.20	1.98	109.83	.7993	.7960	.7812
3659.69	108.52	110.17	1.95	109.78	.7719	.7836	.7808
3659.99	106.72	109.78	1.84	109.72	.7591	.7848	.7804
3660.29	107.43	109.73	1.84	109.66	.7641	.7805	.7800
3660.59	110.36	109.69	1.87	109.61	.7350	.7802	.7796
3660.89	114.28	109.64	1.90	109.55	.8126	.7798	.7792
3661.19	106.80	109.59	1.84	109.49	.7596	.7755	.7788
3661.49	110.50	109.55	1.87	109.44	.7859	.7791	.7784
TOTAL AREA UNDER CALCULATED SPECTRA =					.52536122E+02		
TOTAL AREA UNDER EXPERIMENTAL SPECTRA =					.53801041E+02		
FINAL VALUE OF CHISQ =					.29497665E+01		

[illegible]

